FREQUENCY CONTROL SCHEME FOR ISLANDED DISTRIBUTION NETWORK WITH HIGH PV PENETRATION

MOHAMMAD HUSSEIN MOHAMMAD DREIDY

FACULTY OF ENGINEERING
UNIVERSITY OF MALAYA
KUALA LUMPUR

2017

FREQUENCY CONTROL SCHEME FOR ISLANDED DISTRIBUTION NETWORK WITH HIGH PV PENETRATION

MOHAMMAD HUSSEIN MOHAMMAD DREIDY

THESIS SUBMITTED IN FULFILMENT OF THE REQUIREMENTS FOR THE DEGREE OF DOCTOR OF PHILOSOPHY

FACULTY OF ENGINEERING
UNIVERSITY OF MALAYA
KUALA LUMPUR

2017

UNIVERSITY OF MALAYA

ORIGINAL LITERARY WORK DECLARATION

Name of Candidate: Mohammad Hussein Mohammad Dreidy

Registration/Matric No: KHA140004

Name of Degree: Doctor of Philosophy

Title of Project Paper/Research Report/Dissertation/Thesis ("this Work"):

FREQUENCY CONTROL SCHEME FOR ISLANDED DISTRIBUTION NETWORK WITH HIGH PV PENETRATION

Field of Study: RENEWABLE ENERGY (POWER SYSTEM)

I do solemnly and sincerely declare that:

(1) I am the sole author/writer of this Work;
(2) This Work is original;
(3) Any use of any work in which copyright exists was done by way of fair dealing and for permitted purposes and any excerpt or extract from, or reference to or reproduction of any copyright work has been disclosed expressly and sufficiently and the title of the Work and its authorship have been acknowledged in this Work;
(4) I do not have any actual knowledge nor do I ought reasonably to know that the making of this work constitutes an infringement of any copyright work;
(5) I hereby assign all and every right in the copyright to this Work to the University of Malaya ("UM"), who henceforth shall be owner of the copyright in this Work and that any reproduction or use in any form or by any means whatsoever is prohibited without the written consent of UM having been first had and obtained;
(6) I am fully aware that if in the course of making this Work I have infringed any copyright whether intentionally or otherwise, I may be subject to legal action or any other action as may be determined by UM.

Candidate's Signature Date:

Subscribed and solemnly declared before,

Witness's Signature Date:

Name:

Designation

ABSTRACT

Air pollution due to fossil fuel power plants are causing serious environmental problems, which affect all aspects of life. Due to this, many governments and power utility companies are expressing great interest in Renewable Energy Sources (RESs). Generally, using RESs in a distribution system such as solar Photovoltaic (PV) decreases dependence on fossil fuel. However, at high PV penetration levels, an islanded distribution network suffers from critical frequency stability issues. This occurs due to two main reasons: first, the reduction of the distribution network inertia with high PV penetration, where in this condition, the rate of change of frequency (ROCOF) will be high enough to activate the load shedding controller, even for small power disturbance, and second, this type of networks has a small spinning reserve, where the PV generations are normally providing the maximum output power.

The main aim of this research is to develop a comprehensive frequency control scheme for islanding distribution networks with high PV penetration. This scheme is used to stabilize the frequency of the network to a value that is suitable for the islanded and reconnection processes. To achieve this aim, three different controllers were proposed in this scheme; inertia, frequency regulation, and under-frequency load shedding (UFLS) controllers. The inertia controller is designed for PV generation to reduce the network frequency deviation, which is initiated immediately during disturbance event. After a few seconds, a frequency regulation controller, which consists of primary and secondary frequency controllers, is activated. This frequency regulation controller was proposed to provide sufficient power from the Battery Storage System (BSS) to stabilize the frequency within a few minutes. When inertia and frequency regulation controllers fail to stop the frequency deviation, an optimal (UFLS) controller is initiated from Centralized

Control System (CCS) to shed the required loads. On top of shedding loads, the CCS is used to manage the operation of frequency control scheme and reconnect the grid.

The proposed frequency control scheme and centralized control system were tested using a part of Malaysia's distribution network (29-bus). The distribution network was modeled and simulated for different PV penetration levels using PSCAD//EMTDC software. The simulation results confirmed that the proposed scheme is able to stabilize the frequency of an islanded distribution network, with 50% PV penetration. This scheme is also capable of recovering the network frequency for small load and radiation changes just before it reaches the load shedding limit (49.5 Hz). Furthermore, at high PV penetration and large disturbance events, the proposed scheme can still recover the frequency by shedding the required loads within (0.254 seconds) without overshooting the frequency. Moreover, when the proposed frequency control scheme is coordinated with CCS, the islanded distribution network will be smoothly reconnected to the main grid. Therefore, this frequency control scheme has potential to be applied in real distribution networks with high PV penetration.

ABSTRAK

Pencemaran udara disebabkan oleh loji-loji janakuasa bahan api fosil telah menyebabkan masalah persekitaran yang serius, yang mempengaruhi semua aspek kehidupan. Oleh kerana itu, banyak kerajaan dan syarikat-syarikat utiliti kuasa menunjukkan minat yang mendalam terhadap sumber tenaga yang boleh diperbaharui (RESs). Secara amnya, penggunaan RESs dalam sistem pengagihan seperti solar fotovoltaik (PV) mengurangkan pergantungan kepada bahan api fosil. Walaubagaimanapun, pada tahap penembusan PV yang tinggi, rangkaian pengedaran terpulau akan menderita daripada isu-isu kestabilan frekuensi yang kritikal. Ini berlaku kerana dua sebab utama: pertama, pengurangan dalam inersia pengagihan rangkaian dengan penembusan PV yang tinggi, di mana dalam keadaan ini, kadar perubahan frekuensi (ROCOF) adalah cukup tinggi untuk mengaktifkan pengawal pengurangan beban, bahkan untuk gangguan kuasa kecil, dan kedua, rangkaian jenis ini mempunyai simpanan putaran kecil, di mana penghasilan PV biasanya menyediakan kuasa keluaran yang maksimum.

Tujuan utama kajian ini adalah untuk membangunkan satu skim kawalan frekuensi yang komprehensif untuk pemulauan rangkaian pengedaran dengan penembusan PV yang tinggi. Skim ini akan digunakan untuk menstabilkan frekuensi rangkaian kepada nilai yang sesuai untuk proses pemulauan dan penyambungan semula. Untuk mencapai matlamat ini, tiga pengawal yang berbeza telah dicadangkan dalam skim ini; inersia, peraturan frekuensi dan pengawal frekuensi-terkurang pengurangan beban (UFLS). Pengawal inersia direka untuk generasi PV bagi mengurangkan sisihan frekuensi rangkaian, yang dimulakan dengan serta-merta semasa kejadian gangguan. Selepas beberapa saat, pengawal peraturan frekuensi, yang terdiri daripada pengawal frekuensi rendah dan menengah, diaktifkan. Pengawal kawalan frekuensi ini telah dicadangkan untuk memberikan kuasa yang mencukupi dari sistem penyimpanan bateri (BSS) untuk

menstabilkan frekuensi dalam beberapa minit. Apabila inersia dan pengawal peraturan frekuensi gagal untuk menghentikan sisihan frekuensi, pengawal (UFLS) yang optimum dimulakan dari Pusat Kawalan Sistem (CCS) untuk mengurangkan beban yang diperlukan. Di samping mengurangkan beban, CCS tersebut digunakan untuk mengurus operasi skim kawalan frekuensi dan penyambungan semula grid.

Cadangan skim kawalan frekuensi dan sistem kawalan berpusat telah diuji menggunakan sebahagian daripada rangkaian pengedaran di Malaysia (29-bas). Rangkaian pengedaran dimodelkan dan disimulasikan bagi tahap penembusan PV yang berbeza menggunakan perisian PSCAD//EMTDC. Keputusan simulasi mengesahkan bahawa cadangan skim ini dapat menstabilkan frekuensi pemulauan rangkaian pengedaran, dengan penembusan PV sebanyak 50%. Skim ini juga mampu memulihkan frekuensi rangkaian bagi beban kecil dan perubahan radiasi sejurus sebelum ia mencapai had bagi pengurangan beban (49.5 Hz). Selain itu, pada penembusan PV yang tinggi dan acara-acara gangguan yang besar, skim yang dicadangkan masih boleh memulihkan frekuensi dengan mengurangkan beban diperlukan dalam (0.254 saat) tanpa frekuensi terlebih. Selain itu, apabila skim kawalan frekuensi yang dicadangkan diselaraskan dengan CCS, pemulauan rangkaian pengedaran akan dipasang semula ke grid utama dengan lancar. Oleh yang demikian, skim kawalan frekuensi ini mempunyai potensi untuk digunakan dalam rangkaian pengedaran yang sebenar dengan penembusan PV yang tinggi.

ACKNOWLEDGEMENT

Alhamdullilah, all praise and thanks to Allah for his guides towards the timely completion of my study. I would like to express my deepest and sincere gratitude to my respected supervisors Prof. Dr. Hazlie Mokhlis and Prof. Dr.Saad Mekhelif for their professional guidance, expertise and assistance throughout the period of my Ph.D. I also would like to acknowledge my special thanks to the University of Malaya for providing academic support in order to accomplish my project. Also, special thanks to Palestine Technical University-Kadoorie for their financial support throughout my Ph.D.

To all my friends in the power system lab, thanks for continuously giving me support till the completion of this thesis. Also, special thanks to my best friend, Shiva, for his support, kindness and true friendship.

I wish to express my deepest gratitude to my mother and father for raising me and giving me full support during my study. Most importantly, I would like to thank the most important person in my life, my lovely wife for her encouragement and patience from the beginning till the completion of my Ph.D. thesis.

TABLE OF CONTENTS

LIST OF FIGURES

LIST OF TABLES

LIST OF SYMBOLS AND ABBREVIATIONS

UFLS	:	Under Frequency Load Shedding
MPPT	:	Maximum Power Point Tracking
DGs	:	Distribution Generations
DG	:	Distribution Generation
RESs	:	Renewable energy sources
BEP	:	Binary Evolutionary Programming
BGA	:	Binary Genetic algorithm
BPSO	:	Binary Particle swarm optimization
ROCOF	:	Rate of Change of Frequency
FiT	:	Feed-in Tariff
SEDA	:	Sustainable Energy Development Authority
MBIPV	:	Malaysian Building Integrated Photovoltaic
UVLS	:	Under Voltage Load Shedding
IPCU	:	Imbalance Power Calculator Unit
FCU	:	Frequency Calculator Unit
LSU	:	Load shedding Unit
RE	:	Renewable Energy
IEA	:	International energy Agency
PV	:	Photovoltaic
HPPs	:	Hydropower Plants
RoR	:	Run-of-River
PMSG	:	Permanent Magnet Synchronous Generator
DFIG	:	Doubly Fed Induction Generator
CCS	:	Centralized Control System

PMU	:	Phasor Measurement Unit
TNB	:	Tenaga National Berhad
SOC	:	State of Charge
IC	:	Incremental Conductance
CV	:	Constant Voltage
P&O	:	Perturb and Observe
ANN	:	Artificial Neural Network

LIST OF APPENDICES

CHAPTER 1: INTRODUCTION

1.1 Overview

The consumption and usage of fossil fuels for generating electricity causes several environmental problems. One of the most critical environmental problems pertains to the emission of carbon dioxide (CO_2), which is released from generation power plants. It is one of the main agents for global warming. The fossil fuel power plants in United States (US), China, Russia, and Germany emit 2.2, 2.7, 0.661, and 0.356 billion tons of CO_2 annually, respectively (Lashof et al., 2014).

Interest in environmental problems forced the power industry to increasingly utilize Renewable Energy (RE) to produce electricity. RESs such as photovoltaic, wind, and hydro power plants are able to decrease environmental pollutions by reducing the usage of fossil fuels. Hence, many governments and agencies around the world set targets towards increasing the application of RESs to generate electricity. China and Germany, for example, expects to draw 15% and 35% of their energy needs from renewable energy sources by 2020, respectively (REN, 2012). Malaysia has also begun utilizing RESs for power generation. According to (Shekarchian, Moghavvemi, Mahlia, & Mazandarani, 2011), Malaysia seeks to replace its power production to 11 % from RESs by the end of 2020.

The necessity of providing sufficient energy alongside interest in clean technologies results in increased use of Distributed Generations based on RESs (DG-RESs). In Malaysia, a mini-hydro power plant and photovoltaic generation have been widely installed in the distribution network, as both are cost effective and environmentally friendly (Mekhilef et al., 2012). Currently, based on IEEE std.1547–2003, when the distribution network is islanded from the grid, all DGs must be disconnected from the

network within 2 seconds (Basso, 2004). This operation is important, as it ensures the safety of power system workers and avoid faults that could occur due to re-closure activation. However, separating the DGs after islanding will prevent the grid maximizing the benefits that could be gained from these sources. Research related to islanding operation is progressing to the level that allows islanded distribution network to operate autonomously when disconnected from the main grid. However, after islanding, the distribution networks with high PV penetration will be exposed to critical frequency stability issues. For this reason, the distribution will completely blackout if these issues are not addressed.

1.2 Problem Statement

In the near future, the penetration level of RESs, such as PV generation, will be increased in the distribution network. Therefore, the distribution network will be exposed to several frequency stability issues during the islanding and reconnection processes. Issues pertaining to these processes are discussed in the following paragraphs.

At high PV penetration, the islanded distribution network will suffer from low inertial response because PV generations do not provide any physical inertia. Hence, the system's frequency will quickly drop, preventing frequency restoration via primary frequency controller even if reserve power is available. Many researchers propose installing different inertia controllers for islanded distribution networks (El Itani, Annakkage, & Joos, 2011; Hansen, Altin, Margaris, Iov, & Tarnowski, 2014; Wachtel & Beekmann, 2009). However, most of them proposed increasing the inertia of the distribution networks using only wind turbine technology and Energy Storage Systems (ESS).

Besides reducing inertia, islanded distribution network also faces frequency regulation issues. Due to insufficient reserve power, mainly in a distribution network with high PV penetration, the imbalance of power between the generation and demand commonly takes

place, which result in quick frequency drops. This occurs because PV generation units commonly operate at its maximum power point. In literature, several control techniques, such as droop control and deloading control were proposed for RESs to regulate the frequency of grid-connected distribution systems during disturbances (Eid, Rahim, Selvaraj, & El Khateb, 2014; Josephine & Suja, 2014; Mishra & Sekhar, 2013). However, these techniques may be ineffective for islanded distribution systems, as islanded system is not as stable as grid-connected system. The intermittent nature of the RESs will also contribute to frequency fluctuations in an islanded system. Therefore, many researchers proposed the usage of batteries to provide a stable energy reserve for frequency regulation services. However, most of these techniques used a battery to provide primary frequency controller without taking into account the secondary controller, which is important for grid reconnection.

In the case where the inertia and frequency regulation controllers fail to stabilize the frequency in an islanded distribution network, a potential solution is to apply load shedding. Load shedding is a technique that stabilizes system frequency by removing some loads to ensure a balanced condition between generation and load demands. Although there are various load shedding techniques, only a few were proposed for islanded distribution systems with RESs. However, these techniques do not consider high PV penetration in the distribution system, where the system has a small inertia. For a system with this condition, fast load shedding is required, since its frequency will drop quickly when islanded takes place. Besides fast load shedding, a suitable amount of load shed is also required to ensure that the frequency is within an acceptable limit. (Laghari, Mokhlis, Karimi, Bakar, & Mohamad, 2015) proposed a new Fixed and Random Priority Load Shedding (FRPLS) technique to determine a suitable combination of loads to be shed. This technique is time consuming, since all possible combinations of loads shed need to be determined beforehand. Therefore, it is unsuitable for application in a

distribution network with high PV penetration, which require a fast and correct load shedding technique. Taking into account this shortcoming, metaheuristic optimization methods can be explored to determine the optimal combination of load to be shed within a short period of time.

1.3 Research Objectives

The main aim of this research is to develop a comprehensive frequency control scheme for islanded distribution network with high PV penetration, where the scheme consists of inertia controller, frequency regulation controllers, and UFLS controller. The following are the main objectives of this research:

(A) To design an inertia controller for PV systems based on the deloading technique to address the reduction of inertia response caused by high PV penetration.

(B) To propose frequency regulation controllers (primary and secondary) based on a Battery Storage System (BSS).

(C) To propose an optimal under-frequency load shedding controller based on metaheuristic techniques.

(D) To model a centralized control system to manage the operation of frequency control scheme, load shedding, and grid reconnection process.

1.4 Research Scope and Methodology

This research focuses on an islanded distribution system. The islanding detection and grid disconnection process are beyond the scope of this research. All of the proposed controllers in this research are developed for islanded distribution system with high PV penetration. In this research, technical issues are studied without taking into account economic analyses considerations. Figure 1.1 shows the research methodology pertaining to this work.

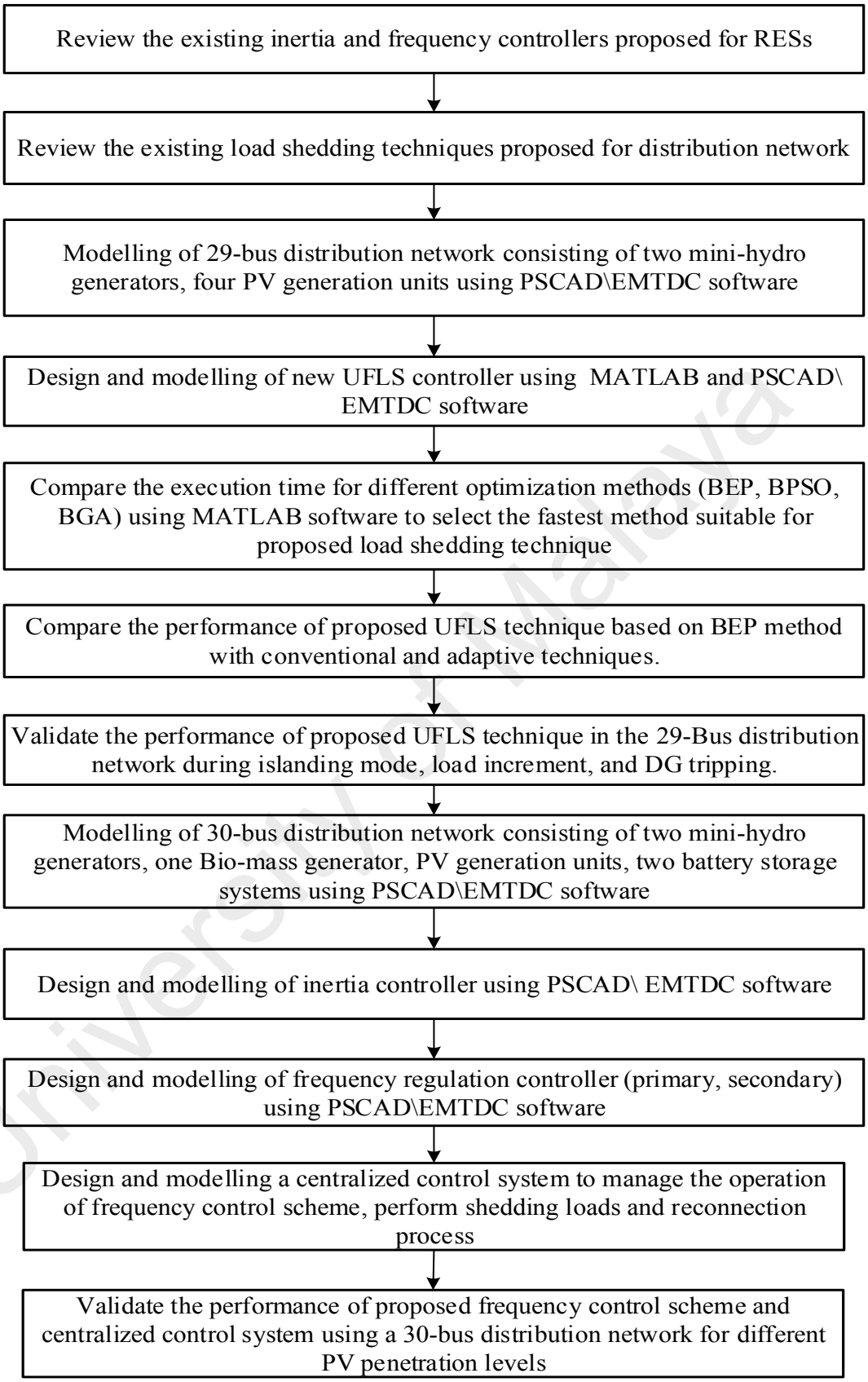

Figure 1.1: Flow chart of research methodology

1.5 Thesis Outline

Chapter 1 describes the changes that took place in the distribution network due to the continual integration of inverter based DGs. The frequency issue following the distribution network islanding will be presented. The importance of stabilizing the frequency of islanding distribution network by inertia, frequency regulation and load shedding controllers will then be discussed. The objectives and research methodology will consequently be presented, followed by the thesis outline.

Chapter 2 will provide an overview of the distributed generation, presenting the various types, the global trend of solar PV and hydropower, and the Malaysian trend of solar PV and hydropower. It will also discuss the operation modes and challenges pertaining to DGs. This chapter will detail the frequency stability issues related to the islanded distribution network. Various frequency control schemes proposed for DGs-RESs will also be discussed, and several types of existing load shedding techniques will be reviewed.

Chapter 3 will present the proposed frequency control scheme for distribution networks with high PV penetration. This scheme consists of inertia controller, frequency regulation controller, and a UFLS controller. The modelling of three controllers will be discussed in this chapter. This chapter will also describe the centralized control system that can be used to manage the operation of the frequency control system and reconnect the grid.

Chapter 4 will detail the modelling of the distribution network used to validate the proposed UFLS technique. The proposed UFLS technique was validated using a 29-bus distribution network for different islanding, DG tripping, and load increments cases. This distribution network is a part of Malaysia's distribution network. In order to show the preference of the proposed UFLS technique compared with existing techniques, various PSCAD simulation results will be presented in this chapter. It will also describe the

utilized metaheuristic optimization methods with the proposed UFLS technique for the selection of the optimal combination of loads to be shed from random and fixed priority loads.

Chapter 5 will detail the modelling of distribution network used to validate the proposed frequency control scheme. The proposed frequency control scheme was validated using a 30-bus distribution network for different islanding, DG tripping, and load increments cases. In order to show the ability of proposed frequency control scheme on stabilizing the distribution network frequency, this chapter will present several simulation case studies such as islanding, generator trip, and load increment. Moreover, various simulation scenarios have been implemented for grid reconnection.

Chapter 6 concludes this thesis by summarizing the research contributions and presents the possible future works for this research.

CHAPTER 2: LITERATURE REVIEW

2.1 Introduction

Recently the world has experienced severe climate changes due to increased environmental pollution levels. Global warming is one of the most serious environmental changes that threatens life on Earth. It is therefore necessary to decrease environmental pollution, particularly air pollution, which are emitted from fossil fuel power plants. The necessity to reduce air pollution alongside growing demand represents the main motivation of using the DGs-RESs. According to (IEEE, IEA), a general definition of DG is a small-scale electric generation technology (sub-kW to a few MW) located close to the power demand.

This chapter provides an overview of the distributed generation, presenting various types, global, and local trends of solar PV generation. It also discusses operation modes and challenges pertaining to DGs. The major subject that will be discussed in this chapter is the frequency stability issue of an islanded distribution network. It also discusses various frequency control schemes implemented alongside renewable energy DGs to stabilize the frequency of islanded distribution network. At the end, this chapter reviews various types of load shedding techniques for recovering system frequency.

2.2 Distributed Generation

Over the last decade, the world has seen a significant development in distributed generation technologies. These DGs are generally classified according to their operation technologies and applications. For frequency stability application, the DG technologies are classified into two main categories: Dispatchable and Non-Dispatchable DGs, as shown in Figure 2.1. The former includes all sources that can adjust their output power at the request of power grid operators, while the latter contains all sources that are naturally

intermittent. Under the dispatchable and non-dispatchable categories, the DGs are classified into rotary based type, which is directly connected with power system, and inverter based type, which is coupled from the power system via power electronic converters.

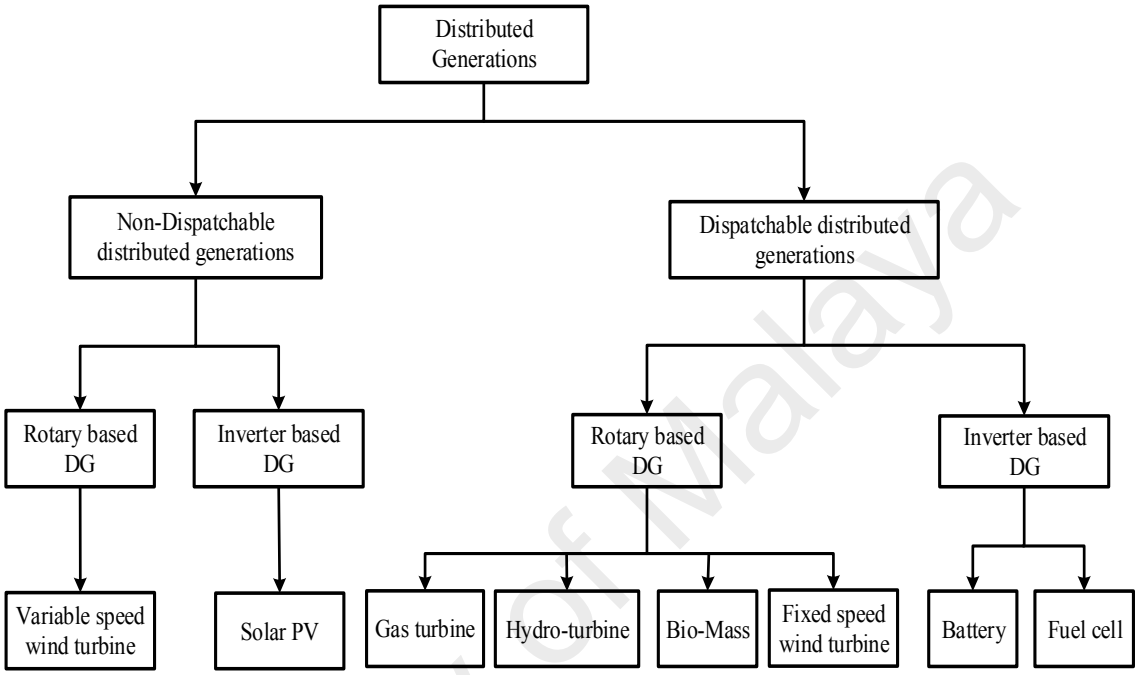

Figure 2.1: Categories of distributed generations

The following subsections provide an overview of PV and mini-hydro DGs considered in this research.

2.2.1 Solar Photovoltaic

The sun is the most important source of renewable energy; it produces power without emitting any pollutants. Solar energy is the light and heat obtained from the sun and harnessed using different technologies, such as solar thermal and solar Photovoltaic PV. Solar PV technologies is used to convert sunlight into electricity via the photoelectric effect. These technologies report several advantages, such as free maintenance, zero emissions, silent operation, and long-life operation. However, it is intermittent, and unavailable at night.

2.2.1.1 Global Trends of Photovoltaic

In 2015, several countries reported an increase in installed capacity of photovoltaic compared with 2014 (REN, 2016). China continue to increase installation targets to increase RESs to prevent severe pollution problems and support local power generation, as shown in Figure 2.2. In 2015, China added an estimated 15.2 GW capacity of solar PV, approaching 44 GW of cumulative capacity. With this addition, China overtook Germany to take the lead in cumulative solar PV capacity. In Japan, growth continued with 11 GW being added to the grid, bringing the total capacity to an estimated 34.4 GW in 2015.

In only three years, Japan doubled its share of RESs, and solar PV accounted for the vast majority of this addition. The US reported continued growth, with 7.3 GW added to the grid, bringing the total capacity to an estimated 25.6 GW in 2015. For the first time, solar PV installations in the US exceeded its natural gas capacity. The utility-scale sector for the US remained the largest in 2015, with more than 4 GW added and ~20 GW under development at the year's end.

In 2015, the European Union (EU) continued to lead the world in solar PV's contribution to electricity supply. Germany installed 1.5 GW, bringing its total capacity to an estimated 40.1 GW, Italy installed 0.3 GW, bringing its total capacity to an estimated 19.1 GW, The United Kingdom (UK) installed 3.7 GW, bringing its total capacity to an estimated 9.1 GW, France added more than 0.9 GW, ranking 7th globally for new installations, and ending the year with 7.1 GW, Spain added more than 0.1 GW, ranking 8th globally for new installations, and ending the year with 6.0 GW, India and Australia installed 2.0 GW, 0.9 GW, respectively, and ending the year with 3.4 GW, 5.1 GW, respectively.

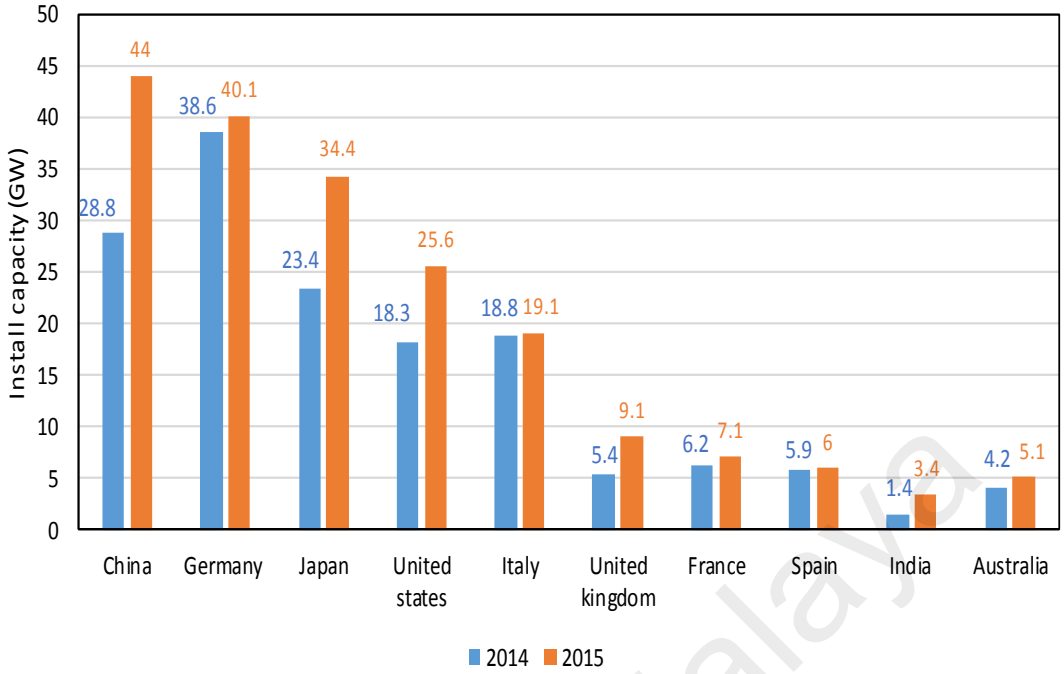

Figure 2.2: Solar PV installed capacity for different country for 2014-2015 (REN, 2016)

2.2.1.2 Malaysian Trends Towards Photovoltaic

Since independence, Malaysia began to realize the importance of RE replacing traditional sources to provide electricity in the country. Malaysia, due to its close proximity to the equator, reports an average solar radiation of 400–600 MJ/m^2 per month, rendering it viable for solar energy harvesting.

Prior to 2005, limited numbers of off-grid PV systems were installed under the rural electrification project. For this reason, the Malaysian Building Integrated Photovoltaic (MBIPV) project was initiated in 2005 for promoting the solar PV market. The United Nations Development Program (UNDP) supported this project to encourage the growth of grid-connected PV systems. The MBIPV project played an important role in the growth of the solar PV market (Mekhilef et al., 2012). From 2006 to 2010, the MBIPV project funded the installation of a 2 MW grid-connected PV systems for residential and commercial buildings. In 2011, Malaysian government introduced the Feed-in Tariff

(FiT) mechanism to address the shortcomings found in the Small Renewable Energy Power (SREP) Program from 2001 to 2010. The FiT mechanism is defined as the mechanism that allows for the selling of the electricity produced from RESs to the power grid at a fixed rate and for a specific period of time. According to the Sustainable Energy Development Authority (SEDA), the cumulative growth of installed capacities for solar photovoltaic connected to the grid increase year by year, as shown in Figure 2.3.

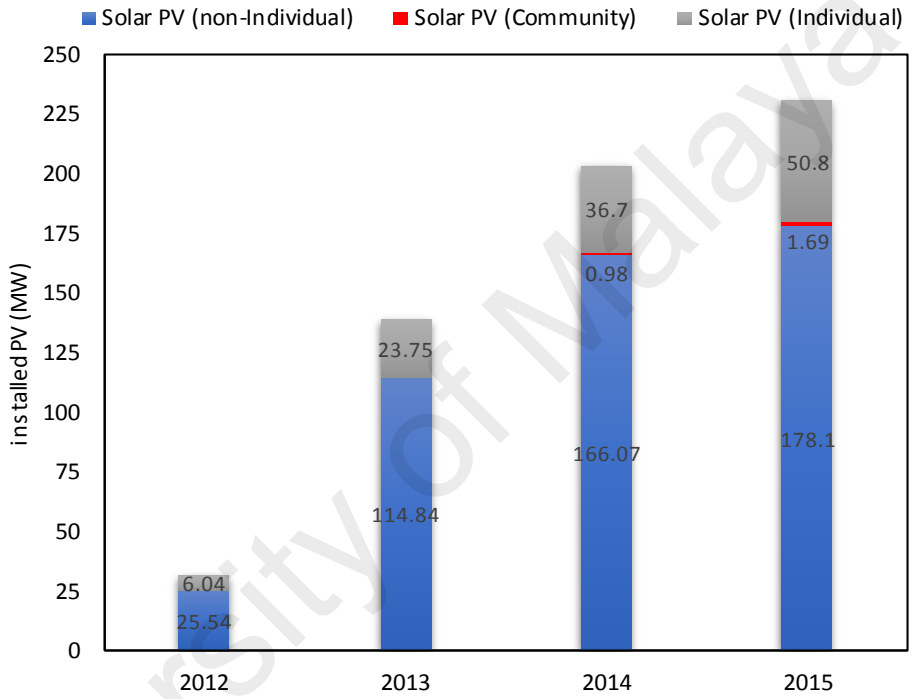

Figure 2.3: Cumulative growth of PV Installed capacities since inception of FiT (MW) (SEDA, 2015)

2.2.2 Hydropower

Hydropower is considered as one of the cleanest technology for producing electricity. It transforms the potential energy of water flowing in a river or stream at a certain vertical fall. Hydroelectricity is the most widely used form of renewable energy, with relatively low electricity generation cost, and several countries take advantage of this fact to install hydropower plants (HPPs) on an annual basis. For example, China installed ~ (290 GW) worth of HPPs in 2015. Figure 2.4 shows the hydropower global capacity for six countries (REN, 2016).

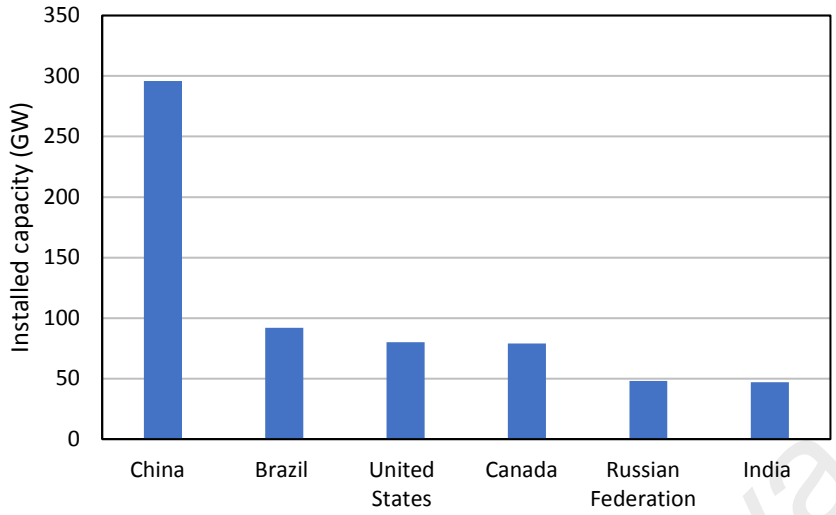

Figure 2.4: Hydropower global capacity for top six countries, 2015 (REN, 2016)

2.2.2.1 Classification of Hydropower Plant

HPPs are normally classified according to multiple perspectives. It can be classified according to operation and type of flow, or according to the capacity.

(A) Classification of HPPs According to the Capacity

The need to provide sufficient electrical energy to meet the growing demand with interest for clean sources led to the development of several types of HPPs. The majority of these plants involved large dams flooding wide areas of land to provide water storage. Recently, the environmental problems associated with large hydro projects have been identified as a matter of interest. Due to opposition from environmental agencies and people living in the flooded area, building additional dams become more and more difficult. This can however be mitigated by constructing mini and micro HPPs. To date, there are no agreed international standards that defines the size of HPPs. For a small-hydro plant, a maximum of 10 MW is the most widely accepted value worldwide, although the definition in China officially stands at 25 MW. According to the industrial definition, mini-hydro plants typically refers to schemes of (0.5 MW-2 MW), micro-hydro plants typically refers to schemes of (10 kW-500 kW) and pico-hydro plants refers to schemes below 10 kW (Paish, 2002).

(B) Classification According to Flow Type

Based on the type of water flow, HPPs are categorized into HPPs with storage (reservoir), pumped storage, and run-of-river (RoR).

i Hydropower Plant with Reservoir

Hydropower projects with a reservoir store water behind a dam for times when river flow is low is shown in Figure 2.5. Therefore, power generation is more stable and less variable. The generating stations are located at the dam toe or further downstream, connected to the reservoir via tunnels or pipelines. Reservoir hydropower plants can have major environmental and social impacts due to the flooding of the land for the reservoir.

Figure 2.5: Kenyir (Sultan Mahmud) Hydroelectric Power Project Malaysia (KualaLumbur-Post, 2016)

ii Pump Storage Hydropower Plant

Pumped storage plants are not energy sources, instead, they are storage devices**.** Water is pumped from a lower reservoir to an upper reservoir, usually during off-peak hours, while flow is reversed to generate electricity during the daily peak load period or at other times of need. Although the losses of the pumping process make such a plant a net energy consumer, the plant provides large-scale energy storage system benefits. Pumped storage is the largest capacity form of grid energy storage that is now readily available worldwide.

It is regarded as one of the most efficient technologies available for energy storage. Figure 2.6 shows such type of plant.

Figure 2.6: Geesthacht pumped-storage power plant (VATTENFALL, 2016)

iii Run-of-River Hydropower Plant (RoR)

This plant produces energy from the available flow and natural elevation drops of a river, as shown in Figure 2.7. Water is diverted and channeled into a penstock to power the turbine, then the water is returned to the river. This type of plant generally includes a short-term storage (hourly, daily, or weekly), allowing for adaptations to the demand profile. The installation of small RoR plants is relatively cheap, and has a minor environmental impact.

Figure 2.7: Run-of-River hydropower plant (Energypedia, 2016)

2.2.2.2 Potential of Hydropower in Malaysia

Malaysia reports an average annual rainfall of 2000 mm, with an abundance of streams and rivers flowing from highland areas (Shekarchian et al., 2011). Consequently, Malaysia's potential for hydropower is very high. Currently, Malaysia has utilized this potential within the range of large and mini hydropower. Malaysia has a substantial amount of hydropower resources, and potential hydropower capacity is estimated at 29,000 MW (Wong et al., 2009). However, according to the international hydropower association, only ~5472 MW is utilized in 2016. Sarawak plans to increase its hydropower capacity to 7723 MW by 2020, and to 20 GW by 2030 (Stockwell, 2009).

2.3 Distributed Generation Operating Modes

The need to provide reliable and clean electrical energy to all consumers led to the rapid expansion of distributed generation. DG can operate in two possible modes; grid-connected mode or islanded mode. In the former, the main grid controls the system operation, while in the latter, system control is realized by the coordination of available DGs.

2.3.1 Issues of Distributed Generation Operating in Grid Connected Mode

Using DGs resulted in many benefits for the distribution network. It reduces the transmission cost and the dependence on fossil fuel. However, when the power system is made up of more distributed generations, it will result in several technical issues. The followings are the main issues of DGs operation in grid connected mode:

(A) Reverse Power Flows

The distribution networks were originally designed as radial systems to allow flow power from the generation to the consumers by decreasing voltage level. However, using DGs in the distribution system leads to increased voltage on connection point, causing the

power to flow bi-directionally. Accordingly, this situation could negatively impact protective devices, such as over-current, fuses, and automatic re-closers.

(B) Voltage Flickers

The intermittent nature of some distribute generation output can cause fluctuations in the operating voltage. According to (IEEE) 1453TM-2011, voltage flicker is defined as "Voltage fluctuations on electric power systems due to illumination changes from lighting equipment". These voltage fluctuations increase the possibility of operation malfunction of devices.

(C) Harmonics

Sometimes, the integration of distributed generation to the main grid takes place via power electronics converters, which might cause harmonics due to the switching operation. The magnitude and order of this harmonic depend on the technology of the converter. Injection harmonics via the grid can distort the voltage profile and increase losses in the distribution system.

2.3.2 Issues of Distributed Generation Operating in Islanding Mode

According to IEEE standard, islanding operation is defined as "A condition in which a portion of a utility system that contains both load and distributed resources remains energized while isolated from the remainder of the utility system". However, separating the DGs after islanding will prevent the grid from exploiting the benefits garnered from these sources. For this reason, at a high penetration level of RESs, there is an increased need for the RESs to power some critical loads of the islanded micro-grid. When the islanding mode occurs, the distribution network is disconnected from the grid using the main circuit breaker, which results in the instability frequency issue.

2.3.2.1 Issue of Small Inertial Response

The frequency response of England and Wales is shown in Figure 2.8. During normal operations, the system frequency is close to 50 Hz. However, when an event happens that causes generation-demand unbalance, the system frequency drop with a rate of change of frequency (ROCOF) depending on the total system inertia and the amount of unbalance power, as per the swing equation (Kundur, Balu, & Lauby, 1994):

$$\frac{df}{dt} = \frac{f_0}{2H_{SYS}S_B}(P_m - P_e) \tag{2.1}$$

where *df/dt* is the rate of frequency change, H_{sys} is the total system inertia constant, S_B is the rating power of the generator, P_m, P_e are the mechanical power and electrical power, respectively, and f_o is the system frequency.

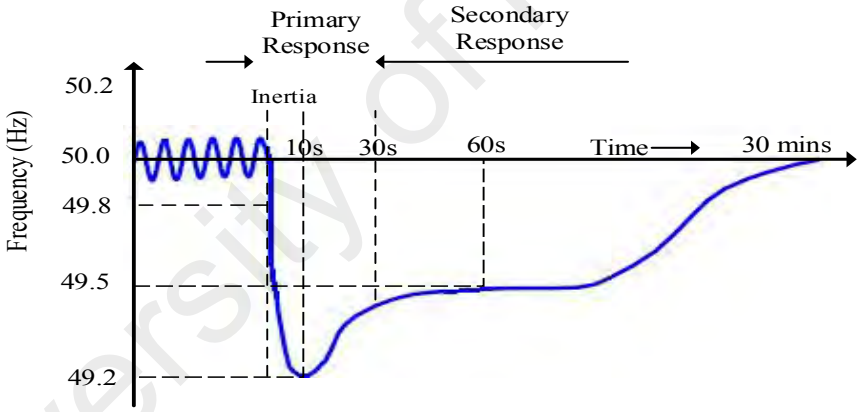

Figure 2.8: Time frames involved in system frequency response (Gonzalez-Longatt, Chikuni, & Rashayi, 2013)

In fact, the RESs have low or non-existent inertial responses (Dehghanpour & Afsharnia, 2015). For example, the wind turbines are connected to the power grid through an electronic converter, which effectively decouples the wind turbine inertia from mitigating the system transients. Furthermore, solar photovoltaic systems do not provide any inertia response to the power system.

This fact is supported by (Jayawardena, Meegahapola, Perera, & Robinson, 2012), where they predicted that the increasing number of RESs in the UK could reduce the inertia constant by up to 70% between 2013/14 and 2033/34. In (Jayawardena et al., 2012), different penetration levels of RESs were used with a Synchronous Generator (SG) to meet the 3.8 MW load demand. As reported in (Jayawardena et al., 2012) and shown in Figure 2.9, the ROCOF of the power system increase whenever the percentage-installed capacity of the RESs increases.

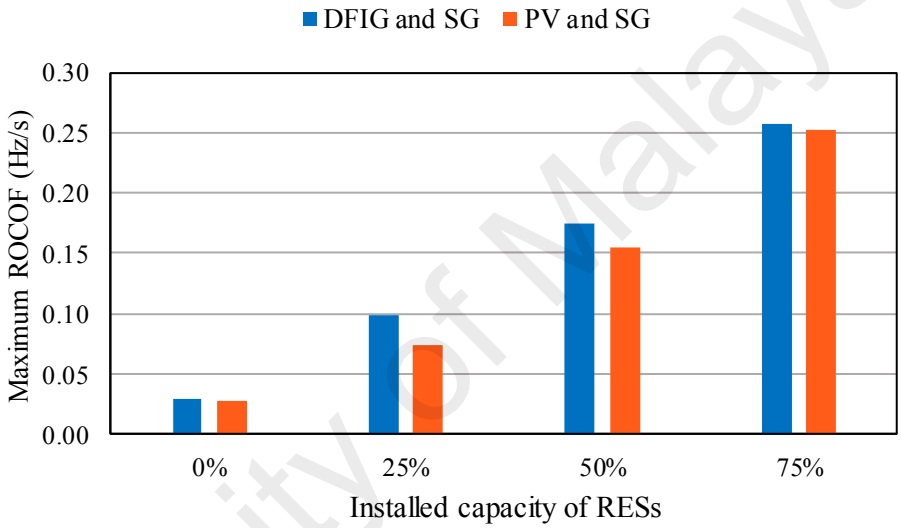

Figure 2.9: The ROCOF of the distribution network for two types of RES supply 3.8MW load (Jayawardena et al., 2012)

According to Figure 2.9, when the conventional sources are replaced by RESs, the rate of change of frequency increases due to the reduced inertia constant. For this reason, the system frequency decreases rapidly, thus wasting the opportunity for other controllers to recover the frequency.

2.3.2.2 Issue of Small Reserves Power

Immediately after an islanding or disturbance event, the inertia controller releases the kinetic energy stored in the rotating mass of synchronous generator, which lasts for 10s (Díaz-González, Hau, Sumper, & Gomis-Bellmunt, 2014). After that, a new controller, called a primary frequency controller, is immediately activated. This controller use the

governor to restore the frequency to acceptable frequency levels within 30s (Yu, Dyśko, Booth, Roscoe, & Zhu, 2014). After 30s, a secondary frequency controller is activated in order restore the system frequency. Finally, the remaining power deviation activates the tertiary frequency control. Figure 2.10 shows the different types of reserve service.

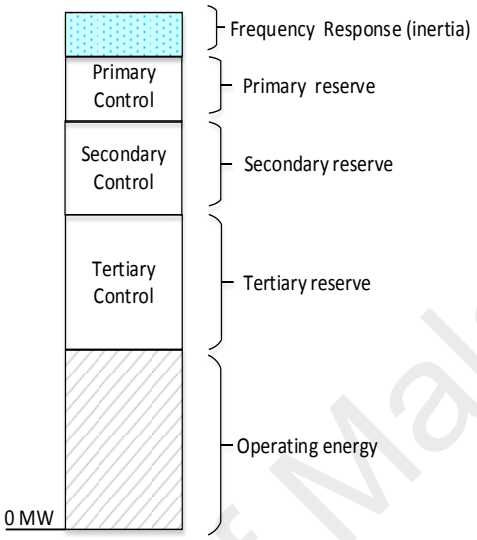

Figure 2.10: Types of reserve services

When the rotating generation units are replaced by RESs, which is normally operating at maximum power point, the islanded distribution networks will report less reserve power, which is normally used to regulate the system frequency. In this situation, the system frequency deviates more for the same imbalance power, which leads to disconnecting the generation units, causing a total blackout. Figure 2.11 shows the system frequency response when the reserve power is halved (Ulbig, Borsche, & Andersson, 2014).

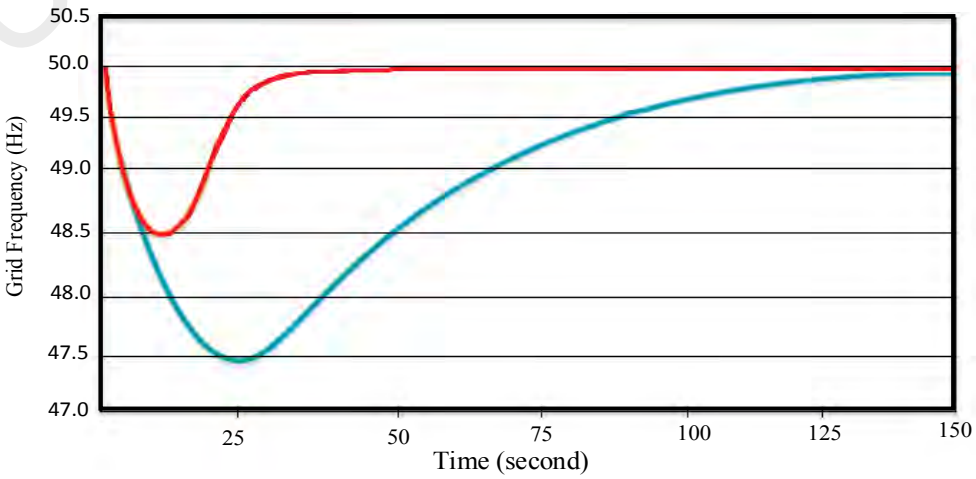

Figure 2.11: Frequency deviation for different reserve power

To overcome these issues and keep the frequency within an acceptable limit, three controllers are required. Inertia controller is the first controller required to increase the inertial response of the power system. Second, a frequency regulation controller must be available to regulate the system's frequency. The under-frequency load shedding (UFLS) is the third controller used to shed the required loads if the inertia and frequency regulation fail to recover the system's frequency. The following sections discuss literature pertaining to these controllers.

2.4 Inertia and Frequency Regulation Controllers Proposed for RESs

Generally, inertia and frequency controllers proposed for RESs are commonly classified into three main categories; inertia and frequency regulation controllers proposed for RESs with Energy Storage System (ESS), controllers proposed for RESs without ESS, and controllers proposed for RESs based on intelligent algorithms. Figure 2.12 shows controller's types for each category:

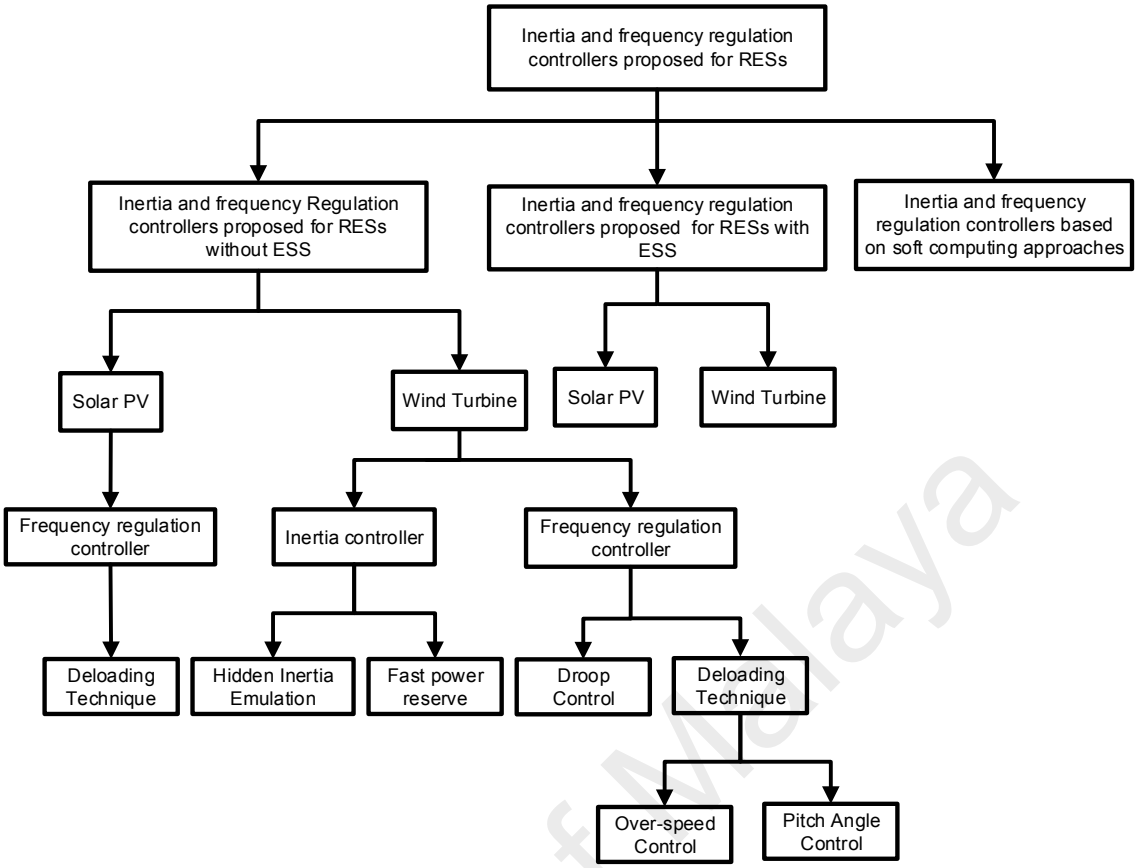

Figure 2.12: Inertia and frequency controllers designed for RESs

2.4.1 Inertia and Frequency Regulation Controllers Proposed for RESs without ESS

To minimize the negative impact of high RESs penetration, several inertia and frequency control techniques with and without ESS can be utilized. These techniques allow the RESs to contribute to frequency regulation.

2.4.1.1 Inertia and Frequency Regulation Controllers Proposed for Wind Turbine without ESS

Wind energy is one of the most used renewable sources in the world. Many countries that report potential for wind energy began replacing conventional power plants with wind energy plants. Statistics show that future wind penetration in the U.S. and Europe will be more than 20% within the next two decades (Thresher, Robinson, & Veers, 2007). There are two main categories of wind turbines; fixed speed and variable speed (Mauricio,

Marano, Gómez-Expósito, & Ramos, 2009). The former generally uses an induction generator connected directly to the grid and can provide an inertia response to the frequency deviation, even though this inertia is small compared to the synchronous generator.

A variable speed wind turbine mainly uses a Permanent Magnet Synchronous Generator (PMSG) or Doubly Fed Induction Generator (DFIG). The PMSG is fully decoupled from the grid; this is because the stator of this type of generator is connected to the power electronic converter in order to inject the power into the grid. The DFIG is similar to PMSG, except that this generator is connected to the grid by the rotor circuit. The power electronic converter used in a variable speed wind turbine enables the wind turbine to regulate the output power over a wide range of wind speeds (Revel, Leon, Alonso, & Moiola, 2014). However, this coupling isolates the wind turbine from the frequency response under disturbance. Furthermore, traditional wind turbines normally follow the maximum power curve, as shown in Figure 2.13. Therefore, they do not have reserve power to support the frequency control. The maximum output power from a wind turbine, defined as a function of rotor speed, is given by (Bianchi, De Battista, & Mantz, 2007).

$$P_{MPPT} = K_{opt}\omega^3 \tag{2.2}$$

where ω is the rotor speed, and K_{opt} is the constant (controller gain) for the tracking of the maximum power curve, obtained from:

$$K_{opt} = 0.5\,\rho\pi R^5\,\frac{Cp_{opt}}{\lambda_{opt}{}^3} \tag{2.3}$$

Where ρ is the air density, R is the radius of the turbine wheel, Cp_{opt} is the maximum power coefficient, and λ_{opt} is the optimum tip speed. The maximum power point controller determines the operating point along the power load line. This operation is conducted by regulating the speed of the wind turbine within the speed limits and pitch regulation after the rated speed.

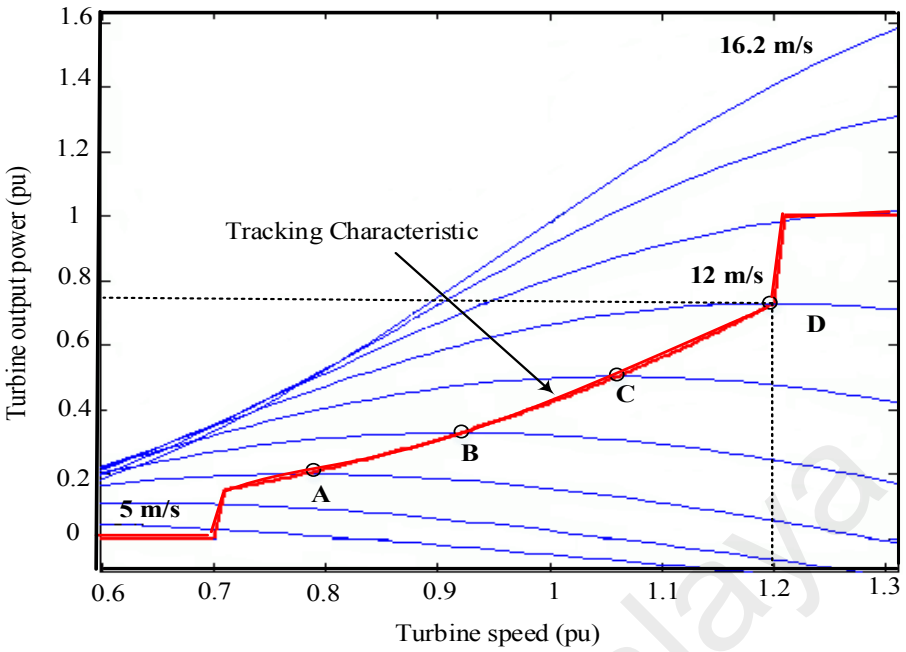

Figure 2.13: Power against rotating speed characteristics at (Pitch angle β=0)

(Lamchich & Lachguer, 2012)

Researchers proposed two main techniques to support frequency control using a variable speed wind turbine; inertia response and power reserve control. Inertia control enables the wind turbine to release the kinetic energy stored in the rotating blades within 10 seconds to arrest frequency deviation, while reserve control technique uses the pitch angle controller, speed controller, or a combination of both to enhance the power reserve margin during unbalanced power events.

(A) Inertia Response Control

Wind turbines lack the ability to automatically release the kinetic energy stored in their rotating mass, unlike conventional generator. For this reason, a suitable controller is needed to provide the wind turbine with an inertia response. Generally, there are two control techniques that can be used to do this; hidden inertia emulation and fast power reserve. The former is the first technique; it proposes new control loops to release the kinetic energy stored in the rotating blades of the wind turbine. This additional power can be used to terminate the frequency deviation during unbalance events. Fast power reserve

is the second technique, which can also be used to terminate the frequency deviation. However, it responds to frequency deviation by releasing constant power for a definite time.

i ***Hidden Inertia Emulation***

Using a power electronic converter with a suitable controller enables variable speed wind turbines to release the kinetic energy stored in their rotating blades. This kinetic energy is used as an inertia response in the range 2-6 seconds (Knudsen & Nielsen, 2005). Generally, there are two types of inertia response; the first one is single-loop inertia response, and the other is the double-loop inertia response. The first type is based on ROCOF, and it is used to release the kinetic energy stored in the rotating blades, while the second type uses two loops based on ROCOF and frequency deviation. In (Gonzalez-Longatt et al., 2013; Sun, Zhang, Li, & Lin, 2010), one-loop inertia response is added to the speed control system to enable the wind turbine to respond to ROCOF. This control loop is called inertia emulation, which exactly emulates the inertia response of conventional power plants, as shown in Figure 2.14.

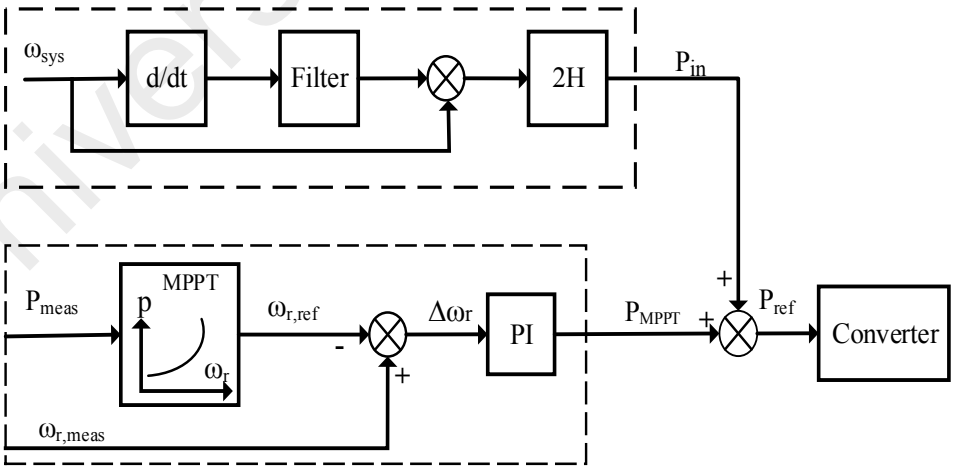

Figure 2.14: Inertia emulation for variable speed wind turbines

The output power from the wind turbine P_{meas} determines the reference rotor speed $\omega_{r,ref}$ that is compared to the measuring rotor speed $\omega_{r,meas}$ and used by the PI controller to provide maximum power. During normal operations, the reference power transferred to

the converter is equal to the maximum power without any contribution from the inertia control loop. After a power deficit, a certain amount of power P_{in}, based on the value of ROCOF and virtual inertia constant H_v, will be added to the power of maximum power point tracking (P_{MPPT}). Due to this power increment, the generator speed will slow down, and the kinetic energy stored in the rotating wind turbine blades will be released. The additional power P_{in} comes from the inertia response loop given by (Morren, Pierik, & De Haan, 2006):

$$P_{in} = 2H_v \times \omega_{sys} \times \frac{d\omega_{sys}}{dt} \tag{2.4}$$

Due to the constant additional power resulting from the inertial control loop, this type of control has two disadvantages. First, the rotor speed is rapidly reduced, leading to big losses in aerodynamic power. Second, the controller takes time to recover energy during rotor speed recovery. These disadvantages can be avoided using the techniques proposed in (L. Wu & Infield, 2013), where they formulated a new inertia response constant. This inertia constant is called the effective inertia response, which is based on the frequency value. Generally, the inertia constant for a wind turbine is defined by:

$$H = \frac{E_{kin}}{S_B} = \frac{J\omega^2}{2S_B} \tag{2.5}$$

where E_{kin} is the kinetic energy stored in the rotating mass of the wind turbine, S_B is the rated power, and J is the moment of inertia. Equation (2.5) can be rewritten by substituting the corresponding power from equation (2.2), making the effective inertia constant:

$$H_e(\omega) = \frac{J{\lambda_{opt}}^3}{\rho\pi R^5 Cp_{opt}} \frac{1}{\omega} \tag{2.6}$$

The main idea is to increase the value of the inertia constant as long as the system frequency continues to decrease. Consequently, the torque transfer to the converter is reduced, as shown in Figure 2.15.

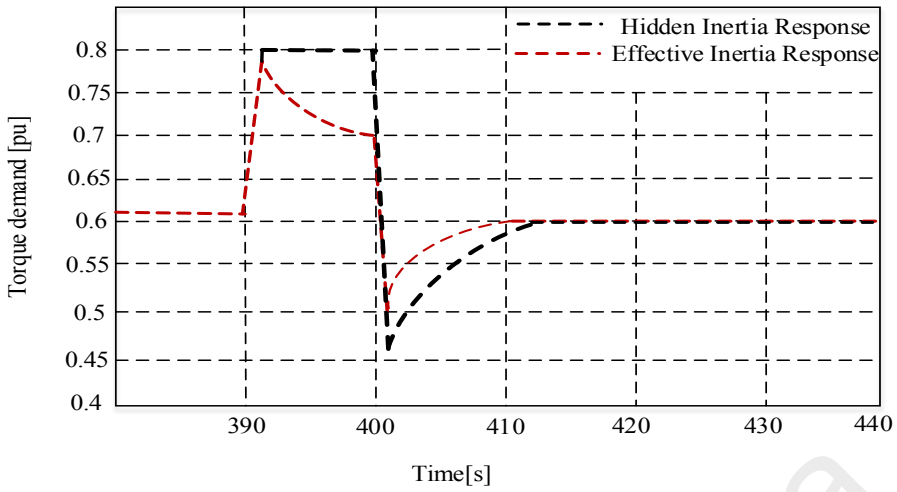

Figure 2.15: Torque demand due to inertia response

The principle of the single-loop inertia response discussed earlier is to provide a decelerating torque signal proportional to ROCOF. This decelerating torque lasts until the frequency is restored. Consequently, without support from another controller, the overall reference torque injected into the converter T_{elec}^{*} will be decreased by the maximum power point, which revert the system to its optimum curve. As a result of this, the power injected into the grid will be reduced directly and recover the frequency support immediately.

In order to avoid this re-acceleration of a wind turbine, (Morren, De Haan, Kling, & Ferreira, 2006) proposed a double-loop control inertia response, as shown in Figure 2.16. This controller provides an additional torque ΔT proportional to frequency deviation, and lasts until the nominal frequency is recovered. The two-loop inertia response control system with two additional modification is presented in (Z. Zhang, Wang, Li, & Su, 2013). A new block called delay speed recovery is added to recover turbine speed as soon as possible. A wave filter is the other modification, which is adapted in the Δf loop to avoid constant value. In this paper, the author also discusses the effect of different values of K_1 and K_2 on system stability.

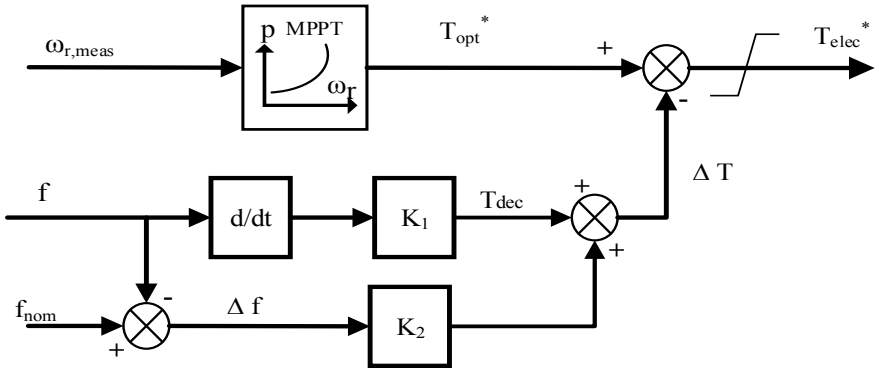

Figure 2.16: Supplementary control loops for inertia response

ii Fast Power Reserve

Generally, the inertia response can be emulated, depending on the frequency deviation or ROCOF, as pointed out previously. It can also be defined as a constant 10% of the nominal active power for 10 seconds, despite various wind speeds (Wachtel & Beekmann, 2009). The short-term constant power, called fast power reserve, is released from the kinetic energy stored in the rotating mass of the wind turbine. This fast power reserve can be achieved by controlling the rotor speed setpoint, which is given by:

$$P_{const}t = \frac{1}{2}\mathrm{J}\omega_{r0}{}^{2} - \frac{1}{2}\mathrm{J}\omega_{rt}{}^{2} \tag{2.7}$$

Where $P_{const,}$ is the constant amount of active power, t is the time duration for the fast power reserve, ω_{ro} is the initial rotational speed, and ω_{rt} is the rotational speed at the end of the inertial response. Thus, the reference rotor rotational speed can be calculated using:

$$\omega_{r.ref} = \omega_{r.t} = \sqrt{\omega_{ro}{}^{2} - 2\frac{P_{const}}{J}t} \tag{2.8}$$

Literature discussed the principle operation of the fast power reserve. (Hansen et al., 2014; Ullah, Thiringer, & Karlsson, 2008) detailed the capability of variable speed wind turbines to provide short-term overproduction power for different wind speeds. In fact, they did not provide any controller design for fast power reserve. However, (Sun et al., 2010) proposed a fast power reserve controller for wind power turbine, as shown in Figure 2.17, where the amount of constant power and time duration determine the rotor speed

based on Equation (2.8). Then, a reference power will be injected to stop frequency deviation.

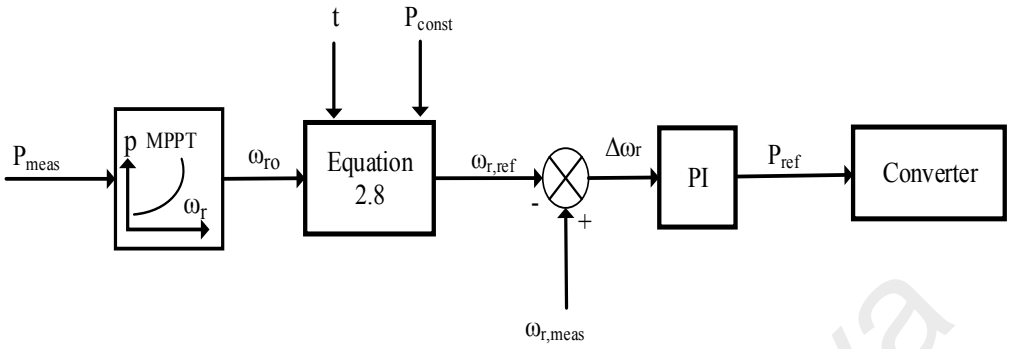

Figure 2.17: Fast power reserve controller for a wind turbine

(El Itani et al., 2011) proposed an architecture for a fast power reserve controller, as shown in Figure 2.18. This figure contains a detecting and triggering scheme, power shaping, and an MPPT controller.

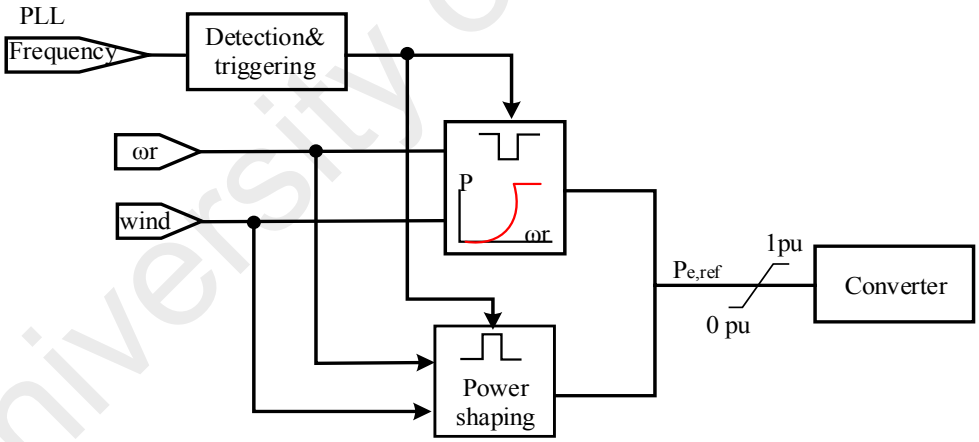

Figure 2.18: Block diagram of fast power reserve controller

The operation of the fast power reserve controller shown in Figure 2.19 starts once the frequency deviation exceeds a certain threshold. A control signal is sent from detecting and triggering scheme to bypass the maximum power point tracking, and enables power shaping block. This scheme continues providing extra power during the over-production period. However, when kinetic energy discharge is complete, the rotor speed recovery function brings the rotor speed back to its pre-event value, and restores maximum power.

This restoration often leads to under-production phase, where power is withdrawn from the grid to bring the rotor speed back to its optimal value. The transition from over-production to under-production is made along a slope to avoid a sudden drop in the output power.

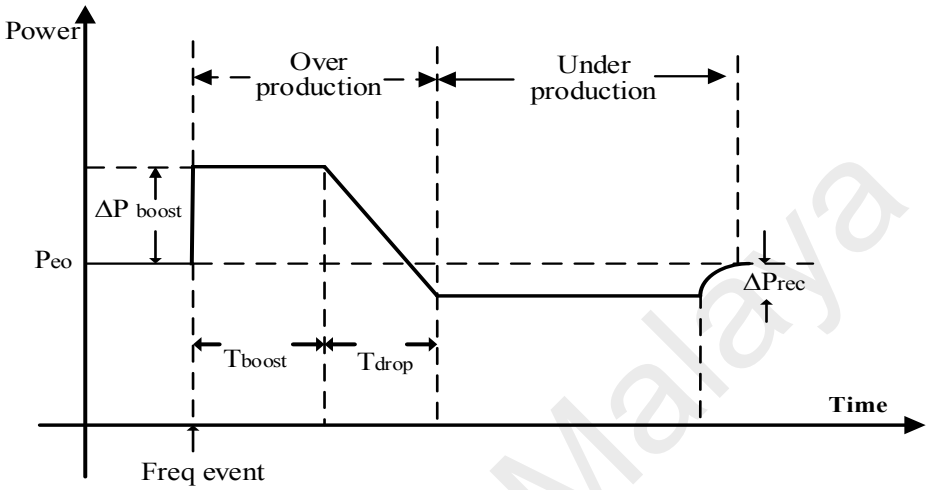

Figure 2.19: Power characteristics for fast power reserve control

Different strategies for fast power reserve for wind farms were proposed by (Keung, Li, Banakar, & Ooi, 2009). They discussed the operation of a centralized controller, which is responsible for frequency regulation. This central controller has two main tasks; the first is to determine the amount of additional power for each wind turbine, and the second is to determine the appropriate time to recover kinetic energy after over production is over.

(B) Droop Control

The droop control scheme shown in Figure 2.20 regulate the active power output from a wind turbine proportional to the frequency change. This controller significantly improves the frequency nadir, as well as the frequency recovery process following disturbances. The active power is adjusted according to linear characteristics, and is given by (Josephine & Suja, 2014; Mishra & Sekhar, 2013; Yao & Lee, 2011).

$$\Delta P = P_1 - P_O = -\frac{f_{meas} - f_{nom}}{R} \tag{2.9}$$

where R is the droop constant, f_{meas} and P_1 are, respectively, the new frequency and wind turbine output power, and f_{nom} and P_o are the initial operating points.

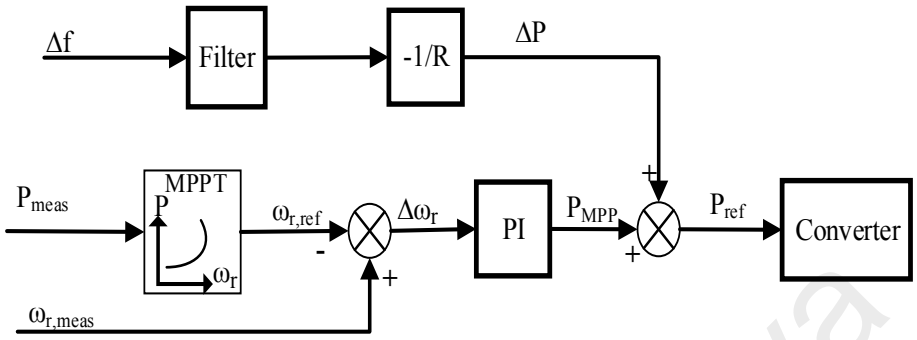

Figure 2.20: Frequency support scheme with droop speed control

The linear relation between frequency and active power of the wind turbine is illustrated in Figure 2.21. When the frequency falls from f_{nom} to f_{meas}, the wind turbine increases its output power from P_o to P_1 to compensate for the frequency deviation (Eid et al., 2014).

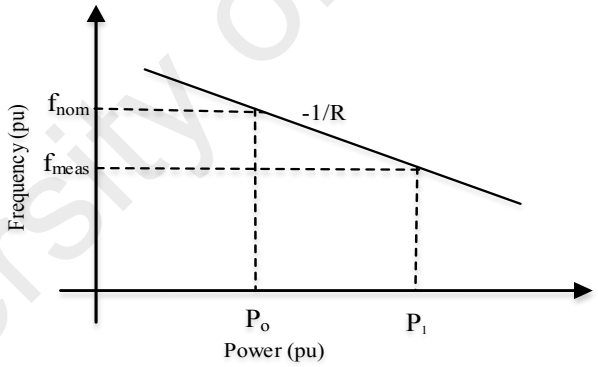

Figure 2.21: Wind turbine droop characteristics

(C) Deloading Control

From an economic perspective, wind turbines are designed to operate at an optimum power extraction curve. As a result of this, they do not participate in frequency regulation. For this reason, sufficient reserve capacity must be available in the system to address any frequency deviation. Deloading is a new technique that ensures a reserve margin by shifting the wind turbine's operating point from its optimal power extraction curve to a reduced power level. Based on the wind turbine's aerodynamic behavior, the mechanical output power captured by the wind turbine will be:

$$P_m = \frac{1}{2}\rho A C_p\,(\lambda, \beta)\, v^3 \tag{2.10}$$

where ρ is the air density, A is the rotor sweep area, v is the wind speed, C_p is the power coefficient, β is the pitch angle, and λ is the tip speed ratio, given by:

$$\lambda = \frac{\omega_r R}{v} \tag{2.11}$$

From equation (2.10), the output power of the wind turbine depends on the tip speed ratio λ and pitch angle β. Generally, the deloading technique has two types of control system; speed control and pitch angle control.

iii Deloading by Speed Control

(Castro, Fuerte-Esquivel, & Tovar-Hernández, 2012) proposed a speed controller to change the value of the tip speed ratio λ by shifting the operating point towards the left or the right of the maximum power point, as shown in Figure 2.22 (a). This figure illustrates the deloading function of a 1.5 MW DFIG-based wind turbine by (1-x) of the maximum power under definite wind velocity (V_W). The wind turbine running at point A can be deloaded by the under-speed or over-speed control. For the under-speed control, the operating point of the wind turbine moves towards point C, while for the over-speed control, the operating point of the wind turbine moves towards point B, which is preferable.

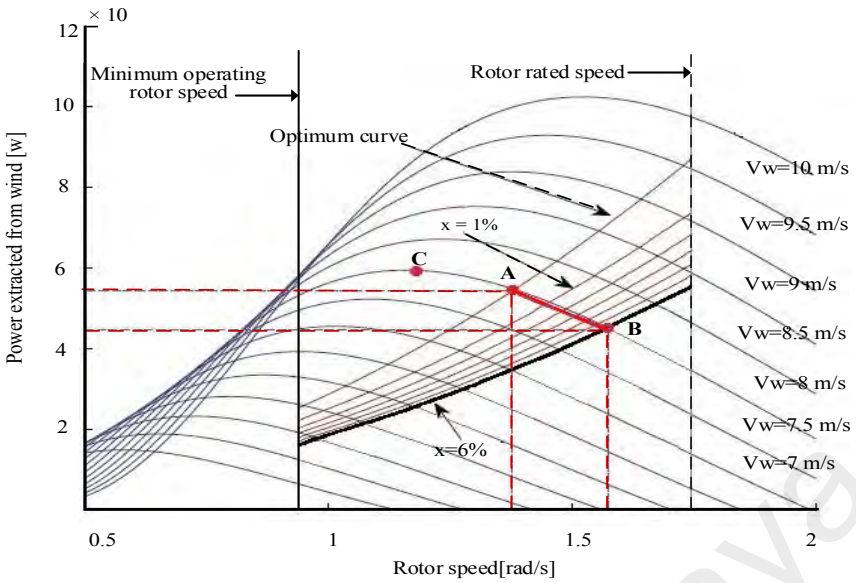

(a)

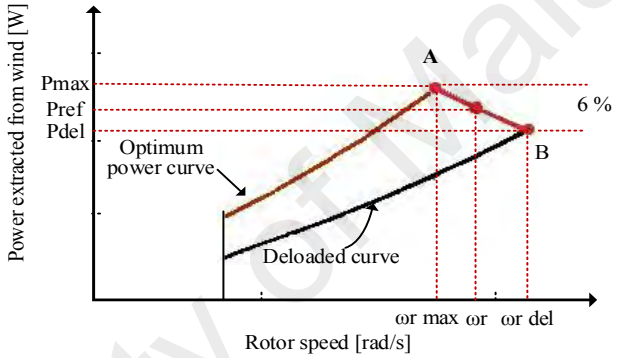

(b)

Figure 2.22: (a) MPPT and deloaded power curves of the wind turbine. (b) Calculation of power reference for 6% deloaded operation (Castro et al., 2012)

As per Figure 2.22 (b), when the system frequency drops, the wind turbine releases a definite amount of active power proportional to the frequency deviation. Then, the operating point will be located between A and B with $P_{ref,}$ which is expressed by:

$$P_{ref} = P_{del} + (P_{max} - P_{del}) \times \left(\frac{\omega_{r\ del} - \omega_r}{\omega_{r\ del} - \omega_{r\ max}}\right) \qquad (2.12)$$

where P_{max} is the maximum power (pu), P_{del} is the deloaded power (pu), $\omega_{r\ max}$ is the rotor speed at maximum power, $\omega_{r\ del}$ is the rotor speed at deloaded power, and ω_r is the rotor speed, corresponding to the reference power. Generally, deloading using the over-speed control is preferred at medium wind speeds.

(A) Deloading by Pitch Angle Control

Pitch angle is the second controller used to deload the wind turbine by increasing the blade angle. This controller is preferably activated when the wind turbine generator arrives at rated speed when the over-speed controller fails to perform this operation. Figure 2.23 shows the power-rotor speed curve for a DFIG wind turbine under different pitch angles. It illustrates the deloading technique for the wind turbine running at point A; in this case, the controller fails to increase the rotation speed over the rated speed. Then, the pitch angle controller begins to increase the angle of the wind turbine blades and shifts the operating point from point A to point B without changing the rotor speed.

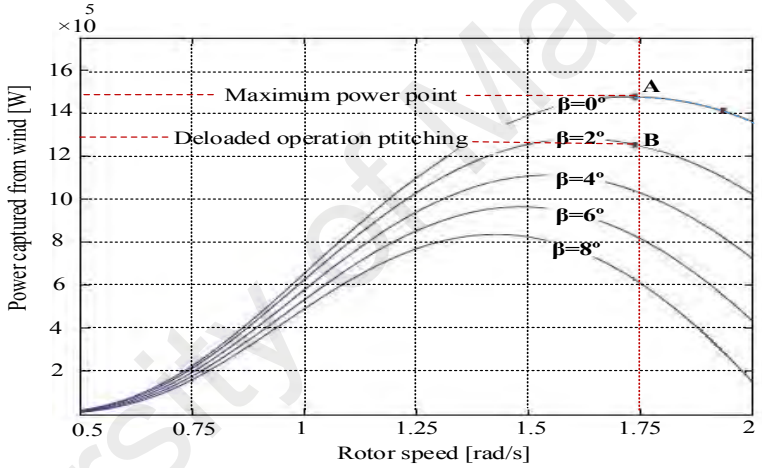

Figure 2.23: Power- rotor speed curves with different pitch angles (Castro et al., 2012)

Generally, several different works in literature discussed the deloading technique being used with a variable speed wind turbine, such as in (Vidyanandan & Senroy, 2013). The deloading technique supports primary frequency control under two operating conditions, as shown in Figure 2.24. In normal conditions, the variable speed wind turbine works at the optimal power curve, extracting the operating point from the look-up table. However, when the deloading switch is turned on, the deloading mode will be activated. In this case, the speed and pitch angle controllers cooperate to allow the wind turbine to reserve some power under different modes. Equation (2.12) determines the reference power for speed and pitch control to provide 10% of reserve power. In order to release the active power

stored in the rotating mass as a result of deloading control, droop control is also presented in this work. The amount of releasing power is proportionated to the frequency deviation, and is limited to 10% of wind turbine rated power.

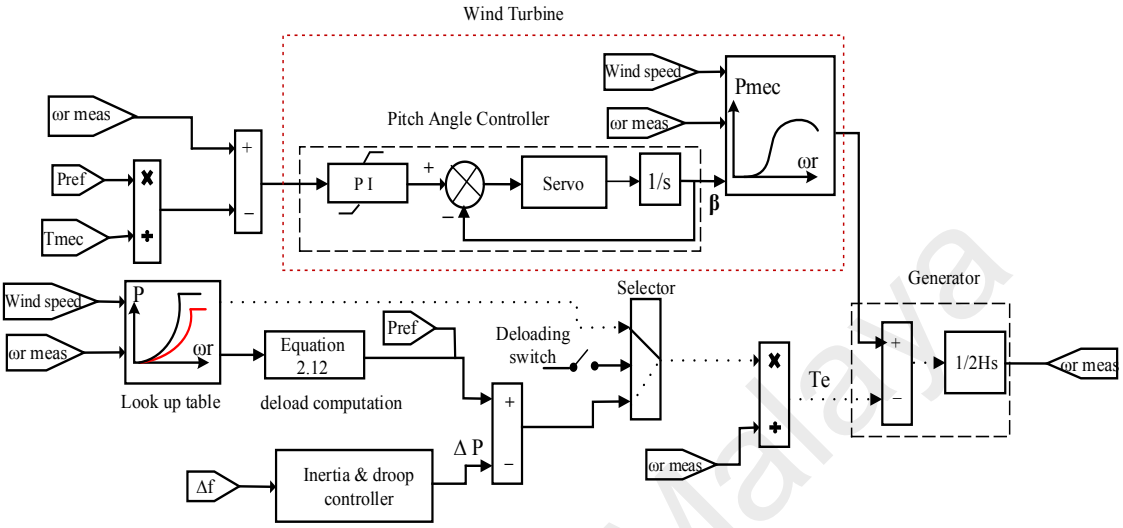

Figure 2.24: Primary frequency control of wind turbine based on deloading control

(Z.-S. Zhang, Sun, Lin, & Li, 2012) presented the inertia response and primary frequency for DFIG-based wind turbines. The inertia controller is emulated to release the kinetic energy stored in the wind turbine rotating blades for a few seconds. It is proposed that a deloading strategy with 90% sub-optimal power works as the primary frequency control. This strategy, based on the cooperation between the speed and pitch controllers, provides the wind turbine with relatively long-term reserve power. Figure 2.25 shows the deloading technique used with a wind turbine in three operating modes. In the first operating mode, the over-speed control is used to deload the wind turbine. For example, the deloading of the wind turbine running at point F by 90% sup-optimal power is conducted by increasing the generator rotor speed towards point C. In the second operating mode, the over-speed and pitch angle controller are combined to achieve a specific sup-optimal power. For example, in order to deload the wind turbine running on point B with 90% sup-optimal power, the over-speed controller needs to shift the operating point towards point D. However, the over-speed controller increases the speed

until the wind turbine arrives at point G. After that, the over-speed controller cannot increase the rotation speed anymore. As a result of this, the pitch angle controller increases the blade pitch angle shifting the operating point towards point A. In the third region, the pitch controller is used on its own to achieve the target deloading value.

The cooperation between pitch angle and speed controller for a variable speed wind turbine is also presented in (Díaz-González et al., 2014). They proposed three operating modes, depending on the range of wind speed, and a decision algorithm to manage the cooperation between pitch angle and the over-speed controller. This algorithm determines the power set value for the pitch angle controller and the power margin for the over-speed controller.

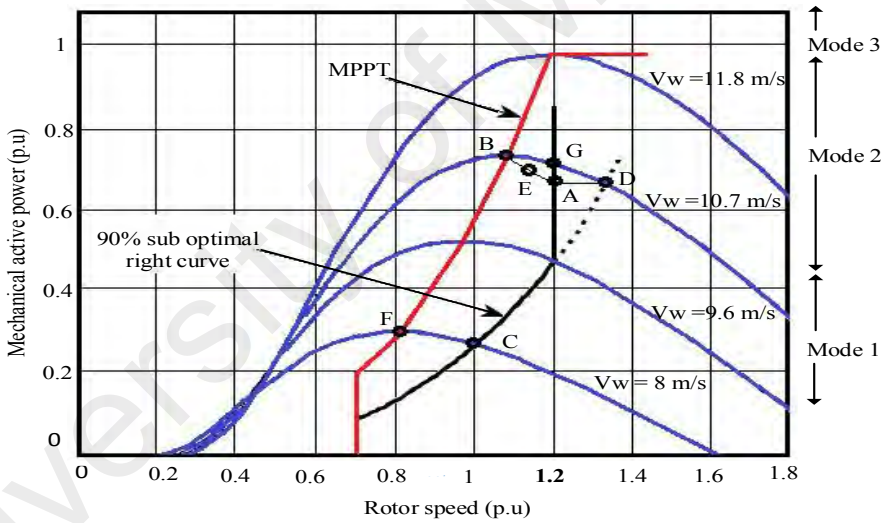

Figure 2.25: 90% sub-optimal operation curve (Z.-S. Zhang et al., 2012)

(De Almeida & Lopes, 2007) used the cooperation between pitch angle and over-speed controller to allow the wind turbine to participate in frequency regulation. However, this time, the controllers decided on the reserve power value based on the network operator request. (Z. Wu, Gao, Wang, & Gu, 2012) reported that the same frequency regulation controllers used for the DFIG wind turbine were redesigned and implemented in the PMSG to enable this type of wind turbine to contribute to primary frequency control.

(Tielens et al., 2012; Zhangjie, Xiaoru, & Jin, 2012) proposed the pitch angle and over-speed controllers, coordinated with the droop control. These controllers are activated by wind speed ranges to enable the DFIG-based wind turbine to participate in frequency regulation. Furthermore, the over-speed control strategy uses wind speed measurements to determine the sub-optimal power based on the deloading tracking curve, and saves this value in the lookup table.

2.4.1.2 Frequency Regulation Controllers Proposed for PV without ESS

Recently, the penetration of solar photovoltaic (PV) into distribution networks has significantly increased. As a result of this, reserve power from the remaining conventional source unit is insufficient to regulate system's frequency under island conditions. Moreover, due to the high cost of solar photovoltaic systems, different MPPT techniques have been introduced to extract maximum power from this source (De Brito, Galotto, Sampaio, e Melo, & Canesin, 2013; Faranda & Leva, 2008; Hua & Shen, 1998). However, the use of MPPT techniques enables the solar photovoltaic (PV) to operate without any reserve power. For these reasons, different modifications have been made to the design of controllers used with a (PV) converter to allow them to effectively participate in frequency regulation.

According to (Hoke & Maksimović, 2013), smart photovoltaic inverters do not have the full commercial control capability to change the output power from (PV) systems, even if they have the ability to provide frequency down-regulation by curtailing power. Moreover, research related to this type of control is still in the early stages, and mainly depends on two types of controller. The first uses solar photovoltaic (PV) supported by ESS to regulate the frequency, which will be discussed later, while the second proposes the deloading technique for solar photovoltaic (PV) without ESS, as presented in (Rahmann & Castillo, 2014; Zarina, Mishra, & Sekhar, 2012a, 2012b). These papers

present a comprehensive control scheme that allows the photovoltaic system to participate in frequency regulation. Figure 2.26 shows the deloading technique, which is performed by increasing the dc voltage beyond *MPP*. This is achieved by increasing the value from V_{MPP} by voltage V_{deload}, which allows the PV array to maintain some reserve power. This reserve power is not released until the system frequency deviates. Under these conditions, a control signal proportional to frequency deviation $V_{dc\Delta f}$ is added to the dc reference voltage.

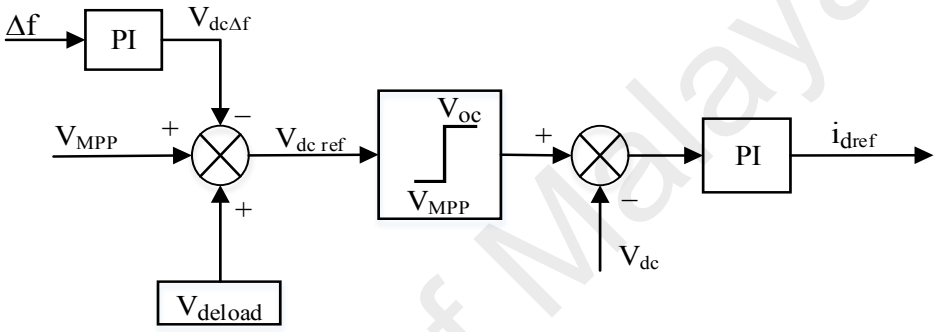

Figure 2.26: Controller for deloaded solar PV

It can be seen in Figure 2.26 that the change in output power from the PV will not only depend on the V_{MPP} value, but also on the frequency deviation, as per equation (2.13).

$$V_{dc\,ref} = V_{MPP} + V_{deload} - V_{dc\,\Delta f} \tag{2.13}$$

The operation of the deloaded controller is illustrated in Figure 2.27, where PV is working at point 3 to reserve some power. This continues until the system's frequency begins to decline, at which point a control signal related to frequency deviation will reduce the PV voltage and make the PV work at point 2.

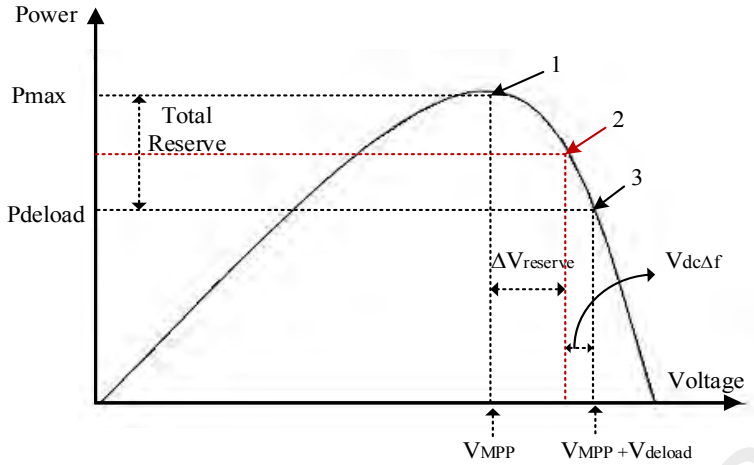

Figure 2.27: Solar PV with deloading technique (Zarina, Mishra, & Sekhar, 2014)

In fact, the controller discussed in Figure 2.26 has a big problem in that it does not take into consideration the remaining reserve power for each PV unit. For this reason, all PV units will release the same amount of active power needed for frequency regulation, even if the reserve power of each unit will not be equal. As a result of this, some of the PV units, which have less reserve power, will reach MPP faster, and will not be able to contribute any further to frequency regulation. This will lead to a non-uniform distribution of frequency regulation. (Zarina et al., 2014) proposed a new modification to the previous controller by adding a new control signal to represent the remaining reserve power $\Delta V_{reserve}$, as shown in Figure 2.28. The reference voltage of the new controller is given by equation (2.14), which clearly shows that the output power released from the PV units is not equal and depends on the reserve power available for each.

$$V_{dc\,ref} = \left(V_{MPP} + V_{deload} - V_{dc\,\Delta f}\right) - \left(\Delta f \times \Delta V_{reserve} \times K_{P2}\right) \qquad (2.14)$$

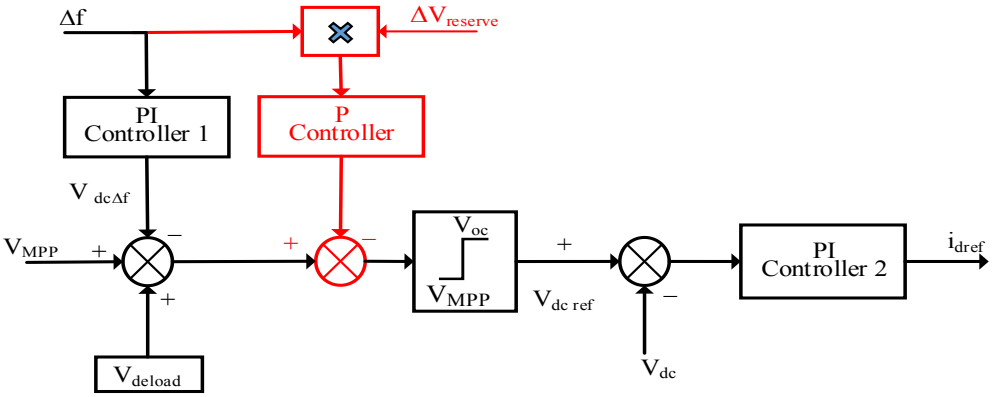

Figure 2.28: The improved controller for deloaded PV

Another technique was proposed in (Pappu, Chowdhury, & Bhatt, 2010) to enable a solar PV plant to participate in frequency regulation. Two algorithms were implemented, the first was the traditional MPPT controller, which is responsible for operating the PV plant on MPP during normal operations. For transient conditions, a control signal would activate the deloading algorithm, which uses a modified fractional open circuit voltage. This modification proposed the use of ratio *K* as a controlled variable, which determines the amount of reserve power for PV plants limited to the range (0.8-0.95). The main findings of this paper show that a PV generator has the ability to regulate the frequency and follow load changes. Furthermore, (Watson & Kimball, 2011) discussed a control scheme designed for a PV panel to regulate the frequency of an islanded micro-grid. Their main objective was to use a tracking algorithm to follow a command signal, which changes according to the frequency deviation of the micro-grid. Following this, the control system continues until the controller reaches the maximum power point, and stays running at this point.

Generally, all control techniques discussed in this paper were designed to provide the solar PV system with reliable control to regulate the frequency in grid connected or off-grid mode. These techniques were mainly based on the MPPT controller running the PV array in the deloading mode. In contrast, (Okou, Akhri, Beguenane, & Tarbouchi, 2012) proposed a frequency regulator consisting of an adaptive frequency scheme, using a nonlinear control to calculate the active power signal P^*, depending on the frequency deviation, as shown in Figure 2.29. This signal is needed to update the reference power P_{ref} used by the power controller to determine the output power of the solar PV by regulating the duty cycle (D) of the power converter.

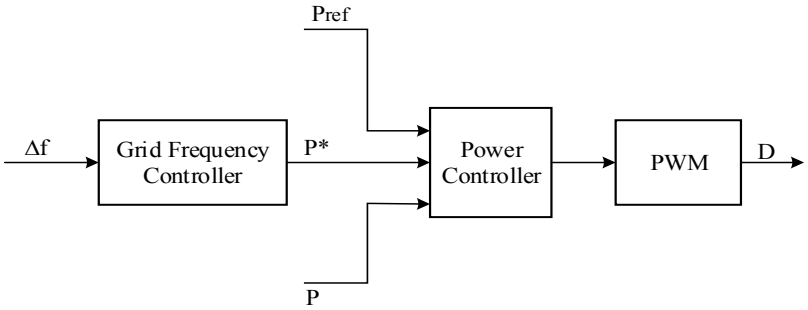

Figure 2.29: Solar PV frequency regulator

2.4.2 Inertia and Frequency Regulation Controllers Proposed for RESs with ESS

Different control techniques have been proposed in the previous sections to provide RESs with the ability to regulate system frequency during disturbances. However, these techniques experience reliability issues, as the nature of the RESs is intermittent. Therefore, the variable speed wind turbines and PV generation need an ESS to increase the reliability of frequency regulation.

2.4.2.1 Inertia and Frequency Regulation Controllers Proposed for Wind Turbines with ESS

In (Miao, Wen, Xie, Yue, & Lee, 2015), a coordination between frequency control techniques and ESS was proposed for the DFIG wind turbine. This coordination helps overcome problems of frequency control techniques, such as frequency oscillation and second frequency drop. In fact, the ESS has two main functions in supporting frequency regulation in all wind speed ranges, in the first function, the ESS provides the active power required for rotor speed recovery to prevent frequency second drop, while in the second, the ESS is considered a backup system to provide power during wind turbine power deficits.

In (Díaz-González, Hau, Sumper, & Gomis-Bellmunt, 2015), a primary frequency control was used in wind power plants to maintain a certain level of power reserve. Flywheel storage supports the wind power plant to fulfil the power reserve requirements set by the

network operator. In steady state conditions, a central controller distributes the power reserve requirement between the wind turbines and the flywheel storage system, as shown in Figure 2.30. The power reserve margin x (p.u) is determined based on the wind speed range, and is given by:

$$1 - x = \begin{cases} \dfrac{P_{del}}{P_{opt}} & if \quad v_w \leq v_{w\,rated} \\ \dfrac{P_{del}}{P_{rated}} & if \quad v_w > v_{w\,rated} \end{cases} \tag{2.15}$$

Where P_{opt} is the maximum power extracted from the wind turbine and P_{del} is the wind turbine output power under deloading conditions.

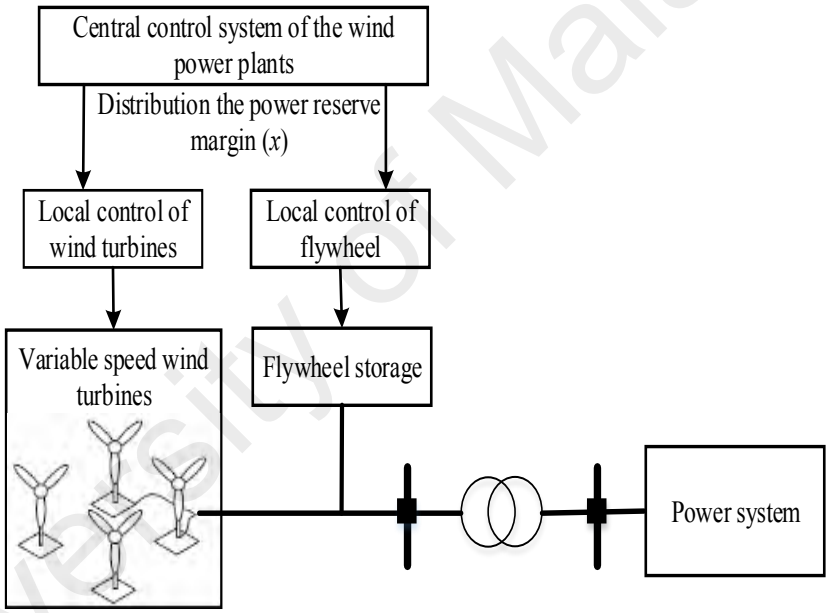

Figure 2.30: Schematic diagram of frequency regulation of wind turbine and flywheel

In (Arani & El-Saadany, 2013), a virtual inertia technique was proposed for the DFIG wind turbine to provide short-term frequency regulation. Since this technique focuses on short term oscillation, there is no need for long power regulation. For this reason, a super-capacitor is connected to the DC-link of the DFIG wind turbine inverter via a DC-DC converter. A comparison study done in this work showed that using the DFIG rotating mass or super-capacitor as the virtual inertia source enhances system stability. However, each type reports different impacts. It was shown that while rotating-mass-based virtual

inertia does not need any new components, its performance is highly dependent on wind speed, which is unpredictable. On the other hand, super-capacitor-based virtual inertia, which significantly improves the system's behavior and is independent of wind speed, require an additional component.

2.4.2.2 Frequency Regulation Controllers Proposed for Solar PV with ESS

In (Kakimoto, Takayama, Satoh, & Nakamura, 2009), the power modulation technique used for PV generation output was described using a double layer super-capacitor, shown in Figure 2.31. It shows a PV generation system, consisting of a PV array, an inverter, and a super-capacitor. The array generates dc power P_S. The inverter then converts the dc power to ac power P, and transmits this power to the utility through a service line. The super-capacitor is used to absorb the difference P_C between P_S and P.

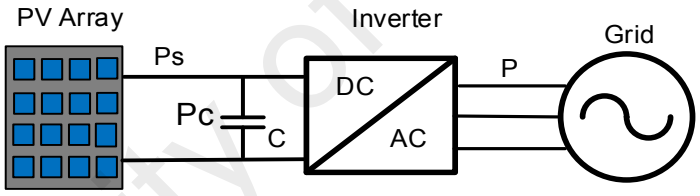

Figure 2.31: PV and super-capacitor used in frequency regulation

The proposed frequency controller is shown in Figure 2.32. It can be seen that if the frequency deviation is smaller than 0.1 Hz, then the output P_f is given by $G\,(f_{ref} - f)$, but is limited to within $\pm P_{mod}$, which is considered 3% of the generation capacity.

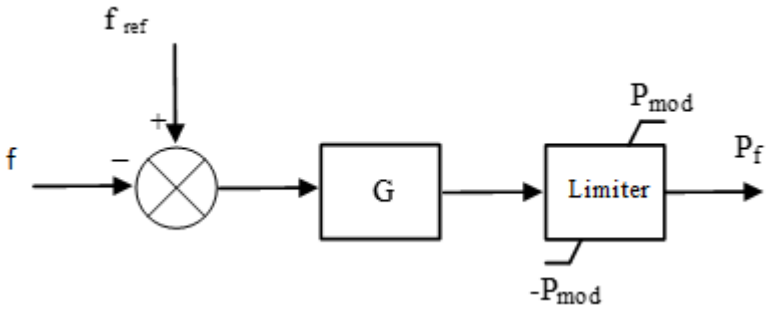

Figure 2.32: Frequency controller using limiter block

A frequency and voltage regulation technique using PV systems and Li-ion BSS coupled to the grid was presented in (Bhatt & Chowdhury, 2011). This technique allows effective control over the active and reactive power available from the system. Two approaches were suggested in this work to allow the system to participate in frequency regulation; the first was down-regulation, where the output power from the PV system and excess power from the grid are absorbed by the storage battery, and the second was up-regulation, where the PV/battery system injects active power into the grid. A proposed system, comprising a 2 kW PV array, 2.64 kWh batteries with bi-directional dc-dc converter, a three-phase inverter, and the grid, was modelled and simulated in MATLAB. The results showed that the PV plant can respond quickly and participate in frequency regulation.

Frequency regulation using a PV plant supported by an Battery Storage System (BSS) was presented in (Chamana & Chowdhury, 2013). This paper proposed a comprehensive control system using P-Q based droop control. This control system automatically regulates the active and reactive power when the demand power exceeds the PV array generation. However, when the power demanded by the grid is less than the PV array, the inverter control switches to regulate the frequency and voltage based on active and reactive set points. The output power from the PV system and battery SOC are included in the proposed controller in order to make the best decision for frequency regulation.

Another research using the same principles of P-Q control for a microgrid with PV generator and BSS was presented in (Adhikari & Li, 2014). This paper proposed the smooth transition of the PV from P-Q control in the grid connected mode to V-f control in the islanded mode. The proposed transition of solar PV to V-f control performed very well in restoring voltage and frequency back to nominal values in a matter of only 2 seconds. The control strategy presented in this paper is operating the PV generator on

Maximum Power Point (MPP) with BSS. This BSS acts to inject and absorb deficit or surplus power using the charge/discharge cycle of the battery.

2.4.3 Inertia and Frequency Regulation Controllers Based on Intelligent Algorithms

In the near future, the complexity/nonlinearity of the power systems will increase due to the continuous integration of RESs. Due to this fact, classical controllers such as proportional-integral (PI) controller is unsuitable for many operations. Therefore, robust control schemes utilizing optimal/intelligent techniques are needed. (Sa-ngawong & Ngamroo, 2013) proposes an inertia and frequency regulation controller based on the fuzzy logic control for the DFIG wind turbine. As shown in Figure 2.33, the fuzzy controller is continuously tuning the values of k_1, k_2, k_f based on the frequency deviation Δf and wind power deviation ΔP_w. Simulation study shows the importance of the proposed fuzzy controller in compelling the power system to respond dynamically to multiple load changes.

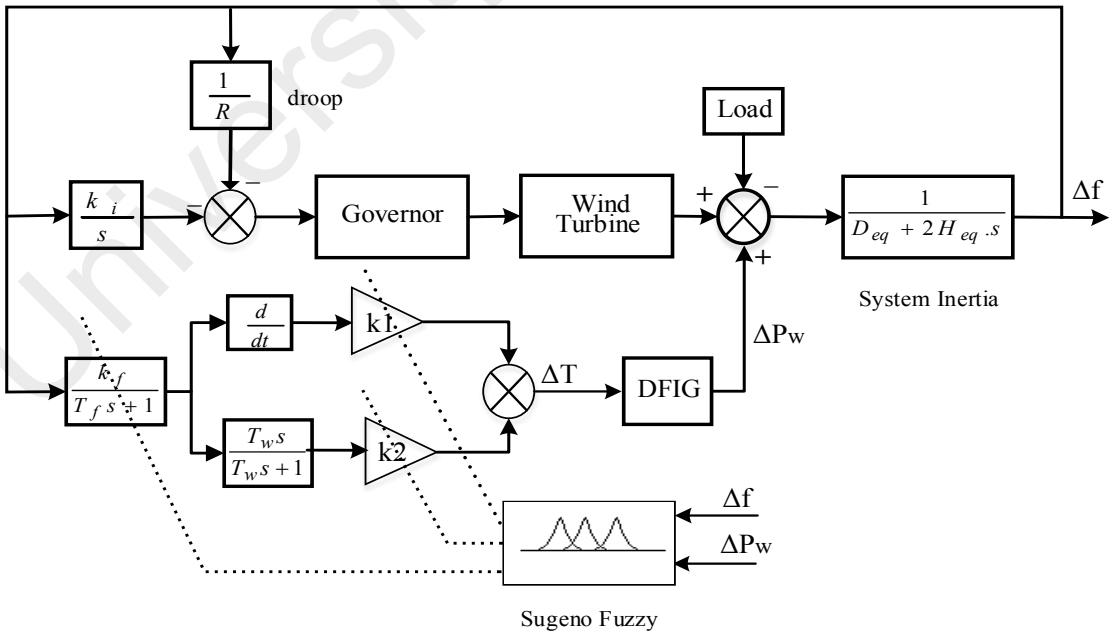

Figure 2.33: DFIG wind turbine frequency regulation using fuzzy tuning-based PI

Another research using the same principles of tuning the classical PI controller by intelligent algorithm was discussed in (Bevrani, Habibi, Babahajyani, Watanabe, & Mitani, 2012). They used the PSO technique to improve the membership functions of the fuzzy controller, which is used to tune the PI controller constants, as shown in Figure 2.34.

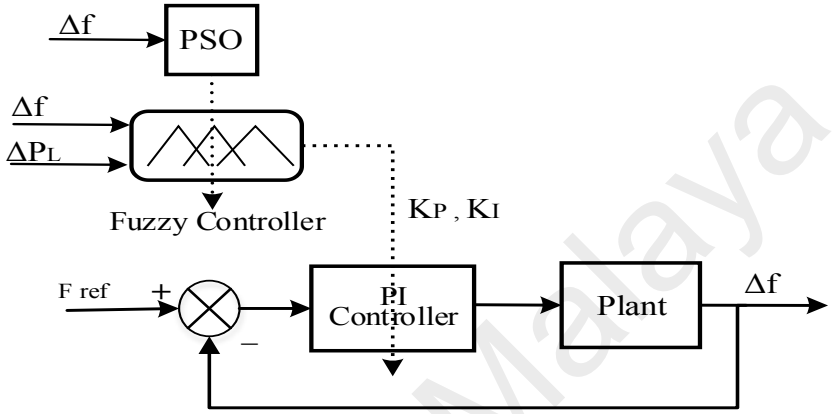

Figure 2.34: Frequency regulation controller using DFIG wind turbine

(Bevrani et al., 2012) compared the classical PI controller, fuzzy tuning approach, and PSO-based fuzzy tuning approach, and confirmed the robustness of the proposed PSO-based fuzzy tuning approach over other methods. (Ali & Hasanien, 2012) compared a classical PID controller and the adaptive neural network (ANN) controller to regulate the frequency of the isolated network. This network contains wind and diesel generators without BSS. The simulation study confirms the advantages of the proposed ANN in terms of overshoot frequency, undershoot frequency, and settling time.

As pointed out earlier, the wind turbine utilizes the deloading technique to reserve the necessary power to regulate the frequency of the controller. However, keeping a fixed value of reserve power will reduce the annual capacity factor (CF) of wind farms, since the output power from this source fluctuates. For this reason, (Pradhan & Bhende, 2015) recommend using an online deloading technique based on the fuzzy logic controller to adjust the deloading factor continuously based on frequency deviation. Furthermore,

(Datta, Senjyu, Yona, Funabashi, & Kim, 2011) propose a frequency regulation control for PV generator based on fuzzy logic controller, as shown in Figure 2.35.

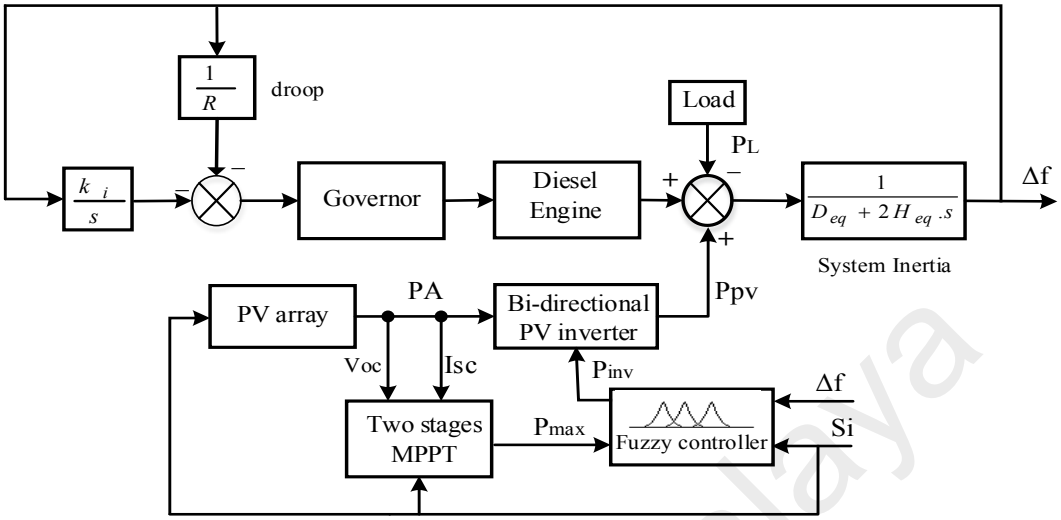

Figure 2.35: Fuzzy-based frequency regulation control for PV diesel system

This controller uses frequency deviation and solar radiation as an input to determine the reference power injected by the PV inverter. The simulation study confirms the effectiveness of the proposed method in frequency regulation.

The overall summary of inertia and frequency control techniques proposed in the literature is shown in Table 2.1. This table shows that no inertia controller is proposed in literature on solar PV. Nevertheless, many studies proposed frequency regulation controllers for PV based on the deloading technique. Due to intermittence of PV generation, a ESS is suggested to support the operation of frequency regulation controller, which increases its reliability. ESS is not only used to increase reliability; it also stops the loss of energy.

Unlike PV generation, several studies proposed inertia controller for wind turbine. This controller provides inertial response by releasing the mechanical power stored in rotating wind turbine blades. In terms of frequency regulation, researchers proposed speed and pitch angle controllers for wind turbines, where the former is used to deload the operation of wind turbine before the rated speed, while the latter is used after the rated speed.

Table 2.1: Summary of inertia and frequency regulation controllers proposed in the literature

Type of RESs	Issues of high penetration level	Proposed technique	Proposed controller	References	Reliability	Power loss	Time response	The ability to adapt according to different changes
Solar PV	Frequency regulation issue	Deloading	Voltage controller based on classical PI	(Rahmann & Castillo, 2014; Zarina et al., 2012b)	Low	Some power is lost due to the deloading technique	Fast response due to the electronic converter	The controller does not adapt, instead, a classical PI is used without tuning
			Voltage controller based on Intelligent Algorithm tuning PI	(Datta et al., 2011)				The controller adapts according to the changes
Solar PV with ESS	Frequency regulation issue	Deloading + ESS	Voltage controller (PV) + Primary frequency controller (ESS)	(Adhikari & Li, 2014; Bhatt & Chowdhury, 2011; Chamana & Chowdhury, 2013)	High reliability due to ESS	No power loss	Fast response due to the electronic converter	The controller does not adapt, instead, a classical PI is used without tuning
Variable speed wind turbine	Reduced inertia response	Inertia response controllers	Hidden inertia Emulation	(Gonzalez-Longatt et al., 2013; Morren, De Haan, et al., 2006)	Low reliability	No power loss	Fast response	
			Fast power reserve	(Wachtel & Beekmann, 2009)				
	Frequency regulation	Deloading	Speed control	(Castro et al., 2012)		Some power is lost due to the deloading technique	Fast response	
			Pitch control	(Vidyanandan & Senroy, 2013; Z.-S. Zhang et al., 2012)			Slow response due to mechanical control	
			Speed control based on Intelligent Algorithm tuning PI	(Sa-ngawong & Ngamroo, 2013)			Fast response	The controller adapts according to changes
Variable speed wind turbine with ESS	Frequency regulation	Deloading + ESS	Speed control + Primary frequency controller (ESS)	(Díaz-González et al., 2015; Miao et al., 2015)	High reliability due to ESS	No power loss	Fast response	The controller does not adapt, a classical PI is used without tuning

2.5 Load Shedding Techniques

As previously discussed, to ensure a successful transition from the grid connected mode to the islanding mode, the frequency and voltage should be within their respective permissible limits, or the distribution network could experience total blackouts (Vahedi & Karrari, 2013). In this situation, the load shedding technique is necessary to prevent total system blackout during frequency and voltage instability issues. In literature, several load shedding techniques have been proposed for selecting the efficient and optimal technique. Generally, load shedding techniques are classed into three main categories; conventional, adaptive, and computational intelligence-based techniques.

2.5.1 Conventional Load Shedding Techniques

The conventional load shedding technique is commonly divided into two main categories; under-voltage load shedding technique (UVLS) and under frequency load shedding technique (UFLS).

2.5.1.1 Under Voltage Load Shedding (UVLS) Techniques

Under voltage load shedding techniques can be used to prevent voltage collapse in power system. From studying major power blackouts, it can be clearly seen that most power blackouts were caused by voltage instability problems (El-Sadek, 1998; Yusof et al., 2017). Generally, voltage collapse occurs due to either tripping generator or overloading, where the reactive power demand changes very quickly, and could cause a blackout if left untreated. For this reason, power utilities typically utilize the UVLS technique to restore power system voltage to its nominal value.

2.5.1.2 Under Frequency Load Shedding (UFLS) Techniques

Under frequency load shedding techniques are used to prevent frequency drop due to the loss of generators or overloading, where the active power demand changes very quickly. The UFLS relay is initialized to shed a fixed amount of load in predefined steps when the

frequency falls below a certain predefined threshold value (Tang, Liu, Ponci, & Monti, 2013). Generally, threshold values vary from one country to another, depending on the power system requirements. An example of conventional under frequency load shedding was reported in 1999 for the Malaysian power system (Zin, Hafiz, & Aziz, 2004). This research proposed a 15-stage load shedding scheme to reflect 5600 MW generation loss. Although this technique is low cost and simple, it is unable to shed the optimal load because it does not estimate the actual amount of the power imbalance, which leads to either over-shedding or under-shedding problems.

2.5.2 Adaptive Load Shedding Technique

The adaptive UFLS technique is advantageous as it uses the swing equation to estimate the imbalance power. The power imbalance can be obtained using this equation:

$$\Delta P = \frac{2H}{f} \times \frac{\partial f}{\partial t} \tag{2.16}$$

Where ΔP is the power imbalance; H is the Inertia constant of generator; f is the nominal frequency (Hz); df/dt is the rate of change of frequency (Hz/s).

When the power system is exposed to disturbance such as faults or overloading, its frequency and its associated rate of change drops quickly. Using these values in the power swing equation will allow us to estimate the power imbalance. After doing so, the adaptive load shedding technique shed the required amount of load in order to stabilize the frequency.

Many adaptive UFLS techniques have been reported in literature. (Terzija, 2006) showed that the adaptive UFLS technique shed less amount of load compared to its conventional counterpart. However, this technique suffers from overshoot frequency, which means that the amount of the shed load is not optimal.

Calculating the power imbalance using the frequency of the center of inertia was reported by (Rudez & Mihalic, 2011). In their work, they proposed shedding lower amounts of load from an islanded power system. The calculated imbalance power is distributed among the different stages; for a large power imbalance, the author suggested using larger steps prior to smaller ones. Two centralized adaptive algorithms were presented in (Pasand & Seyedi, 2007). They proposed these algorithms to protect the power system blackouts, following combinational disturbance by a combination of response-based and event-based techniques. This load shedding technique was proposed to overcome the improper imbalance power, as well as the slow response of under-frequency relays for the conventional load shedding technique. To enhance the conventional UFLS technique operation, (Marzband, Moghaddam, Akorede, & Khomeyrani, 2016; Saffarian & Sanaye-Pasand, 2011) proposed an adaptive load shedding technique based on three combinational factors. This technique utilizes ROCOF, disturbance location, and system voltage status. The load priority of shedding load was determined according to the system voltage, in other words, loads with high voltage will be shed first. In literature, the adaptive UFLS techniques were based on fixed priority load shedding. Accordingly, load shedding techniques suffer from surplus or insufficient loads being shed, which led to total blackouts. To address this issue, (Laghari et al., 2015) proposed a new adaptive UFLS technique with random and fixed priority loads. By using this feature, the UFLS technique can shed the appropriate combination of loads. However, this technique takes quite a while, which is unsuitable for fast frequency changes.

2.5.3 Computational Intelligence Based Load Shedding Techniques

Recently, the structure of power systems is becoming very complex due to the integration of more distribution generation. In this situation, traditional load shedding techniques cannot function efficiently in disturbance events. Thus, an efficient load shedding technique is necessary to shed the optimal load and maintain power system stability. Since

the late 1980s, interest in using computational intelligence techniques in power systems has increased. Accordingly, various load shedding technique based on computational intelligence have been proposed. An ANN-based load shedding technique was proposed by (Cheng-Ting Hsu, Chuang, & Chen, 2011). This technique considers the total generation, total load demand, and frequency drop rate as inputs and the minimum amount of load shedding as an output. They did a comparative study to show that the proposed load shedding is faster than the conventional technique. Other applications of ANN for shedding the optimal load in the isolated power system are reported by (Hooshmand & Moazzami, 2012). They use a 39-bus New England power system to verify the operation of this technique. From the simulation results, it can be clearly seen that the proposed technique can stabilize the power system by shedding the optimal load. To increase the reliability of Taiwan's power system, an ANN-based load shedding technique was proposed in (C-T Hsu, Kang, & Chen, 2005). The simulation results showed that the proposed technique can shed the exact amount of load, making it suitable for real-time applications. (Javadian, Haghifam, Bathaee, & Firoozabad, 2013) proposed an ANN-based load shedding technique to protect the DG-based distribution network from severe faults and disturbances. They split the distribution network into several zones, each of it capable of operating in islanding mode. Despite the advantages of ANN over conventional techniques, research has proven that ANN will not give accurate results for cases not included in the training process.

(Sallam & Khafaga, 2002) proposed a new fuzzy UFLS technique for islanded micro-grid. This technique is dynamic and robust in regulating frequencies in different cases. Using the fuzzy logic application to prevent the voltage collapse by shedding the optimal load is reported by (Sasikala & Ramaswamy, 2011). It was verified on IEEE 14, 30, and 57-bus systems. The simulation results confirmed that the proposed technique can be successfully implemented on a system of any size. (Mokhlis, Laghari, Bakar, & Karimi,

2012) proposed a new fuzzy logic based UFLS technique for islanded distribution network that is able to restore the frequency as soon as possible. It uses frequency, the rate of change of frequency, and load priority to do this.

The GA is also applicable in some load shedding problems. (Sanaye-Pasand & Davarpanah, 2005) proposed a genetic algorithm application for load shedding technique. It was verified on an IEEE 30-bus system. Another GA-based load shedding technique to minimize the amount of load shed is proposed in (Chen et al., 2011). A comparative simulation study between the proposed and conventional techniques was performed to confirm the ability of GA-based technique in shedding optimal loads.

Furthermore, an optimal load shedding technique based on the PSO method is reported by (Amraee, Mozafari, & Ranjbar, 2006) to determine the maximum loading point. The technique was verified on an IEEE 14-bus system. A comparative simulation study between PSO and GA methods was also performed, and it was clearly shown that the UFLS technique based on the PSO method can find the optimal solution more quickly compared with genetic algorithm method. (Sadati, Amraee, & Ranjbar, 2009) is another research involving the usage of a particle swarm-based-simulated annealing optimization method to provide long-term voltage stability. The most important feature of the proposed method is its capability to determine the global optimum solution within a smaller number of iterations. (Ketabi & Fini, 2017) proposed an UFLS technique based on the forecast of the minimum frequency. In this technique, the system frequency samples are taken after disturbance; then, PSO method is used to forecast the minimum frequency and shed the required loads.

The overall summary of inertia and frequency control techniques proposed in literature is shown in Table 2.2. It can be seen that the conventional, adaptive, and computational intelligence UFLS techniques have over-shedding or under-shedding problems. In fact,

these problems occur due to the fixed priority shedding loads. For this reason, (Laghari et al., 2015) proposed a Fixed and Random Priority Load Shedding (FRPLS) technique to shed the optimal combination of loads. However, this technique need time to select the optimal combination of shedding loads.

Table 2.2: Summary of UFLS techniques proposed in the literature

UFLS technique	References	Method used in UFLS technique	Priority of shedding loads	The ability to shed the appropriate loads	Execution time to select the appropriate loads	Effect of network configuration on the UFLS technique
Conventional UFLS technique	(Tang et al., 2013; Zin et al., 2004)	Predetermined frequency steps	Fixed priority load shedding	Suffers from over-shedding or under-shedding loads	No time consumed (fixed priority load)	The predetermined steps need to be selected according to the network configuration
Adaptive UFLS technique	(Marzband et al., 2016; Rudez & Mihalic, 2011)	Swing equation				This technique does not depend on network configuration
Computational Intelligence Based Load Shedding Techniques	(Mokhlis et al., 2012; Sallam & Khafaga, 2002)	Fuzzy logic method	Fixed priority load shedding	Suffers from over-shedding or under-shedding loads	No time consumed (fixed priority load)	These techniques need to be trained to use operational network data, therefore it depends on network configuration
	(Sanaye-Pasand & Davarpanah, 2005)	Genetic algorithm method				
	(Amraee et al., 2006)	PSO method				
	(Hooshmand & Moazzami, 2012; Javadian et al., 2013)	ANN method				
Fixed and random priority load shedding technique (FRPLS)	(Laghari et al., 2015)	Swing equation	Fixed and random priority load shedding	Appropriate shedding loads	0.5 second (ten random priority loads and two fixed priority loads)	This technique does not depend on the network configuration

2.6 Summary

This chapter provided an overview of distributed generation, detailing various types, global, and local trends of hydropower and solar PV. The major topic addressed throughout this chapter is the frequency issues experienced in islanded distribution network due to the high penetration level of RESs. To overcome these issues, various inertia and frequency regulation controllers were developed for RESs.

Based on literature, it was observed that most of existing inertia controller proposed to increase the inertia of the distribution networks using only wind turbine technology and ESS. Furthermore, most frequency regulation controllers may be ineffective for islanded distribution systems, as islanded system is not as stable as grid-connected system. Therefore, many researchers proposed the usage of batteries to provide a stable energy reserve for frequency regulation services. However, most of these techniques used a battery to provide primary frequency controller without taking into account the secondary controller. In addition, this chapter presented several types of load shedding technique. It can be seen that the existing load shedding techniques experience an over-shedding problem due to fixed priority shedding loads. Thus, this research will propose a new UFLS technique for shedding optimal combination of loads.

CHAPTER 3: RESEARCH METHODOLOGY

3.1 Introduction

This chapter details the modelling of the proposed frequency control scheme using PSCAD and MATLAB software. This scheme consists of the inertia controller, frequency regulation controllers, and UFLS controller. This chapter discusses the modelling of Centralized Control System (CCS), which is used to coordinate the operation of frequency control scheme and grid reconnection process. It consists of a reconnection controller, the frequency management unit, and UFLS controller.

3.2 Overview of the Overall Proposed System

This research proposes a frequency control scheme for islanded distribution network with high PV penetration. Figure 3.1 shows the interaction between (A) distribution network, (B) proposed frequency control scheme, (C) Centralized Control System, (D) Phase synchronization controller, and (E) Voltage synchronization controller. Each part will be discussed in the following sub-sections.

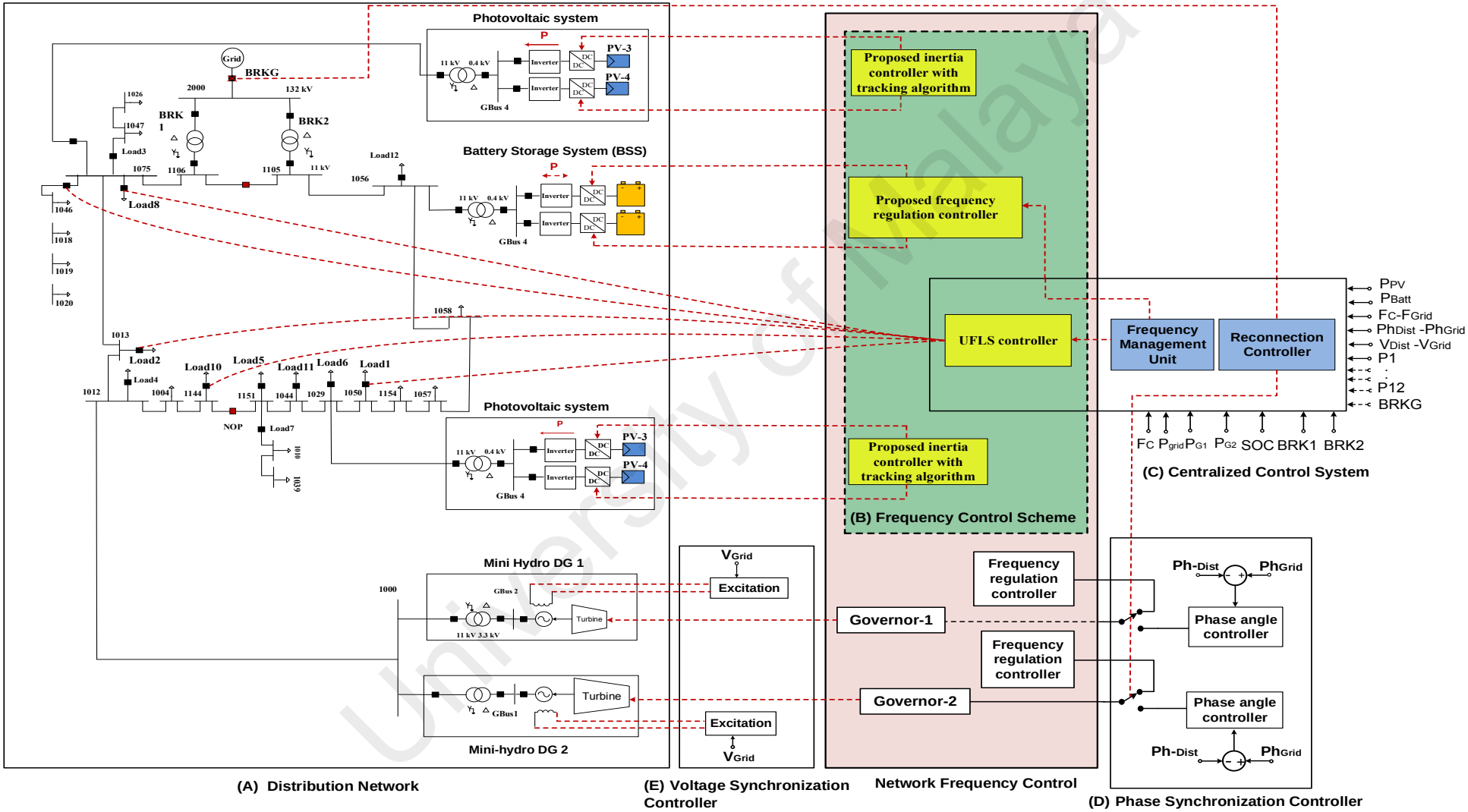

Figure 3.1: The schematic diagram of control architecture for frequency control scheme

3.2.1 Proposed Frequency Control Scheme

The frequency control scheme proposed in this thesis is developed for distribution networks with high PV penetration. After the distribution network is islanded from the main grid, the frequency control scheme can be used to restore the network's frequency. As shown in Figure 3.1 b), the frequency control scheme consists of an inertia controller, frequency regulation controllers, and under-frequency load shedding controller. The operation of frequency control scheme is discussed below.

Immediately after islanding, the inertia controllers start releasing reserve power from PV units to improve the overall network inertial response and reduce the rate of change of frequency. After 10 seconds, a primary frequency controller of Battery Storage System (BSS) is initiated in the parallel with governor system of mini-hydro governors to stop the frequency deviation and restore it within an acceptable level. After that, a secondary frequency controller of BSS is used to offset the frequency deviation by synchronizing the frequency of islanding distribution network with the main grid; this controller is necessary for the reconnection operation. According to Malaysian grid code, the secondary controller starts after 30 seconds, and continue for 30 minutes. When the proposed inertia and frequency regulation controllers fail to recover the system's frequency, a proposed UFLS controller activates to shed the optimal combination of loads. Since the formation of an island operation is only temporary, a reconnection process with main grid is necessary. When the synchronization requirements (frequency, voltage, and phase) are achieved, the islanded network is reconnected with the main grid.

3.2.1.1 Inertia Controller

The solar PV arrays normally work on the maximum power point. Therefore, integrating more PV units will reduce the inertia response, which leads to increased rate of change of frequency. Therefore, it necessary to operate the solar PV below the maximum power

point to keep some amount of reserve power that can be released at disturbance events. The main parts of inertia controller are shown in Figure 3.2. It consists of de-loading process, inertia response, and PV voltage controller. The parameters of the inertia controller are included in Appendix A, section A.9.

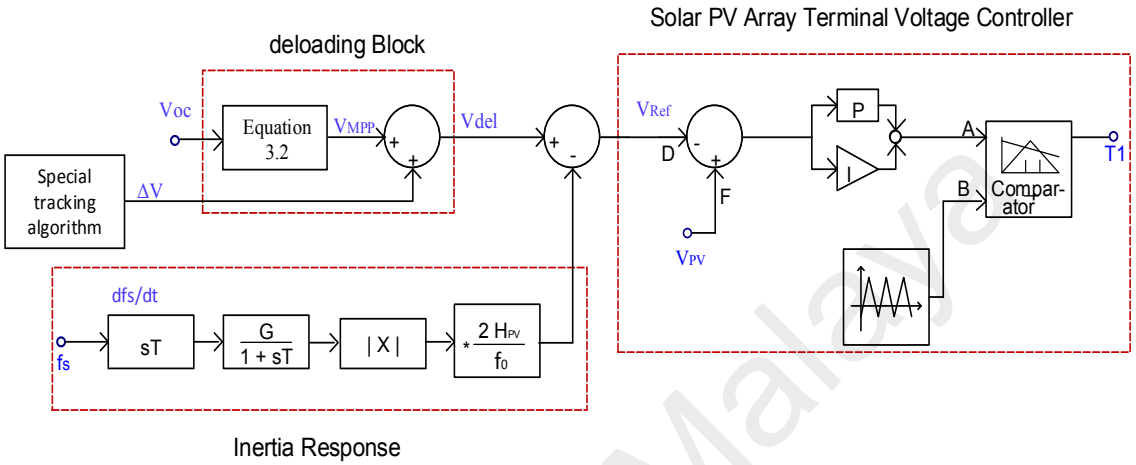

Figure 3.2: Block diagram of inertia controller

Like most inertia controllers applied in a variable speed wind turbine, the PV generation can operate below their maximum power point to maintain power reserves required for an inertial response, which can be achieved by increasing the PV voltage. In this block diagram, the deloading voltage (V_{del}) is calculated by adding a specific value ΔV to the maximum power point voltage (V_{MPP}), as expressed in Equation 3.1.

$$V_{del} = V_{MPP} + \Delta V \tag{3.1}$$

Where ΔV is a specific value determined by a special tracking algorithm as shown in Figure 3.3, and V_{MPP} is the maximum power point voltage calculated using open circuit voltage technique (OCV), as per equation 3.2:

$$V_{MPP} = K \times V_{OC} \tag{3.2}$$

Where V_{OC} is the open circuit voltage of reference module, and K is a constant estimated to be within the range of (0.7–0.80) (Zhou et al., 2010).

As shown in Figure 3.3, special tracking algorithm is used to track the PV generation unit below the Maximum Power Point (MPP) based on the deloading factor (*X*%). A fixed value of deloading factor is set in this research.

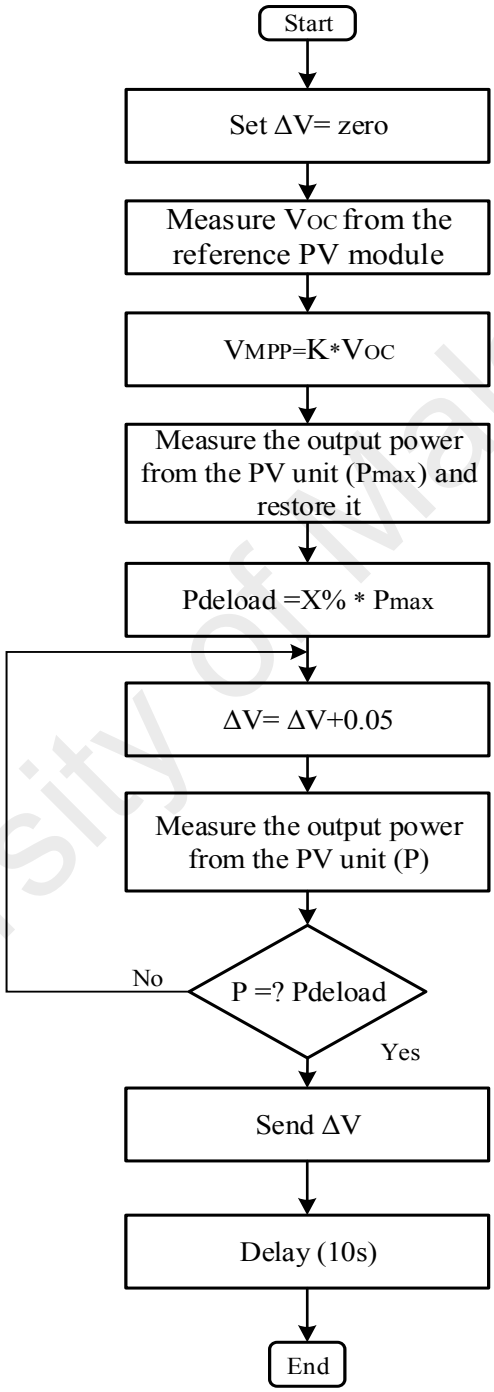

Figure 3.3: Block diagram of special tracking algorithm

Figure 3.4 is used to illustrate the operation of inertia controller and de-loading technique of PV generation, which represents the relationship between PV voltage and power,

where during grid-connected mode, the solar PV is operating on point (2) instead of point (1). When the system's frequency starts to decrease due to islanding (or other factors), the inertia response block increases the generated power based on the rate of change of frequency and the virtual inertia constant (H_{PV}) values. This is done by shifting the operating point from point (2) towards point (1). After that, the reference voltage (V_{ref}) is subsequently compared with its actual value (V_{PV}), and the error is sent to a PI controller, which generates switching signals to control the converter.

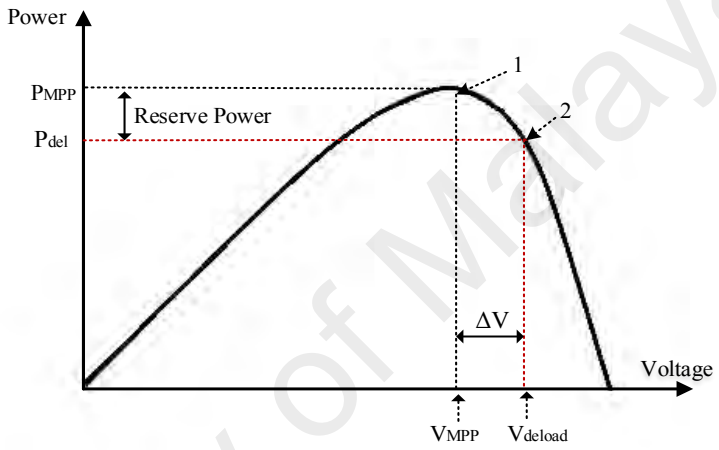

Figure 3.4: Photovoltaic system P-V curve illustrates the de-loading technique

3.2.1.2 Frequency Regulation Controllers

Normally, traditional power generations such as hydro and coal-fired units are used to provide frequency regulation service for the power system. However, the traditional frequency regulation units report various limitations, especially in power systems with a high penetration level of renewable energy sources. Traditional frequency regulation units respond slowly, and its climbing rates are quite low.

On the contrary, BSS responds quickly (in ms) with two-way regulation. The trend of using BSS as a regulation unit is not only related to technical characteristics, but also in terms of the economy, where the prices of future BSS tend to significantly decrease. Due to this, a frequency regulation controller is combined with a BSS to regulate frequency

services for islanded distribution network, as shown in Figure 3.5. The parameters of frequency regulation controller are included in Appendix A, section A.8.

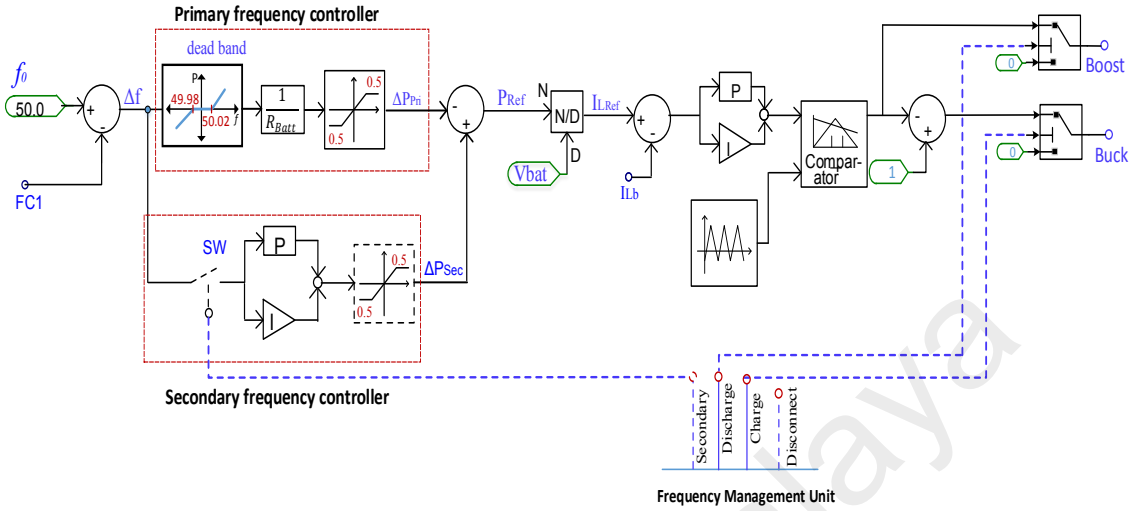

Figure 3.5: Proposed frequency regulation controller

The main feature of the proposed frequency regulation controller is its ability to provide both primary and secondary frequency services for the distribution network. When any disturbance occurs, the primary frequency control is directly initiated and continue for few seconds to stop further frequency deviation and bring the frequency back to an acceptable value (Díaz-González et al., 2014). The relation between frequency deviation and change in the active power can be expressed as:

$$\Delta P_{Prim} = R_{Batt} \times \Delta f \tag{3.3}$$

Where R_{Batt} is the frequency droop given in MW/Hz.

Despite the ability of primary frequency control to bring the frequency back to an acceptable value, it still reports errors due to proportional control. Primary control can thus only stop further deviations from the nominal frequency, but the frequency cannot be brought back to the nominal value. Therefore, a second level control should be available to compensate for the remaining active mismatch. This controller is called the secondary frequency controller, or Load Frequency Control (LFC). According to

Malaysian grid code, the LFC starts after 30 seconds, and return the frequency to its nominal value within 30 minutes.

As shown in Figure 3.4, the summation of primary and decentralized secondary frequency controller output is divided by battery voltage to determine the reference current. The reference current is then injected to the PI controller, which provide suitable control signals required for charging and discharging the battery via a bidirectional DC-DC converter. Two BSS were used in this work, where each can provide 0.5 MW for primary frequency control and 0.5 MW for secondary frequency control. A frequency management unit was developed to control the BSS.

3.2.1.3 Proposed UFLS Technique

From the literature, it is clear that the existing UFLS techniques are limited by over-shedding or under-shedding loads, due to fixed load priorities. Therefore, a Fixed and Random Priority Load shedding (FRPLS) technique is proposed in (Laghari et al., 2015) for shedding the optimal combination of loads. However, this technique takes too long, since all possible combination of loads needs to be accounted for in the calculations. Due to this fact, we used three metaheuristic methods with the UFLS technique to shed the optimal combination of loads from islanded distribution network; Binary Genetic Algorithm (BGA) method, Binary Particle Swarm Optimization (BPSO) method, and Binary Evolutionary Programming (BEP) method.

The most important advantages of the proposed load shedding technique are (A) it is designed to shed the optimal combination of loads for under frequency events, and (B) it is designed to restore the distribution network frequency after it gets islanded. In this technique, the application of metaheuristic methods is used to select the optimal combination of loads needed to be shed from ten-random priority loads and two-fixed priority loads.

The term ‘fixed priority’ is related to the loads separated from the network sequentially based on lookup table, while the term ‘random priority’ is related to the loads that can be shed randomly without any sequence. Figure 3.6 shows the main units of the proposed UFLS technique; (A) Frequency Calculator Unit (FCU), (B) Imbalance Power Calculator Unit (IPCU), and (C) Load Shedding Unit (LSU).

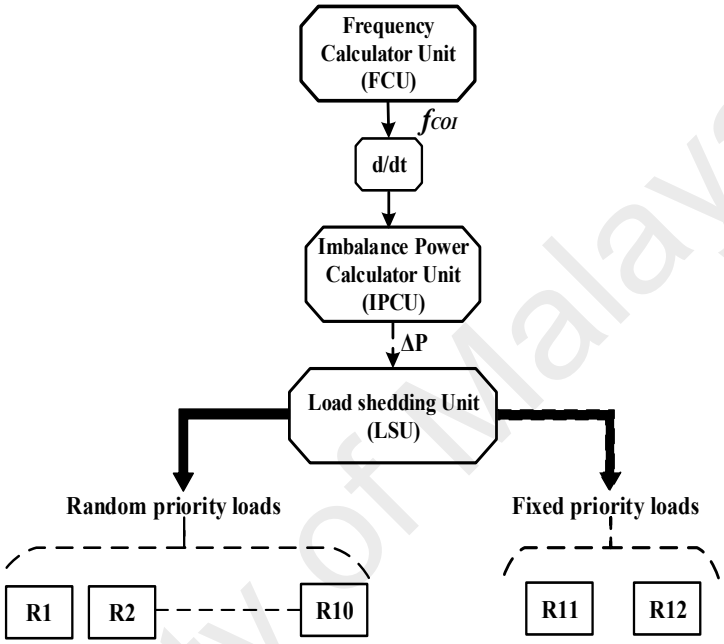

Figure 3.6: Flow chart of proposed load shedding technique

The UFLS technique proposed in this research is simulated by PSCAD/EMTDC and MATLAB software. The distribution network and load shedding technique runs under PSCAD, while the metaheuristic method is executed in MATLAB. When the UFLS technique is initiated due to islanding or imbalance events, PSCAD send the required data to MATLAB. After MATLAB optimized the process, it returns the optimal combination of loads to PSCAD to complete the shedding process. The interface between PSCAD and MATLAB is shown in Appendix A, section A.11.

(A) Frequency Calculator Unit (FCU)

The operation of FCU is shown in Figure 3.7. For the grid connected mode, the FCU use the grid frequency and send it to IPCU, while for the islanded mode, the FCU calculate

the value of f_{COI} based on Equation (3.4) (Terzija, 2006) and send it to IPCU. Furthermore, at every moment of time, the FCU checks the connection state of each generator. When any disconnection event occurs, a new equivalent value of f_{COI} will be calculated.

$$f_{COI} = \frac{\sum_{i=1}^{N} H_i f_i}{\sum_{i=1}^{N} H_i} \tag{3.4}$$

Where f_{COI} is center of inertia frequency (Hz); H_i is inertia constant of each generator (seconds); f_i is the frequency of each generator (Hz); N is the number of DGs.

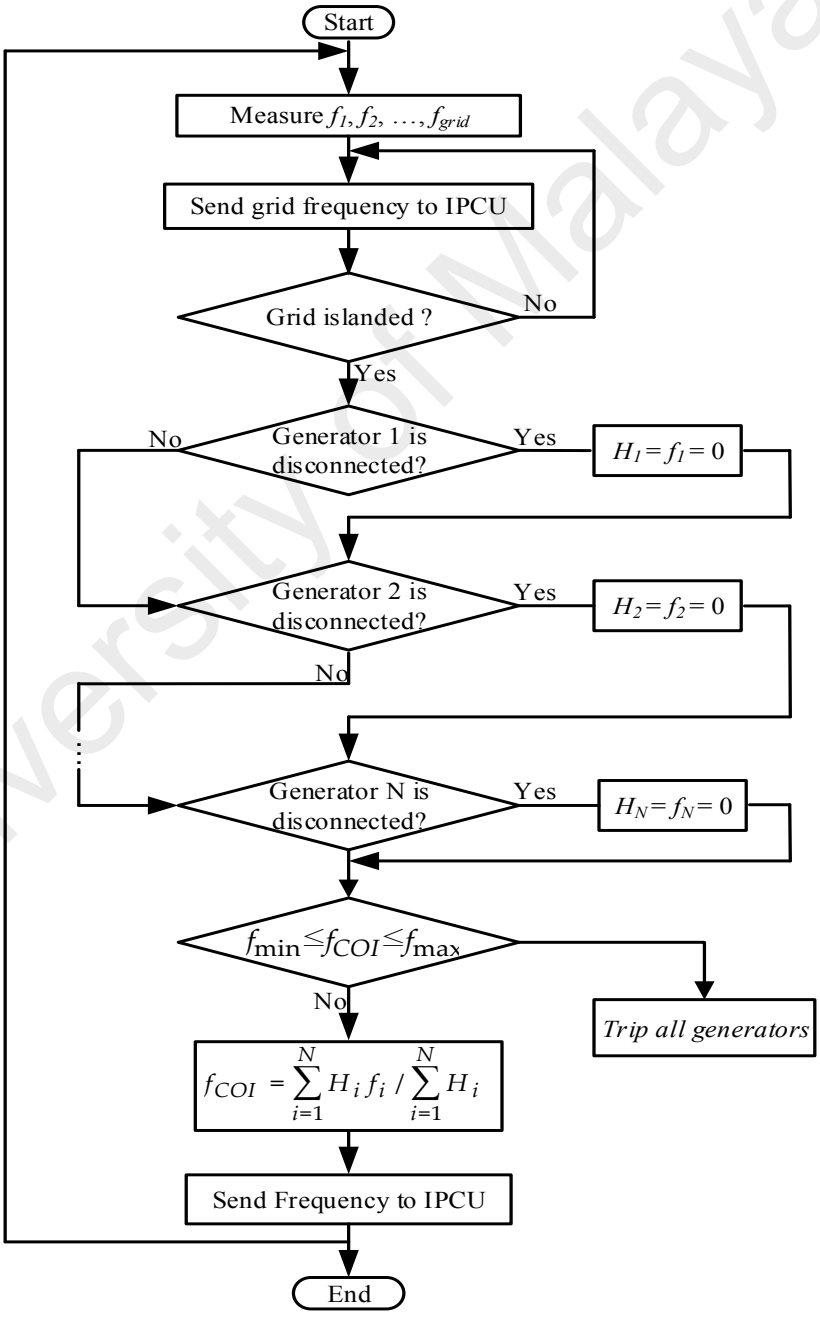

Figure 3.7: Flow chart of FCU

Besides frequency calculation, FCU provides a type of frequency protection for connected generators. It will check whether the value of f_{COI} lies within the frequency protection range. If the value of f_{COI} lies beyond that range, the protection relays will directly disconnect the generators from the network. Generally, the frequency protection range for each generator are based on the distribution network and generator types. According to the Malaysian distribution code, the protection frequency range is (47.5Hz – 52.5Hz). The PSCAD model of FCU is shown in Appendix A, section A.3.

(B) Imbalance Power Calculator Unit (IPCU)

Depending on the value of ROCOF received from FCU and breaker state of grid and DGs, the IPCU has two different strategies to determine the imbalance power, which are:

i Event Based

In this work, the IPCU algorithm is designed to follow the event based in three cases: (A) intentional islanding; (B) DG tripping; (C) irradiance change. For the islanding event, the imbalance power will be equal to the grid power, which is supplied to the distribution network. For the DG tripping event, the power imbalance will be equal to the output power of DG tripped from the network, while for irradiance change, the imbalance power will be calculated based on Equation (3.5):

$$\Delta P = P_{V0} - P_V \tag{3.5}$$

Where P_{v0} is the total PV power at the radiation change event, and P_v is the total PV power at 0.01 ms after radiation changing event.

ii Response Based

Response based occurs due to the sudden increment of load demand in the islanded distribution network. In this case, the load shedding amount is based on the disturbance value that can be estimated by the swing equation (Kundur et al., 1994)

$$\Delta P = \left(\left(2 \times \sum_{i=1}^{N} \frac{H_i}{f_n} \right) \times \frac{df_{COI}}{dt} \right) \tag{3.6}$$

Where ΔP is the imbalance power; H_i is the inertia constant of each generator (s); df_{COI}/dt is the rate of change of center of inertia frequency (Hz/s); N is the number of rotating based DG; f_n is the nominal frequency (Hz). In order to determine the amount of load to be shed for event or response based strategies, the same equation will be followed:

$$Load\ shedding\ amount = \Delta P - TR \tag{3.7}$$

Where the TR is the total reserve power, and can be calculated by Equation (3.8).

$$TR = \sum_{i=1}^{N} Max.P_{Gi} \; - \; \sum_{i=1}^{N} P_{Gi} \tag{3.8}$$

Where $Max\ P_{Gi}$ is the maximum generator power of ith DG; P_{Gi} is the generator power of ith DG; N is the number of DGs. Finally, the PICM send the load-shed amount to the LSU via a communication link to shed the optimal load combination. The PSCAD model of IPCU is shown in Appendix A, section A.4.

(C) Load Shedding Unit (LSU)

The LSU is the most important part of the proposed UFLS technique. It reports the preference of the proposed technique over existing techniques. As shown in Figure 3.8, when the load shedding value exceeds the total random priority loads, the LSU directly shed all random priority loads and start shedding from fixed priority loads. Otherwise, one metaheuristic method is initialized to shed the optimal combination of loads. Since the PSCAD//EMTDC software does not provide a toolbox for metaheuristic methods, the proposed UFLS technique is modelled in MATLAB and integrated with PSCAD. The PSCAD model of the FCU is shown in Appendix A, section A.5.

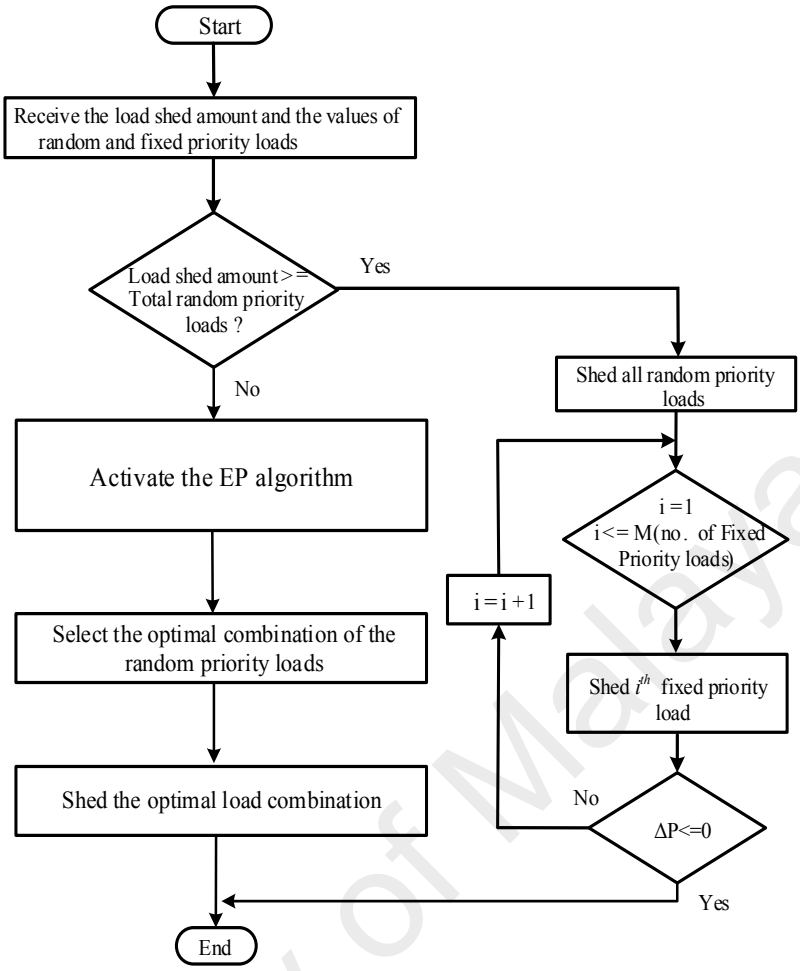

Figure 3.8: Flow chart of the LSU

i Implementation of Binary Evolutionary Programming (BEP)

For the past two decades, the interest in solving real-world search problems by Stochastic optimization techniques and metaheuristic methods has invariably increased. These methods use some biological principles to search for the best solutions. The Evolutionary Programming (EP) method is regarded as a special case of Evolutionary Computation (EC) methods, which was first utilized by Dr. Fogel in 1960.

It is proposed that a BEP method be used to determine the optimal combination of loads that needs to be shed from the distribution network, as shown in Figure 3.9. Similar to other evolutionary methods, the BEP is made up of five phases; initialization, fitness, mutation, recombination, and selection.

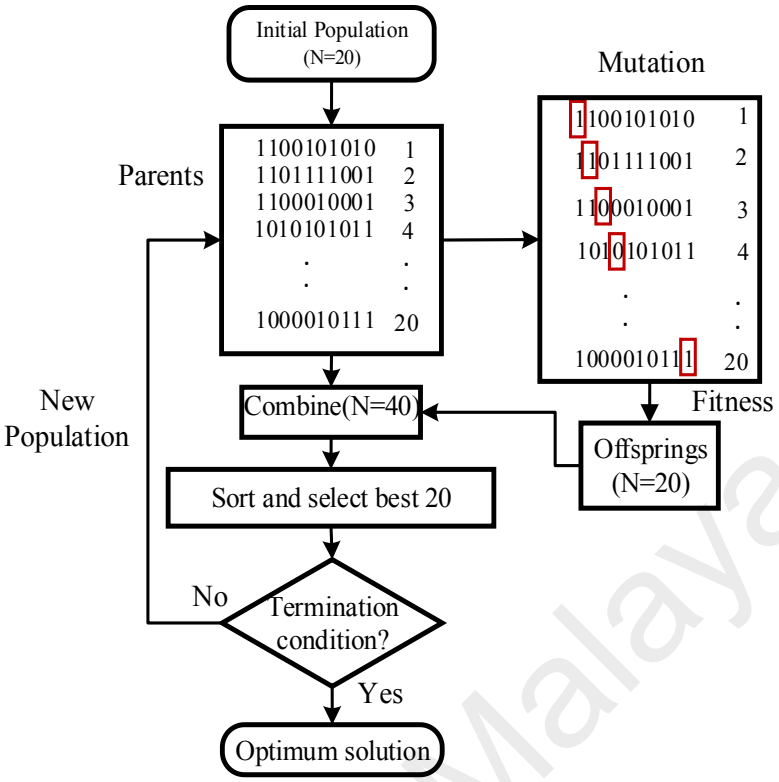

Figure 3.9: Flow chart of BEP method

➢ **Initialization**

In this phase, an initial population of (x_i) chromosomes will be randomly generated, as shown in Table 3.1, where each chromosome represents the connection status of 10 random priority loads. Figure 3.10 shows the random and fixed priority loads connection with the distribution network.

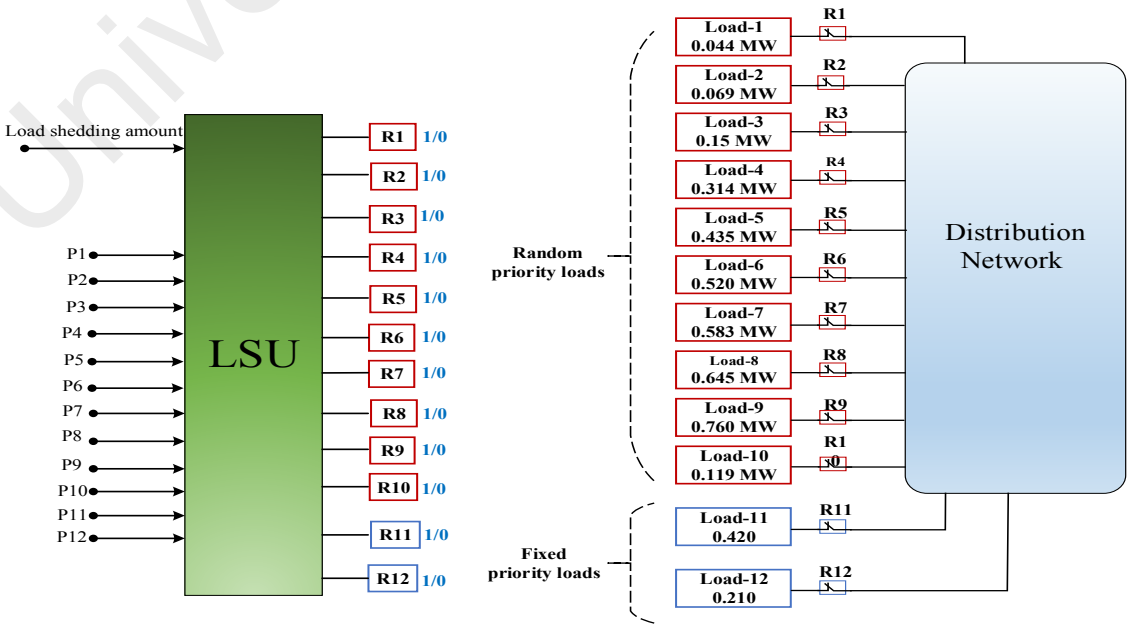

Figure 3.10: LSU connected with fixed and random priority loads

- **Fitness**

This phase involves calculating the fitness value for each chromosome using the fitness function:

$$f_i = Min(E_i) = \left| Load\ shed\ amount - \sum P_{i-combination} \right| \quad (3.9)$$

Where $\sum_{Pi\text{-}combination}$ is the summation of loads power for each chromosome.

To illustrate the calculation of fitness values, an example of 1 MW load shedding amount is considered, as shown in Table 3.1, where the number 1 means that the load is connected to the distribution network, while the number 0 means that the load is separated from the distribution network.

Table 3.1: The initial population and fitness values for individual

x_i	x_{i10}	x_{i9}	x_{i8}	x_{i7}	x_{i6}	x_{i5}	x_{i4}	x_{i3}	x_{i2}	x_{i1}	∑ Pi-combination (MW)	*(fi)*
x_1	1	1	0	1	0	1	0	1	0	1	$P_1+P_3+P_5+P_7+P_9+P10=2.091$	1.091
x_2	0	1	0	1	0	1	0	1	1	1	$P_1+P_2+P_3+P_5+P_7+P_9=2.041$	1.041
x_3	0	0	0	0	1	0	0	1	1	1	$P_1+P_2+P_3+P_6=0.783$	0.217
x_4	0	0	0	1	1	0	0	0	1	0	P2+P6+ P7=1.172	0.172
-						-					-	-
-						-					-	-
-						-					-	-
x_{20}	0	0	0	0	0	1	1	1	1	1	$P_1+P_2+P_3+P_4+P_5=1.012$	0.012

- **Mutation**

The mutation is an operator used to avoid the local optima by preventing the generations from becoming similar to one another. In this phase, one bit in each chromosome is checked for possible mutation, as shown in Table 3.2 (Aman, Jasmon, Naidu, Bakar, & Mokhlis, 2013). This is done by generating a random number in the range of (0-1), and if this number is less than or equal to the mutation probability L, then the bit state will be changed. The probability of a mutation for each bit is 1/L, where L is the number of bit in each chromosome.

Table 3.2: The binary mutation operation used in BEP method

Generation	x_i	x_{i10}	x_{i9}	x_{i8}	x_{i7}	x_{i6}	x_{i5}	x_{i4}	x_{i3}	x_{i2}	x_{i1}
First generation											
	x_1	1	1	0	1	0	1	0	1	0	1
	x_2	0	1	0	1	0	1	0	1	1	1
	x_3	0	0	0	0	1	0	0	1	1	1
	-	-	-	-	-	-	-	-	-	-	-
	x_{10}	1	0	0	0	0	1	1	0	0	1
	x_{11}	1	1	1	0	0	1	1	0	0	1
	x_{12}	1	0	1	0	1	0	1	0	1	0
	-	-	-	-	-	-	-	-	-	-	-
	x_{20}	0	0	0	0	0	1	1	1	1	1
Second generation	x_1	1	1	0	1	0	1	0	0	0	1
	x_2	0	0	0	1	0	1	0	1	1	1
	x_3	0	0	1	0	1	0	0	1	1	1
	-	-	-	-	-	-	-	-	-	-	-
	x_{10}	1	1	1	1	1	0	0	0	0	1
	x_{11}	0	0	0	0	0	1	1	0	0	1
	x_{12}	1	0	0	0	0	1	1	1	1	1
	-	-	-	-	-	-	-	-	-	-	-
	x_{20}	1	0	1	1	1	1	1	1	1	0

- **Combined and Selection**

In this phase, the offspring produced from the mutation phase and parents are combined within the same competition pool. After that, the survivals are ranked in an ascending order based on fitness value. Then, the first half is selected to be the parents of the next generation. This operation continues until the convergence condition is achieved, as shown in the following equation:

$$fitness_{max} - fitness_{min} \leq 0.005 \quad (3.10)$$

Finally, the BEP technique selects the optimal load combination that has a minimum fitness value. After that, the LSU sends the signal to the breakers to shed the optimal combination of loads. The delay time that includes the measurements, communication, and CB operation time is assumed to be 100 ms, based on practical considerations (Laghari et al., 2015).

ii Implementation of Binary Genetic Algorithm (BGA)

The binary genetic method is one of the metaheuristic search methods based on the evolutionary ideas of natural selection and genetics (Oluwadare, Iwasokun, Olabode, Olusi, & Akinwonmi, 2016). Different from the evolutionary programming, the BGA is mainly based on crossover operator in finding the optimal solution, as shown in Figure 3.11.

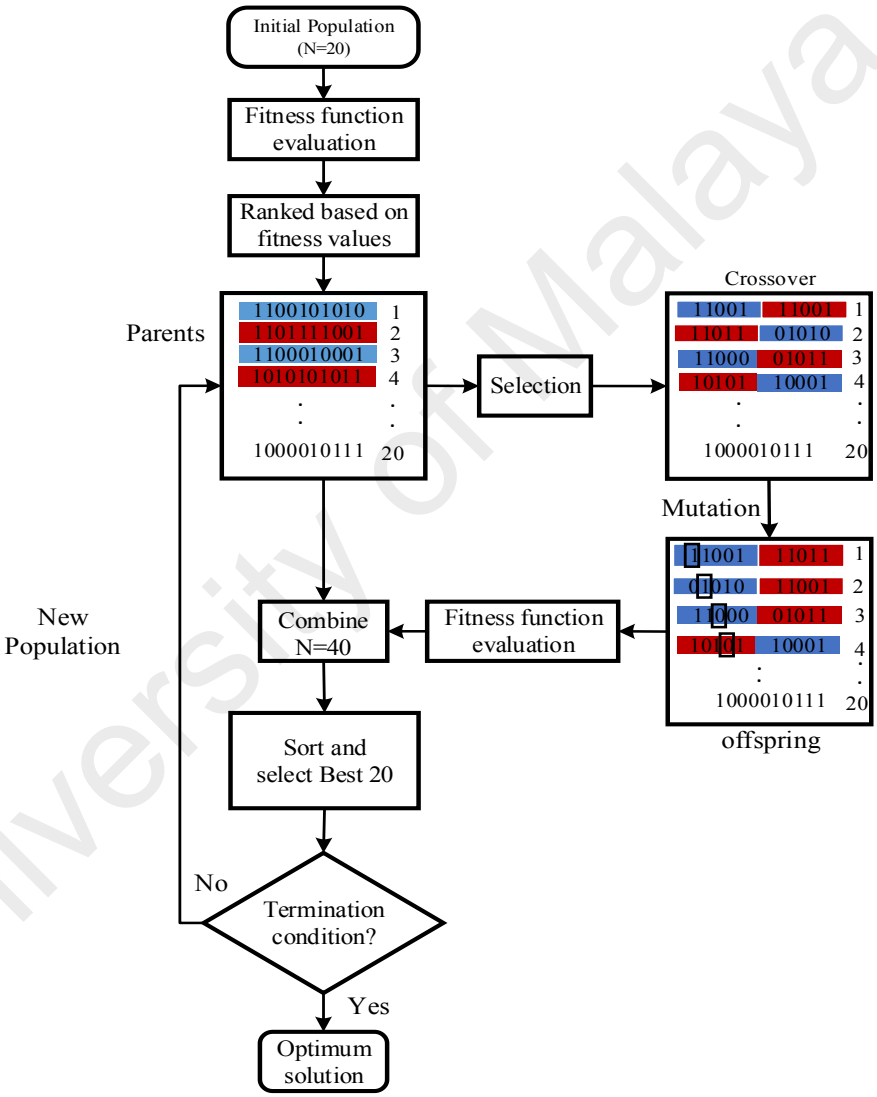

Figure 3.11: Flow chart of BGA method

The BGA method is very similar to the BEP. However, an initial population of 20 chromosomes is randomly generated in BGA, which will then be ranked depending on their respective fitness value. After that, a crossover is performed between each consecutive pair of the parent's chromosomes. Generally, the crossover is made up of

many types, such as single-point crossover, two-point crossover, and uniform crossover (Thakur & Singh, 2014). In this work, a single point crossover is used, as per Figure 3.12.

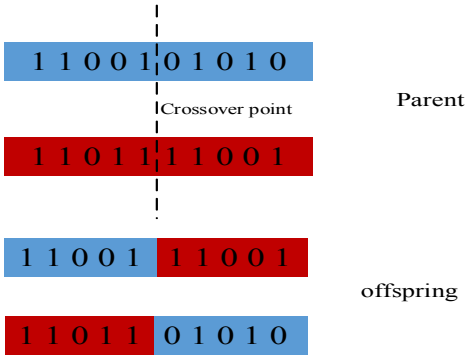

Figure 3.12: Single point cross over used by BGA optimization method

iii Implementation of FRPLS Technique Proposed in (Laghari et al., 2015)

When the LCU receive the imbalance power, it generates all possible combinations of ten random priority loads. This research proposes ten loads as a random priority loads, accordingly the number of combinations of loads will be (1023) based on Equation (3.11). After that, the algorithm of LCU calculates the fitness value for all combinations of loads, and select the combination with lesser fitness value to be shed from the distribution network.

$$Number\ of\ combination = 2^n - 1 \qquad (3.11)$$

Where n is the number of random priority loads. Table 3.3 shows the possible combinations of ten random priority loads when the imbalance power is 0.15 MW.

Table 3.3: The initial population and fitness values of the FRPLS technique

No.	Load combinations	∑ Pi-combination (MW)	Fitness=| load shedding-∑ Pi-combination |
1	0000000001	P_1=0.044	0.106
2	0000000010	P_2=0.069	0.081
3	0000000100	P_3=0.15	0
4	0000001000	P_4=0.314	0.164
5	0000010000	P_5=0.435	0.285
-	-	-	-
11	0000000011	P_1+P_2=0.113	0.037
-	-	-	-
1023	1111111111	P_1+P_2+ P_3 +P_4+P_5 +P_6+P_7+ P_8 +P_9+P_{10}=3.639	3.489

Best combination

Minimum value

iv Implementation of Binary Particle Swarm Optimization (BPSO)

The PSO is a parallel intelligent method that consists of particles, which search in a multidimensional space to find the optimal solution. The particle position and velocity of are adjusted according to its own experience and other particles experience, where this process is expressed by equations (3.12) & (3.13) (Eberhart & Shi, 2000).

$$v_i{}^{n+1} = w \times v_i{}^{n} + c_1 \times r_1 \ (p_i{}^{n} - x_i{}^{n}) + c_2 \times r_2 \ (p_g{}^{n} - x_i{}^{n}) \tag{3.12}$$

$$x_i{}^{n+1} = x_i{}^{n} + v_i{}^{n+1} \tag{3.13}$$

where i is the number of particles; n, w are the generation number and the inertia weight respectively; $x_i{}^{n}$, $v_i{}^{n}$, $p_i{}^{n}$ are the position, velocity, and particle best position; $p_g{}^{n}$ represents the global best position; c_1, c_2 are the cognitive and social components, respectively; r_1, r_2 are uniform random numbers between 0 and 1. In the BPSO, the global and previous best positions are mutated to a manner similar to the real PSO method. The main difference between the BPSO and the real PSO is that the component of each particle is represented by a binary value of 0 or 1, where this value is updated according to equation (3.14).

$$\begin{cases} x_{id}{}^{n+1} = 1 \ if \ rand \ < s(v_{id}{}^{n+1}) \\ x_{id}{}^{n+1} = 0 \ if \ rand > s(v_{id}{}^{n+1}) \end{cases} \tag{3.14}$$

Where the sigmoid limiting transformation is expressed by:

$$s(v_{id}{}^{n+1}) = \frac{1}{\left(1 + e^{-v_{id}{}^{n+1}}\right)} \tag{3.15}$$

Where $x_{id}{}^{n+1}$ and $v_{id}{}^{n+1}$ represent the dth component of $x_i{}^{n+1}$and $v_i{}^{n+1}$, respectively; rand represent random numbers uniformly distributed between 0 and 1

3.2.2 Modelling of Centralized Control System (CCS)

CCS plays an important role in managing the operation of frequency control scheme, shedding loads and reconnecting grids. It receives/transmit the signal from/to the grid and the islanded distribution network via a fast and reliable communication link. The CCS

consists of frequency management unit, reconnection controller, and UFLS controller. The model of UFLS technique is discussed in subsection (3.2.1.1). The following sections will discuss the frequency management unit and reconnection controller.

3.2.2.1 Frequency Management Unit

The frequency management unit is mainly designed to manage the operation of frequency control scheme. The flowchart shown in Figure 3.13 illustrate its basic function, while the PSCAD model of frequency management unit is shown in Appendix A, section A.6.

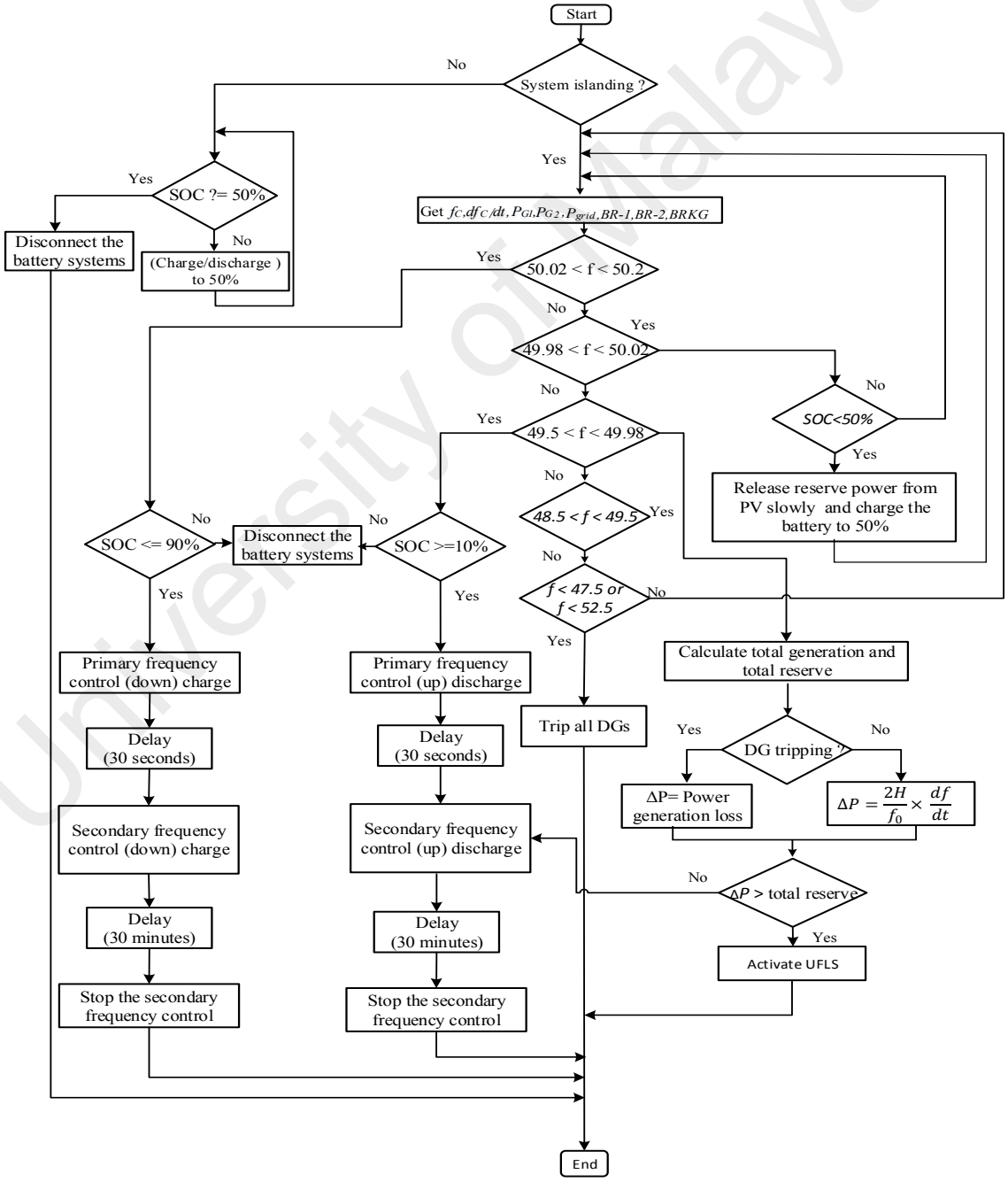

Figure 3.13: Flowchart of frequency management unit

(A) Control Strategies of Frequency Management Unit in Grid Connected State

In this state, the battery state of charge (SOC) is continuously monitored. Based on this value, the frequency management unit selects the battery charging or discharging mode. For example, when the SOC value less than 50%, the frequency management unit activates the charging mode. This charging mode continue until the battery SOC reach 50% then the frequency management unit disconnects the battery. The same procedure is followed when the battery SOC is more than 50%, while this time the discharging mode is activated. Normally SOC value is set to 50% to give an equal reserve power for under and over frequency regulation.

(B) Control Strategies of Frequency Management Unit in Islanded State

In this state, the main functions of frequency management unit are summarized in the followings:

i Down regulation by charging the battery

This function initiates the frequency regulation controller, when the distribution network frequency exists within (50.02< f <50.2 Hz) and the SOC of battery is less than 90%.

ii Up Regulation by Discharging the Battery

This function initiates the frequency regulation controller, when the distribution network frequency exists within (49.5 Hz < f < 49.98 Hz) and the SOC of battery more than 10%.

iii Battery Disconnection

This function is activated when the SOC of the battery is more than 90% or less than 10%.

iv Under-Frequency Load Shedding

This function is activated when the distribution network frequency is less than 49.5 Hz and the active power reserve of mini hydro and battery system is insufficient to compensate the power deficit.

v Charging the Battery

This function is activated when the islanded distribution network is operating in normal condition (49.98 Hz < f < 50.02 Hz). In this situation, the frequency management unit sends a control signal to charge the battery systems by using the solar PV reserve power, which is released slowly so as not to increase the frequency value.

vi Trip all Distribution Generators

This function is activated when (f > 52.5 Hz or f < 47.5 Hz), then the frequency management unit sends a command to separate all DGs.

In this research, the frequency bands are chosen based on Tenaga National Berhad technical guide book (TNB, 2013).

3.2.2.2 Reconnection Controller

The formation of an island is only temporary, and it must be reconnected to the main grid once the fault has been identified and removed. For this reason, the island must remain synchronized with the main grid at all times even when it is electrically disconnected. It is a crucial issue, and need a governor and an excitation controller to regulate the voltage, frequency, and voltage angle of the island so that it remains within the permissible limit. (Best, Morrow, McGowan, & Crossley, 2007; Caldon, Stocco, & Turri, 2008) utilized a Phasor Measurement Unit (PMU) to keep the island synchronized with the main grid. The reference signal from the grid is compared with the signal in the island and sent to the controller to reduce the difference between the two signals.

The practical technique is to reconnect manually based on the indication of synchroscope. However, the manual reconnection needs to be done by substation personnel, which could delay operations. Therefore, a fast reconnection controller is proposed in this research, which utilizes the deadline charging procedure. By using this procedure, a breaker at one

end of a tripped line is reclosed first to allow the line to be re-energized. The breaker at the other end of the line is reclosed after synchronism between the two has established. The flowchart shown in Figure 3.14 illustrates the reconnection controller operation. When an island is detected, the voltage and frequency response is first controlled to their synchronization limit. After the fault is cleared and the island response is stabilized, the dead line charging procedure is initiated.

As indicated in Figure 3.15, for the dead line charging, breaker BRK1-BRK4 are closed. Subsequently, the bus section breaker, which connects feeder 1105 and 1106, is disconnected. After a specific interval of time, the phase controller receives the phase measurements at both ends of BRKG to minimize the phase difference to achieve a nearly zero value. Finally, when the synchronization requirement of frequency, voltage, and phase angle on both ends are fulfilled, the reconnection is issued by closing BRKG. Details for phase and voltage synchronization controllers are discussed in the following sub-sections. The FCU PSCAD model is shown in Appendix A, section A.7.

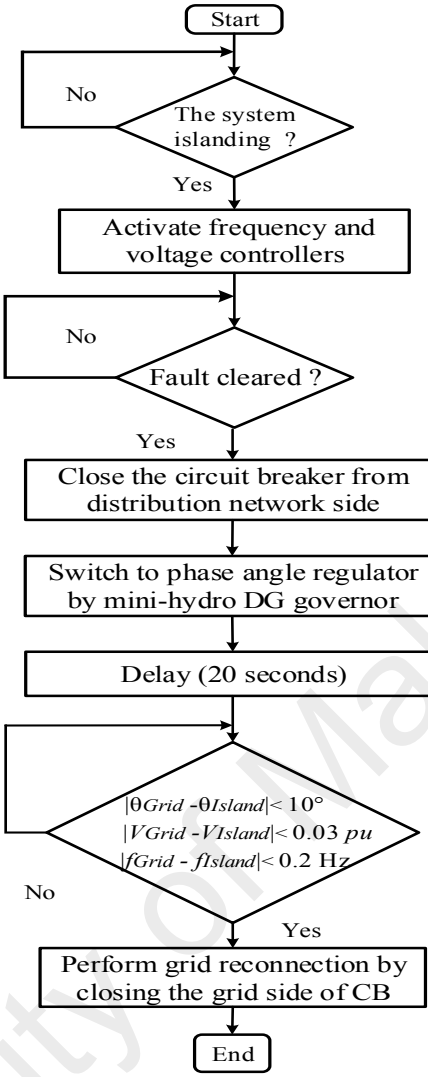

Figure 3.14: Flow diagram of reconnection controller

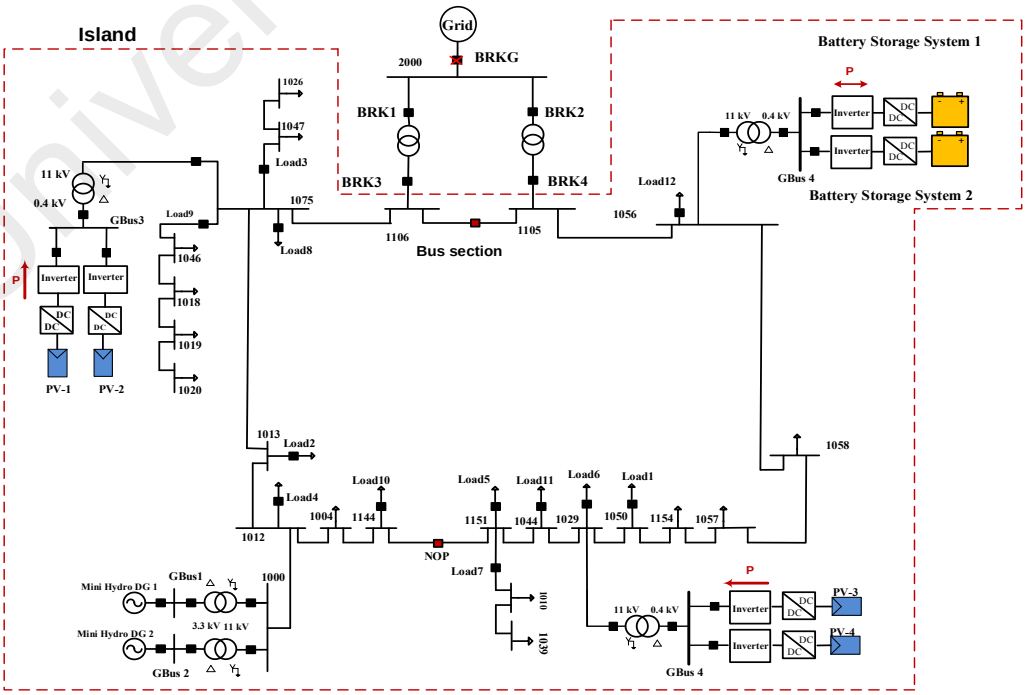

Figure 3.15: The distribution network illustrates the reconnection procedure

3.2.2.3 Phase Synchronization Controller

As seen in Figure 3.16, the phase synchronization controller is designed to work in two operational modes; frequency and phase control. Immediately after islanding, the governor begins regulating the system's frequency using a PID controller. The PID controller helps maintain the stability of the islanded network. It is used to bring the frequency as close as possible to their reference value. Then, when the reconnection process is required, the reconnection controller sends a control signal to switch the operation for phase control. In this research, the inclusion of phase angle controller will not create instability in the frequency response. Furthermore, a new PID controller is utilized in phase synchronization controller for it to be more suitable for the phase control process. The parameters of the mini-hydro DG controllers are included in Appendix A.10.

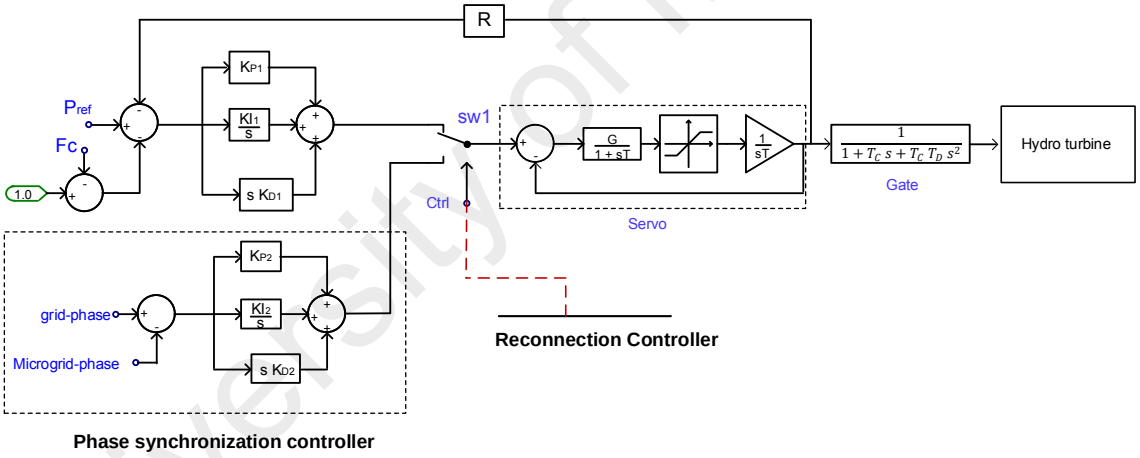

Figure 3.16: Phase synchronization controller

3.2.2.4 Voltage Synchronization Controllers

The basic requirement of excitation system is that it keeps the machine terminal voltage within a percentage range from their nominal value by regulating the machine field current. For a synchronous generator, there are various type of IEEE excitation systems available for use in stability analyses. In this research, the AC1A exciter model is used in the voltage synchronization controller for a mini-hydro synchronous generator. The control block diagram of voltage synchronization controller shown in Figure 3.17 is

designed to work in two operational modes; islanded and grid connected. During the grid-connected mode, the voltage synchronization controller regulates the excitation voltage based on a predetermined reactive power, while for islanding mode, the voltage synchronization controller tries to keep the terminal voltage at its typical nominal value of 1 p.u or within the permissible value.

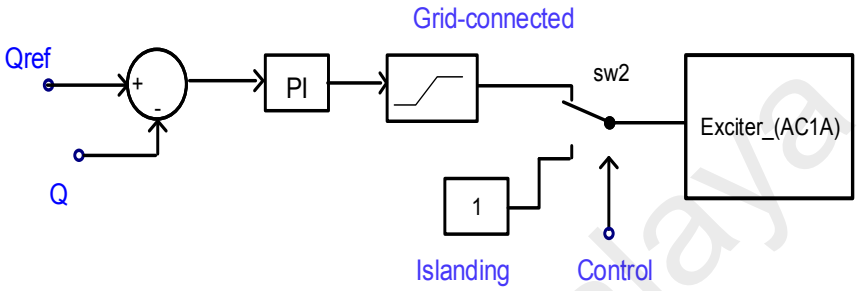

Figure 3.17: Voltage synchronization controllers

3.3 Summary

This chapter discuss the methodology of the proposed frequency control scheme proposed for distribution network with high PV penetration. This scheme is expected to overcome frequency stability issues occurring after islanding; it consists of inertia controller, frequency regulation controller, and an optimal UFLS controller. Inertia controller proposed for PV units increases the total inertia of distribution network. The main principle of inertia controller is operating the PV generation below the maximum power point to keep a definite reserve power, which is delivered directly after the disturbance events and last for a few seconds. After 10s, a frequency regulation controller is used to provide the required power from BSS.

When the two previous controllers fail to stop the frequency deviation, an UFLS technique is initiated to stop the frequency deviation. It has been observed that placing all of the loads in the distribution system with fixed priority results in un-optimum load shedding. For this reason, the proposed UFLS technique uses metaheuristics methods to select the optimal combination of loads from fixed and random priority shedding loads.

This chapter also described the coordination between frequency control scheme and synchronization system, where this coordination is necessary to stabilize the islanded network frequency and achieve a seamless reconnection process with the main grid.

CHAPTER 4: VALIDATION OF PROPOSED UFLS TECHNIQUE

4.1 Introduction

This chapter discusses modelling of the distribution network used to validate the proposed load shedding technique. It also deals with the validation of the proposed load shedding techniques using various case studies, such as including islanding, DG tripping, and load increments. Furthermore, the proposed UFLS is compared with the adaptive UFLS techniques in order to confirm its ability in shedding the optimal amount of power from the distribution network. Different metaheuristic optimization methods (BEP, BGA, BPSO) are applied for load shedding, and their performance are presented here.

4.2 Modelling of 29-Bus Distribution network for Proposed UFLS Technique

The test system considered in this research is a part of the Malaysian distribution network shown in Appendix A, section A.2. The test system consists of two mini-hydro DGs operated at a voltage level of 3.3 kV, each DG rated 2 MVA capacity (maximum power dispatch is 1.8 MW). The distribution network also consists of one Bio-Mass DG; the total load demand of the distribution network is 6 MW, 2 Var. The mini-hydro units were connected to the distribution network using two step-up transformers (3.3 kV-11 kV).

The mini-hydro DGs are modelled using the PSCAD/EMTDC library models of the exciter, the governor, and hydraulic turbine. The turbine chosen for mini-hydro units is the hydraulic turbine with non-elastic water column without a surge tank model. For excitation and governor system, the IEEE type AC1A model and PID governor with pilot and servo dynamics were selected. The entire line is modelled according to a nominal π form. The length of each line does not exceed 6 km.

To validate the operation of proposed UFLS technique for high PV penetration, the same network is used with the replacement of Bio-mass DG by four PV generation units, as shown in Figure 4.1.

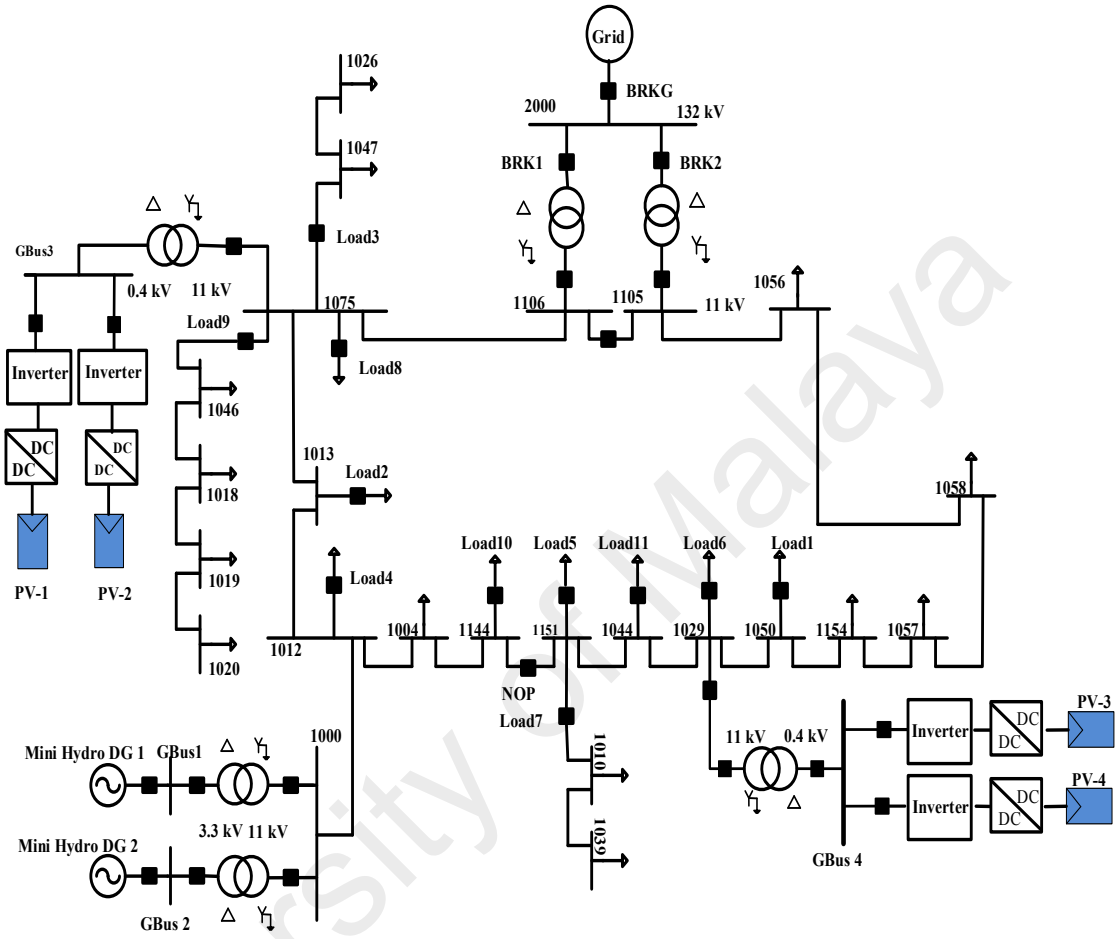

Figure 4.1: Distribution network used for validation of proposed UFLS technique

As shown in Figure 4.1, four units of solar PV were connected with the network to work each rated 0.55 MWP. Two parallel units of solar PV plants were connected to 2MVA step-up transformer (0.4KV/11kV). The distribution network is connected to the transmission grid via two feeders, with each feeder using 30MVA step down transformer (132KV/11kV). The islanding operation is performed by opening the circuit breaker (BRKG) of Bus 2000. The modelling of the various components of the test system is explained in the following sections:

4.2.1 Modelling of Mini-Hydro DG

A simplified block diagram of a hydropower plant with essential features is shown in Figure 4.2.

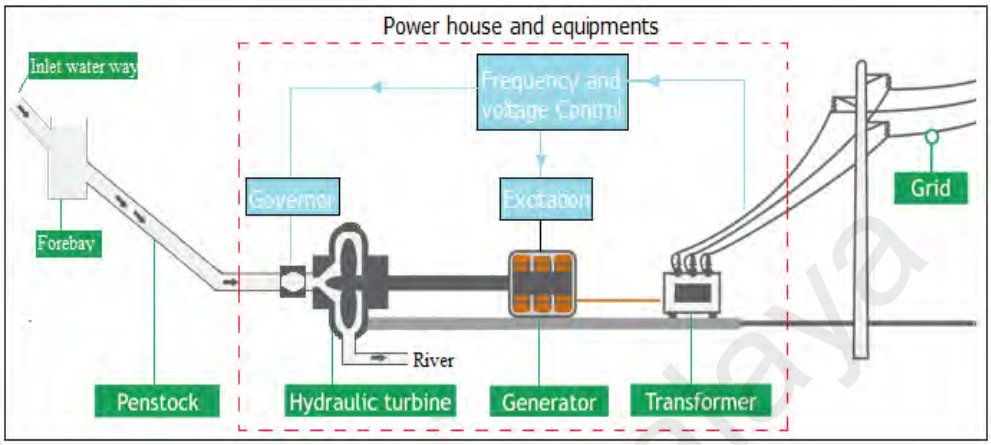

Figure 4.2: Layout of Run of River Hydropower Plant (Sharma & Singh, 2013)

The main elements of a hydropower plant are:

(A) Inlet water ways: Inlet water ways are the passages through which water is conveyed from the dam to the power house. It includes a canal, penstock (closed pipe) or tunnel, flume, fore way, and a surge tank (Paish, 2002).

(B) Forebay: Forebay is the tank at the head of penstock pipe that supplies water regularly at a constant head. The forebay serves as a miniature reservoir for the turbines. Its primary functions are to serve as a settling area for water-borne desires to provide storage for the periods of low flow or increased demand of power.

(C) Penstock: Water may be conveyed to turbines through open conduits or closed pressure pipes called penstocks made of reinforced concrete or steel. It is desirable that the penstock should be sloping towards the power house and its grade is adjusted according to the topography. The thickness of the penstock increases as working pressure or the head of the water increases.

(D) Power House and equipment's: The power house is a building where the turbines, alternators, and the auxiliary plant are housed. Here, the conversion of energy of

water to electrical energy takes place. The following are some of the main equipment's provided in a power house:

i *Prime movers (turbines) coupled with governor*

ii *Generator*

iii *Generator Excitation*

iv *Transformers*

v *Switch board equipment and instruments*

4.2.1.2 Hydraulic Turbine

This research considers a non-linear hydraulic turbine with non-elastic water column without a surge tank. Nonlinear turbine models are required when speed and power changes are large during an islanding, load rejection, and system restoration conditions. The non-linearity of the model comes from the valve characteristic of the turbine. The block diagram of a hydraulic turbine is shown in Figure 4.3.

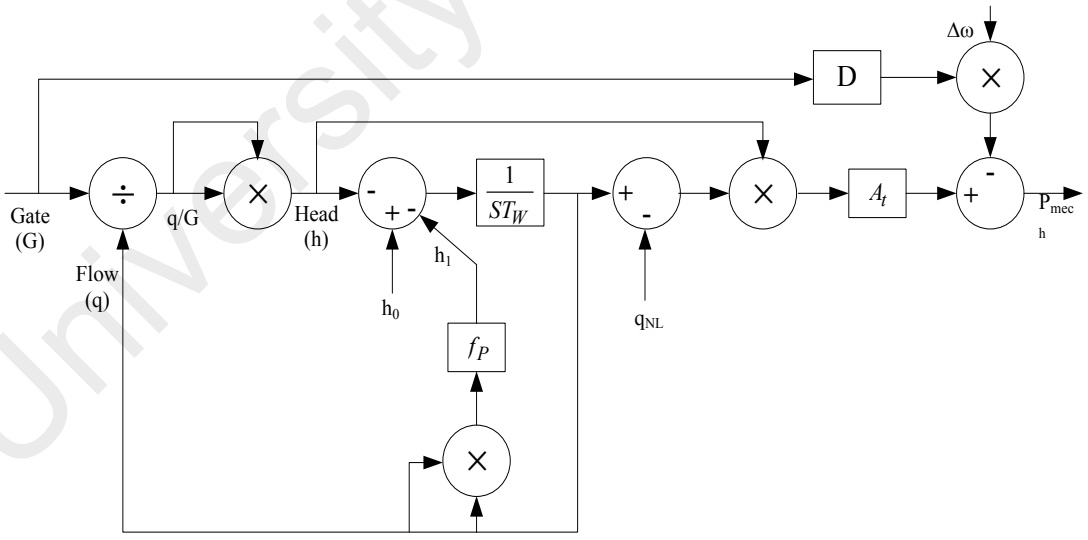

Figure 4.3: Block diagram of hydraulic turbine

In this model, the head losses h_1 are proportional to flow squared and the head loss coefficient f_P. In the modelling of the turbine itself, both its hydraulic characteristics and mechanical output power must be modelled. The parameter values of hydraulic turbine used in this research are shown in Table 4.1.

Table 4.1: Value of hydro turbine parameters

Parameter	Value	Parameter	Value
TW	1.0	Initial output power	0.7
f_p	0.02	Initial operating head	1.0
D	0.5	Rated output power	1.0

4.2.1.3 Governor Model

The main function of the governing system is to regulate the turbine-generator speed in response to load variation. The speed control mechanism includes equipment such as relays, servomotors, power amplifying devices, and governor-controlled gates. The speed governor normally actuates the governor-controlled gates that regulate the water input to the turbine through the speed control mechanism. The general block diagram consisting of hydraulic turbine and governor is shown in Figure 4.4.

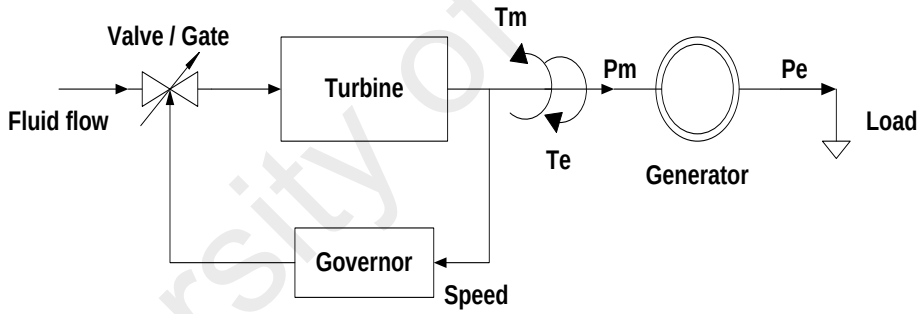

Figure 4.4: Block diagram of turbine speed control with governor

As shown in Figure 4.4, when the load demand in the system decreases, the generator speed will increase accordingly. In this situation, the turbine governor responds immediately and divert water flow by closing the gate to prevent hydro turbine from over-speeding. However, in high load demand situations, the turbine governor opens the hydraulic valve to increase the generator speed. In this research, an electro-hydraulic PID governor for speed control is used to regulate the generator speed. Figure 4.5 shows the block diagram of electro-hydraulic PID governor.

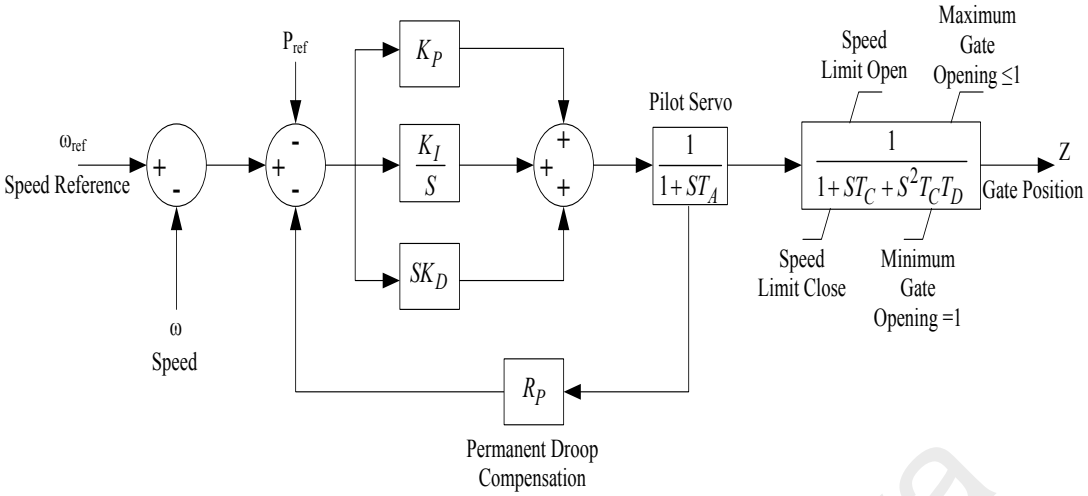

Figure 4.5: Block diagram of electro-hydraulic PID based governor

Where T_A is the time constant of pilot valve and servomotor. T_C is a gate servo gain, T_D is the gate servomotor time constant, and R_P is the permanent droop that determines the amount of change in output a unit produces in response to a change in unit speed. The parametric values used for governor are given in Table 4.2. However, the values for K_P, K_I, and K_D are tuned using trial-and-error method to provide satisfactory results.

Table 4.2: Parameters of the hydraulic governor

Parameter	Value	Parameter	Value
K_P	2.25	T_C	0.2 s
K_I	0.37	T_D	0.2 s
K_D	0.9	Max gate opening	0.16
T_A	0.05 s	Max gate closing	0.16
R_P	0.04	Dead band value	0
Max gate position	1.0	Min gate position	0

4.2.1.4 Synchronous Generator Model

Synchronous generators are the main sources used to provide energy in power systems. For this reason, it is very important to study the performance of synchronous machines. The synchronous machine is assumed to have a three-phase stator armature winding, a rotor field winding, and two rotors damper winding–one in the d-axis and one in the q-axis. In this research, two synchronous generators of 2 MW capacity are driven by

hydraulic turbines and governor control mechanism. The synchronous generator parameters for this test system are tabulated in Table 4.3. The specifications of both generators are similar.

Table 4.3: Synchronous generator parameters

Parameter	Value
Rated RMS line-to-line voltage	3.3 kV
Rated RMS line current	350 A
Inertia constant (***H***)	2.5 s
Iron loss resistance	300 p.u
Base angular frequency	314.159 rad/s
Armature resistance [***Ra***]	0.01 p.u
Potier reactance [***Xp***]	0.104 p.u
Unsaturated reactance [***Xd***]	0.838 p.u
Unsaturated transient reactance [***Xd'***]	0.239 p.u
Unsaturated transient time [***Tdo'***]	8.0 s
Unsaturated sub transient reactance [***Xd''***]	0.12 p.u
Unsaturated sub transient time [***Tdo''***]	0.05 s
Unsaturated reactance [***Xq***]	0.534 p.u
Unsaturated sub transient reactance [***Xq''***]	0.12 p.u
Unsaturated sub transient time [***Tqo''***]	0.1 p.u
Air gap factor	1.0

4.2.1.5 Exciter Model for Synchronous Generators

The main function of excitation system is to maintain the terminal voltage of synchronous machine and control reactive power flow. This operation is performed by adjusting the field current of the synchronous generator. The excitation systems have taken many forms over the years. In this research, the IEEE type AC1A standard model from the PSCAD/EMTDC library is used for interfacing with synchronous machines, as shown in Figure 4.6.

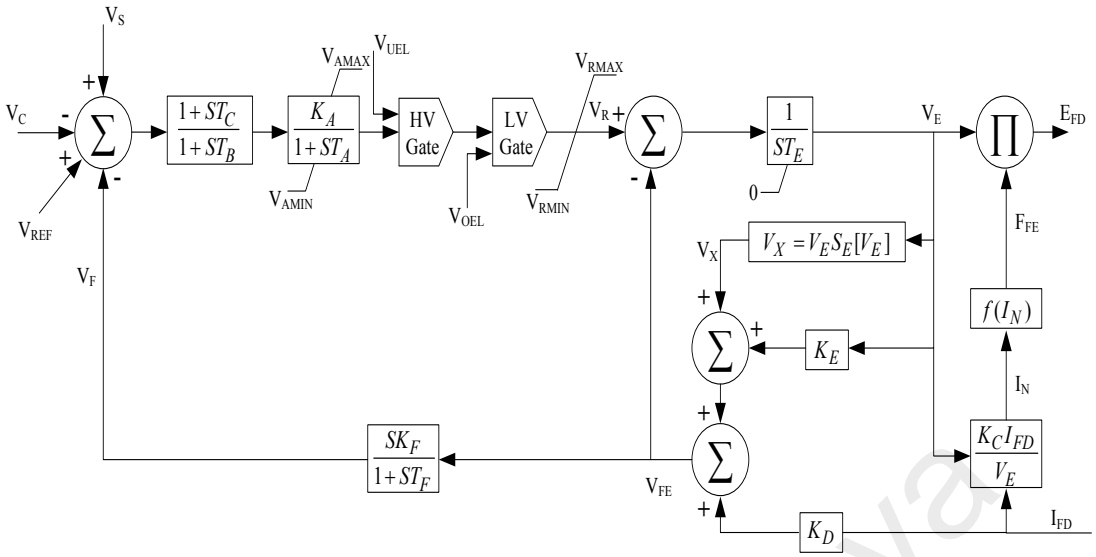

Figure 4.6: Block Diagram of IEEE type AC1A excitation system model

This model provides a field-controlled alternator excitation system with un-controlled rectifiers, and is applicable to brushless excitation systems. The typical parameters used in this research are presented in Table 4.4.

Table 4.4: Sample data of IEEE AC1A excitation model parameters

Parameter	Value	Parameter	Value
T_c	0	K_F	0.03
T_B	0	T_F	1
K_A	400	T_E	0.8
T_A	0.02	K_E	1
V_{AMAX}	14.5	K_C	0.2
V_{AMIN}	-14.5	K_D	0.38
V_{RMAX}	6.03	V_{RMIN}	-5.43
$SE(VE_1)$	0.1	$SE(VE_2)$	0.03
VE_1	4.18	VE_2	3.14

Figure 4.7 shows the synchronous generator with PID based governor, hydraulic turbine, and excitation control modelled in PSCAD.

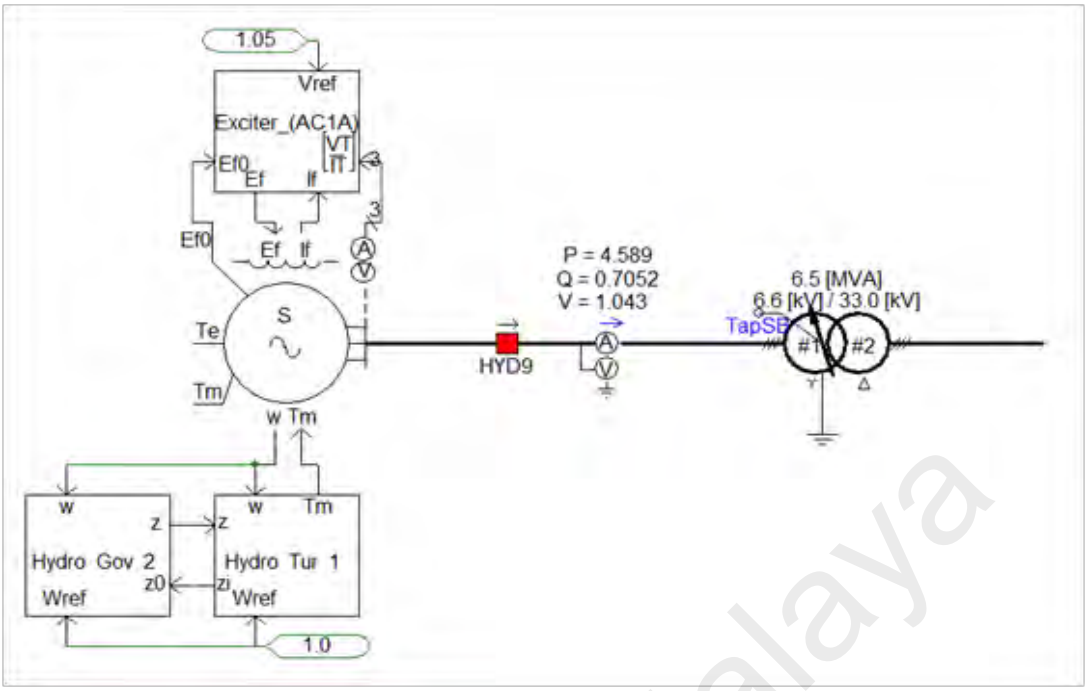

Figure 4.7: Mini-hydro power plant model in PSCAD/EMTDC software

4.2.2 Load Modelling of Distribution Network

The distribution network being tested consist of 29 buses and 21 lumped loads. In real power systems, the load characteristics always depend on the voltage and frequency, and static model is used to represent the distribution network loads, as per (Kundur et al., 1994).

$$P = P_0 \times \left(\frac{V}{V_0}\right)^a \times \left(1 + K_{pf} \times df\right) \tag{4.1}$$

$$Q = Q_0 \times \left(\frac{V}{V_0}\right)^b \times \left(1 + K_{qf} \times df\right) \tag{4.2}$$

where P, Q are active and reactive power for corresponding voltage and frequency, respectively; P_o, Q_o are active and reactive power at a base voltage and frequency, respectively. K_{pf} and K_{qf} are the coefficients of active and reactive load dependency on frequency, respectively; a and b are the load model parameters that determine if this model represents constant power, constant current, or constant impedance characteristics. df is the frequency deviation. In this work, the value for K_{pf}, K_{qf}, a, and b are set to 1.0, -1.0, 1.0, 2.0, respectively. In order to apply the proposed load shedding technique, 11

loads from the distribution network have been determined. Generally, loads are typically divided into commercial, industrial, and residential types. Since industrial and commercial loads are more important than the residential loads, commercial loads (Load 11 and Load 12) take the fixed priority, while residential loads (Load1- Load 10) take the random priority. The loads, with their priority rankings, are tabulated in Table 4.5.

Table 4.5: Load data and their priority

Load Ranked	Bus No.	P (MW)	Load Priority
Load 1	1050	0.044	Random
Load 2	1013	0.069	Random
Load 3	1047,1026	0.15	Random
Load 4	1012	0.314	Random
Load 5	1151	0.5	Random
Load 6	1029	0.55	Random
Load 7	1010,1039	0.583	Random
Load 8	1075	0.645	Random
Load 9	1018-1020, 1046	0.7	Random
Load 10	1144	0.119	Fixed
Load 11	1044	0.223	Fixed

4.2.3 Modelling of Photovoltaic System

The PSCAD model used in this research is shown in Figure 4.8; It mainly consists of PV array model, DC-DC converter, DC link capacitor, three phase-inverter, AC filter, transformer. The following sections detail these devices.

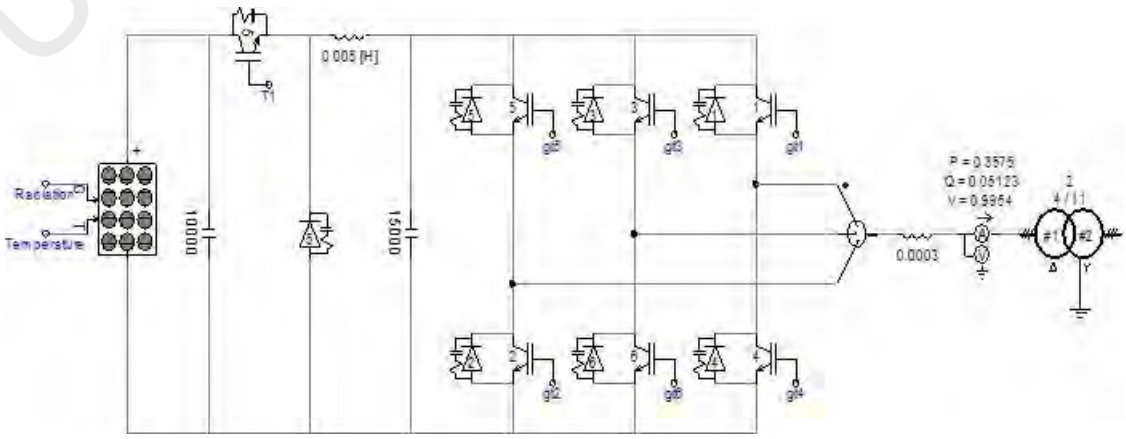

Figure 4.8: PSCAD model of solar PV generation unit

(A) PV Array

Solar PV is used to convert sunlight into electricity via the photoelectric effect. The PSCAD/EMTDC dynamic PV model is used to developed four solar PV units to be integrated with the distribution network. By using the default values tabulated in Table 4, the final output power of the single module is 380 W and 548 KW, for a total 1440 modules.

Table 4.6: Parameters of solar PV module (SM 380(48) P1946×1315)

Parameter	Symbol	Value
Peak power	P_{max}	380 W
Open circuit voltage	V_{oc}	59.75 V
Short circuit current	I_{sc}	8.56 A
Max. power voltage	V_m	47.9 V
Max. power current	I_m	7.93 A
Number of modules connected in series	NS	17
Number of modules connected in parallel	NP	82

To obtain the desired power level, the PV modules are connected in series and parallel. Figure 4.9 shows 82 strings connected in parallel; each string has 17 modules connected in series.

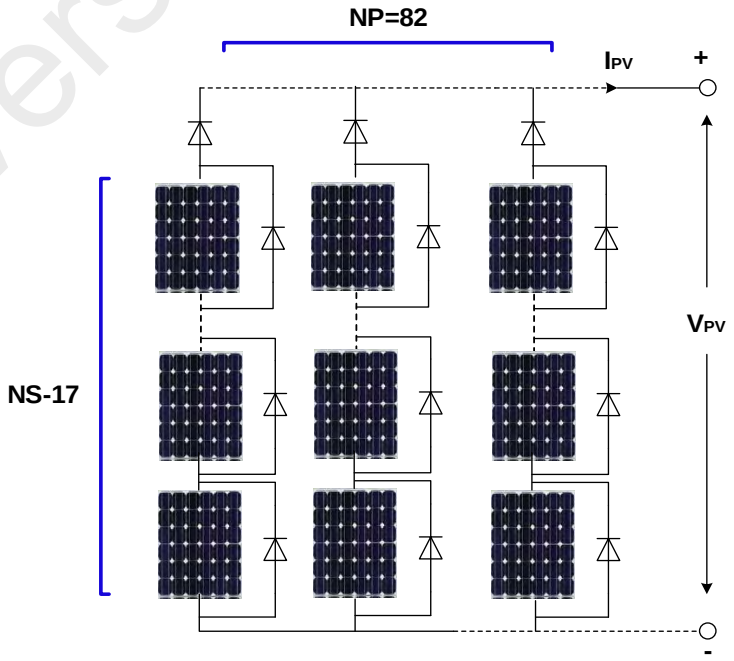

Figure 4.9: PV module connected in series and parallel in array

For describing the typical I-V and P-V characteristics of the PV unit at standard test conditions (E=1000W/m^2, T= 25C°), it is important to define three main parameters points. They are 1) maximum power point 2) open circuit voltage 3) short circuit current. Figure 4.10 and Figure 4.11 illustrate these points, the MPP is the maximum power point at which the photovoltaic system delivers the maximum power for a particular irradiance and temperature from which the voltage at MPP, V_{MPP}, and the current at the MPP, I_{MPP}. Short circuit measurement with zero voltage can give short circuit current, I_{sc}, while the open circuit voltage measurement with disconnected load can provide the open circuit voltage, Voc.

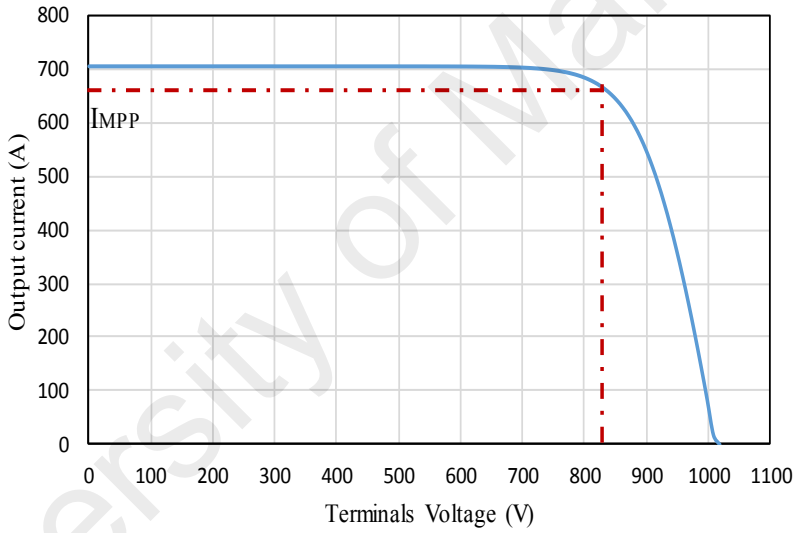

Figure 4.10: I-V curve of solar PV generation unit

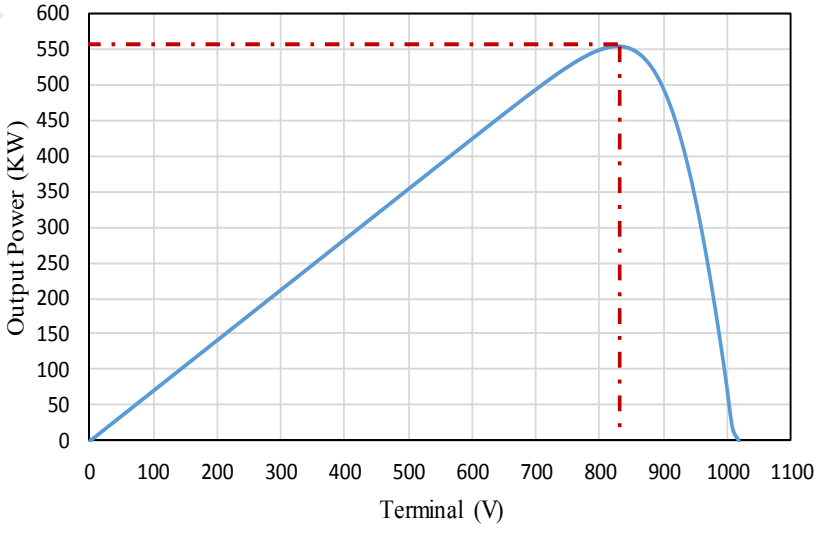

Figure 4.11: P-V curve of solar PV generation unit

(B) Buck DC-DC Converter

The DC-DC converter is an electronic circuit that is used either to step down the input voltage (buck converter) or to step up the input voltage (boost converter). The buck converter consists of Insulated Gate Bipolar Transistor (IGBT) switch, inductor, capacitor and free-wheel diode, as shown in Figure 4.12.

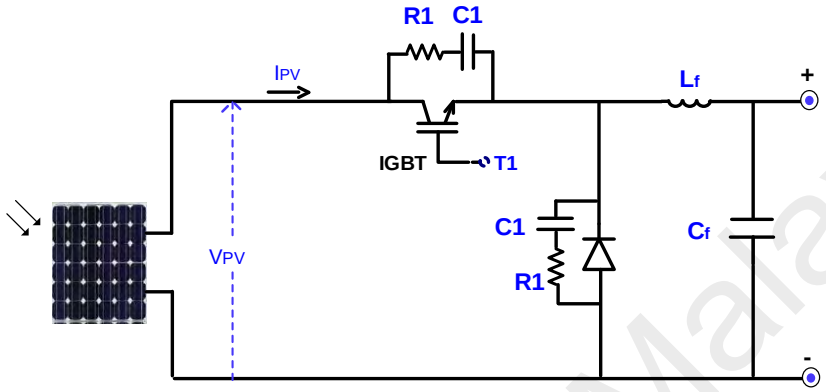

Figure 4.12: Buck DC-DC converter of solar PV unit

The parameters of buck converter are shown in Table 4.7. The input voltage represents the renewable source of the solar PV system, while the output voltage of the boost controller is fixed at 700 V DC.

Table 4.7: Parameters of buck DC-DC converter

Parameter Symbol Target	Parameter	Parameter
Input Voltage	V_{IN}	830 V
Output Voltage	V_{OUT}	700 V
Switching Frequency	f_{SW}	1KHz
Inductor Current Ripple Ratio	LIR	0.3
Capacitor Voltage Ripple	CVR	0.04
Maximum Output Current	$I_{OUT, MAX}$	700 A
The minimum inductance	L_{min}	550 µH
The minimum capacitance	C_{min}	1000 µF

$$D = \frac{V_{out}}{V_{in}} = \frac{700}{830} = 0.84 \tag{4.3}$$

$$L_{MIN} = \frac{(V_{in} - V_{out}) \times D}{L_I \times I_{out,MAX} \times f_{sw}} = \frac{(830 - 700) \times 0.84}{0.3 \times 700 \times 1000} = 520\ \mu H \tag{4.4}$$

$$C_{MIN} = \frac{LIR \times I_{out,MAX}}{8 \times f_{SW} \times CVR \times V_{out}} = \frac{0.3 \times 700}{8 \times 1000 \times 0.04 \times 700} = 937\mu F \quad (4.5)$$

(C) Converter Control of Solar PV Unit

In this PSCAD model, control of the buck converter has two operational functions; first, it is used to reduce the terminal voltage of PV array to match the inverter input voltage, and second, it is used for Maximum Power Point Tracking (MPPT) by controlling the voltage across the PV array. The difference between the solar panel output voltage (V_{PV}) and the reference maximum power (V_{MPP}) is used as an input to the Proportional-Integral (PI) controller, shown in Figure 4.13.

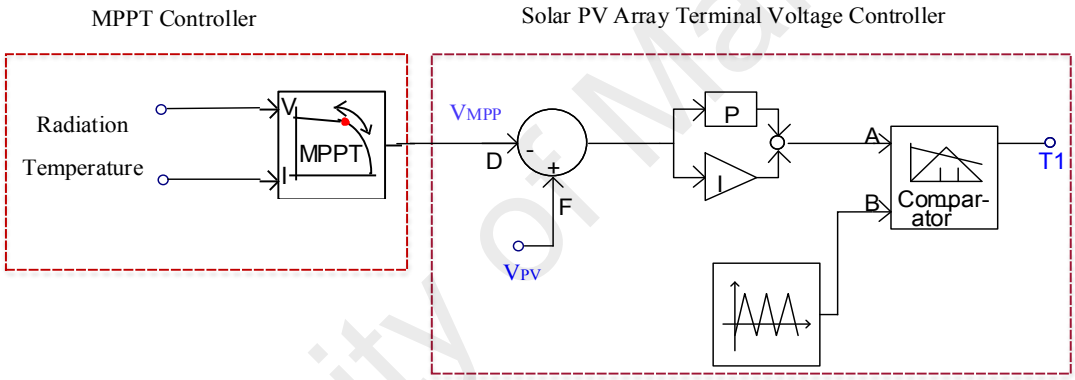

Figure 4.13: Converter control of solar PV unit

(D) Maximum Power Point Tracking (MPPT)

When a PV module is directly coupled to a resistive load, the PV module's operating point will be at the intersection of its I–V curve, with a slope of 1/RL, as shown in Figure 4.14. This means that the load value determines the operating condition of the PV module. A study shows that a direct-coupled system utilizes more than 31% of the PV's capacity. Due to this fact, the PV array is usually oversized to compensate for a low power yield during winters. This mismatch between a PV module and a load requires further over-sizing of the PV array, which increases the overall system's cost. To mitigate this problem, a maximum power point tracking (MPPT) can be used to maintain the PV module's operating at the Maximum Power Point (MPP).

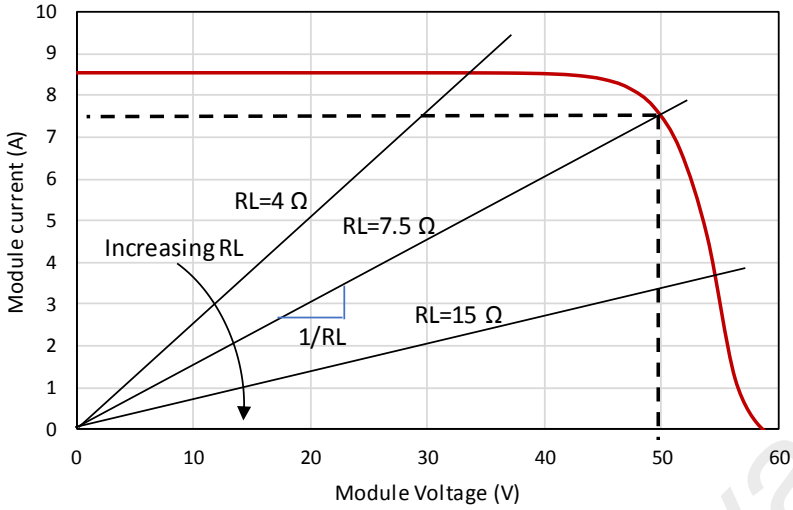

Figure 4.14: I-V curves of SM 380 PV module and various resistive loads

The MPPT techniques are used to control DC converters in order to extract the maximum output power from a PV array under given weather conditions. The DC converter is continuously controlled to operate the array at its maximum power point despite possible changes in the load's impedance. Several techniques have been proposed for this, such as Constant Voltage (CV) method, Incremental Conductance (IC) method, Perturb and Observe (P&O) method, and Artificial Neural Network (ANN) method. The PSCAD model of converter control use Perturb and Observe (P&O) methods to determine the maximum power voltage V_{MPP}.

(E) Three Phase Inverter

The inverter is an electronic circuit that converts the DC output power of the DC-DC converter into a three phase AC power suitable for utility connection. In this PSCAD model, the three-phase inverter consists of a simple active and reactive power controller, a firing pulse generator, and a three-phase inverter bridge.

i Active and Reactive Power Controllers

The active power controller is used to establish a constant DC bus voltage (dcvag) at 0.7 kV between the DC-DC converter and the inverter. The output of the controller will be

used as an input to the current controller, while the reactive controller sets the reactive power (Q) of the grid to zero, which forces the inverter to operate at unity power factor so that it produces sinusoidal voltage and current that are in phase. The active and reactive power controllers are shown in Figure 4.15.

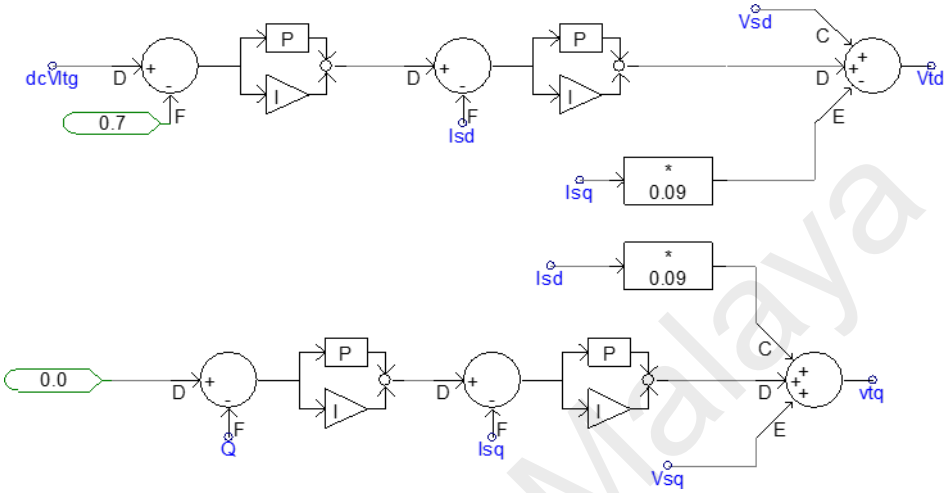

Figure 4.15: Active and reactive power controller of solar PV Inverter

ii Firing Pulse Generation

The switching signals of the six IGBT switches of the 3-legged inverter bridge is shown in Figure 4.16. It starts with creating three sinusoidal modulating waves with a frequency of 50 Hz and a phase shift equal to the output of the previous reactive controller (Vtq). The magnitude of the modulating waves is controlled by (Vtd) from a previous active controller. Then, the three sinusoidal modulating waves were compared with a triangular carrier wave, with magnitudes between -1 and 1.

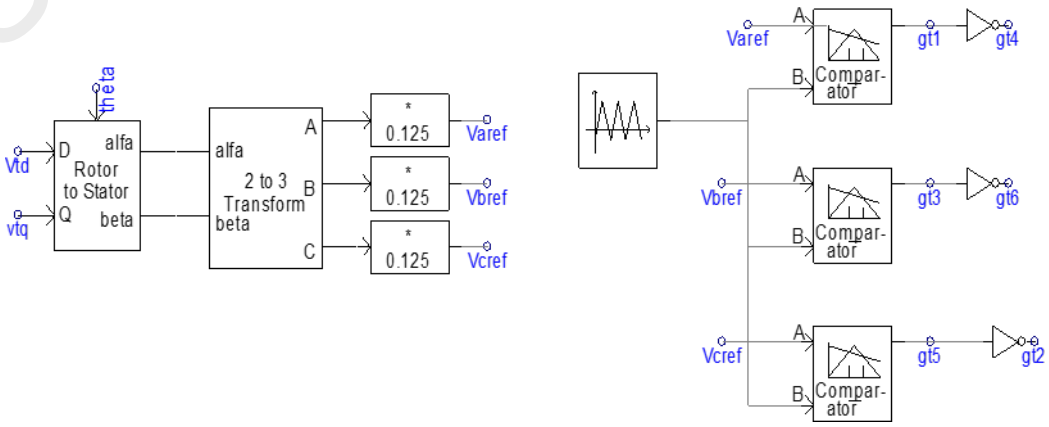

Figure 4.16: Firing pulse generation of solar PV inverter

iii Three Phase Inverter Bridge

Three phase inverter bridge is used to convert the DC bus voltage to AC voltage of 400 V/50 Hz. As shown in Figure 4.17, three phase bridge consists of six IGBT, where each IGBT switch is controlled by a firing signal. Due to the switching operation of IGBT, the output voltage of the inverter will be distorted. For this reason, an LC filter was implemented to improve the shape of the output voltage of the inverter.

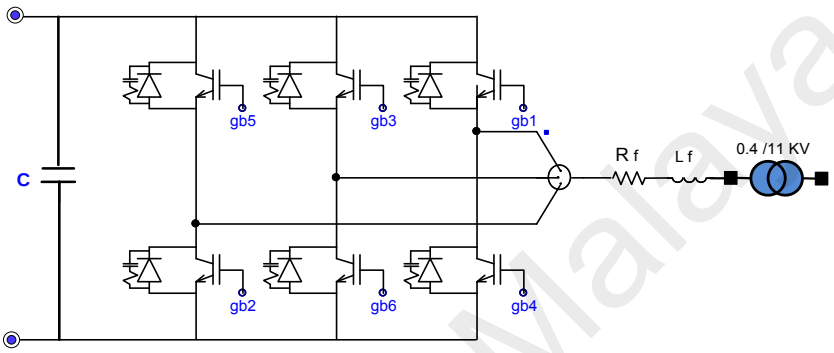

Figure 4.17: PSCAD model of solar PV inverter

4.3 Simulation Results for Proposed UFLS Technique

The validation of the proposed UFLS technique are divided into three case studies;

Case study 1: Comparison Between Metaheuristic UFLS Technique (BEP) and Adaptive UFLS Technique, represents the comparative study between the UFLS technique based on BEP method and the adaptive UFLS technique, which is conducted to show the importance of assuming some flexibility in load shedding priority.

Case study 2: comparison between different Metaheuristic techniques in term of execution time, represents a comparative simulation results between FRPLS technique proposed in (Laghari et al., 2015), BGA, BPSO, and BEP techniques in terms of execution time and convergence curves.

Case study 3: comparison between different load shedding techniques, represents a comparative simulation results between proposed UFLS controller, which uses the BEP technique compared with other UFLS techniques.

4.3.1 Case Study 1: Comparison Between Metaheuristic UFLS Technique (BEP) and Adaptive UFLS Technique

This comparative study is required to show the preference of the proposed UFLS technique over the adaptive UFLS technique, where this preference is due to the flexibility in load shedding priority. This comparative study is performed for load increments of 1.0 MW and 1.8 MW occurring at 40s.

(A) Load Increment of 1.0 MW

Immediately after islanding at 10s, the system frequency begins to decline in response to an excess load of 0.32 MW. Accordingly, the mini-hydro generators use their spinning reserves 0.48 MW to cover the unbalance of power. The UFLS controller will only be activated when the total load power exceeds 5.8 MW. At 40s, the total power demand will be 6.68 MW. For this reason, the UFLS automatically activate its event-based to stop the frequency declination by shedding the loads 2, 3, 8 for BEP UFLS or loads1-5 for adaptive UFLS, as shown in Table 4.8. The frequency responses of proposed UFLS controller and adaptive UFLS controller are shown in Figure 4.18.

Table 4.8: UFLS parameters for load increment of 1.0 MW after islanding

Parameter	UFLS controller based BEP	Adaptive UFLS controller
ΔP (MW)	1.0	1.0
Reserve (MW)	0.16	0.16
Total Load Shed Power (MW)	0.84	0.84
Shedding loads (MW)	Load 2 (0.069) Load 3 (0.15) Load 8 (0.645)	Load 1 (0.044), Load 2 (0.069) Load 3 (0.15), Load 4 (0.314) Load 5 (0.5)
Nadir Frequency (Hz)	49.3	49.5
Frequency Overshoot (Hz)	-	50.25

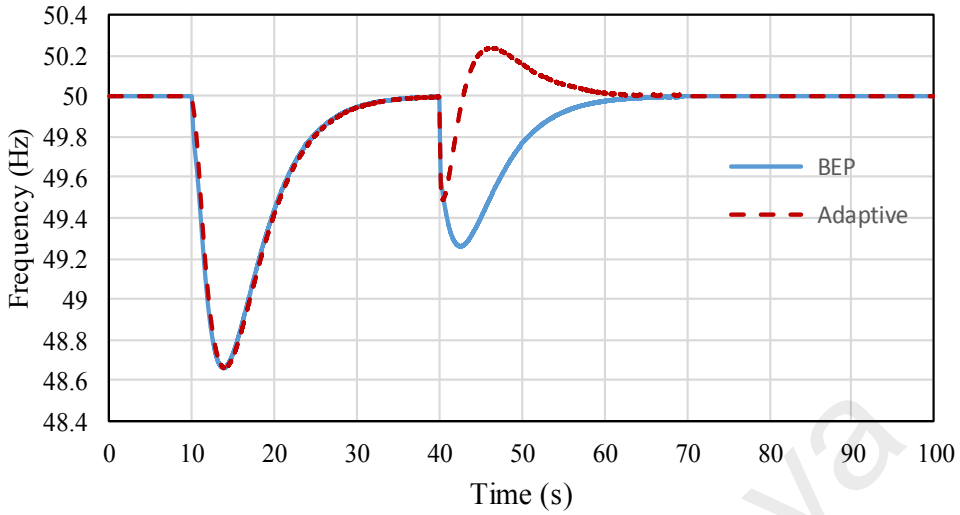

Figure 4.18: The Frequency response for 1.0 MW load increment scenario

Figure 4.18 and Table 4.8 show that due to the fixed priority of loads, the adaptive UFLS techniques will shed more load 1.07 MW, which leads to overshoot in the system's frequency. However, the proposed UFLS technique can shed the appropriate load 0.86 MW without overshooting frequency.

(B) Load Increment of 1.8 MW

Immediately after islanding at 10s, the system frequency begins to decline in the response to an excess load 0.32 MW. Accordingly, the mini-hydro generators use their spinning reserves 0.48 MW to recover the unbalance of power. At 40s, the power demand increased by 1.8 MW. Due to this, the UFLS controller based on BEP stop the frequency declination by shedding the loads 1, 5, 7, 8. While adaptive UFLS shed the loads 2-7, as shown in Table 4.9. The frequency responses of the proposed UFLS controller and adaptive UFLS controller are shown in Figure 4.19.

Table 4.9: UFLS parameters for load increment of 1.8 MW after islanding

Parameter	UFLS controller based BEP	Adaptive UFLS controller
ΔP (MW)	1.8	1.8
Reserve (MW)	0.16	0.16
Total Load Shed Power (MW)	1.64	1.64
Shedding loads (MW)	Load 1 (0.044), Load 5 (0.5) Load 7 (0.583), Load 8 (0.645)	Load 2 (0.069) Load 3 (0.15), Load 4 (0.314) Load 5 (0.5), Load 6 (0.55) Load 7 (0.583)
Nadir Frequency (Hz)	49.3	49.5
Frequency Overshoot (Hz)	-	50.25

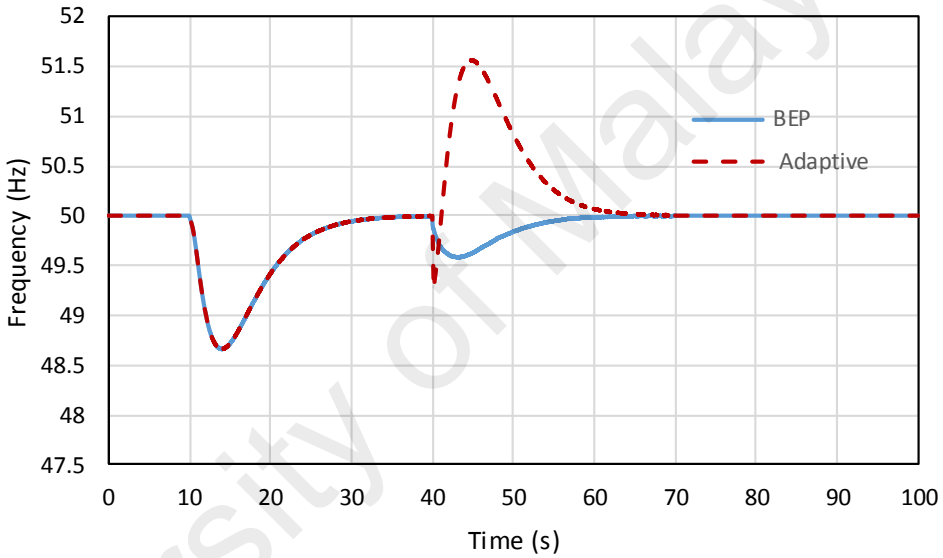

Figure 4.19: The Frequency response for 1.8 MW load increment scenario.

Figure 4.19 and Table 4.9 show that due to the fixed priority of loads, the adaptive UFLS techniques will shed more load (2.21 MW), which leads to overshoot in the system's frequency. However, the proposed UFLS technique shed less load (1.77 MW) and recover the system's frequency without overshooting.

4.3.2 Case Study 2: Comparison Between Different Metaheuristic Techniques in Term of Execution Time

Generally, the success of the load shedding technique not only depends on shedding optimal number of loads, it also depends on the execution time needed to perform the shedding operation. As pointed out previously, the islanded distribution network with

high penetration of solar PV generation suffers from rapid frequency changes. Accordingly, the load shedding controller will have a short time to make a decision, and this necessitates a simulation study to compare the execution time of different metaheuristic methods and determine the best approach. The PC used in this work has a core i7 processor of 2.1 GHz speed (8 CPUs) and 6MB RAM. Table 4.9 shows the execution times of four load shedding methods for six trials. It can be seen in Table 4.10 that the average of six execution times of BEP method is 24% of BPSO, 85% of BGA, and 31% of FRPLS technique proposed in (Laghari et al., 2015). Therefore, the BEP method is the best for the proposed UFLS technique.

Table 4.10: The execution time for different load shedding

Trial number	Execution time (second)			
	BPSO	BGA	BEP	FRPLS technique proposed in (Laghari et al., 2015)
1	0.646	0.196	0.162	0.5
2	0.609	0.179	0.152	0.5
3	0.626	0.172	0.155	0.5
4	0.657	0.178	0.150	0.5
5	0.605	0.176	0.153	0.5
6	0.607	0.189	0.153	0.5
Average	0.625	0.182	0.154	0.5

To demonstrate the overall performance of BGA, BPSO, and BEP techniques, different convergence curves corresponding to these techniques are shown in Figure 4.20, 4.21, 4.22, respectively. It can be seen that the performance of these techniques is reliable, as they report the lowest losses in all six trials.

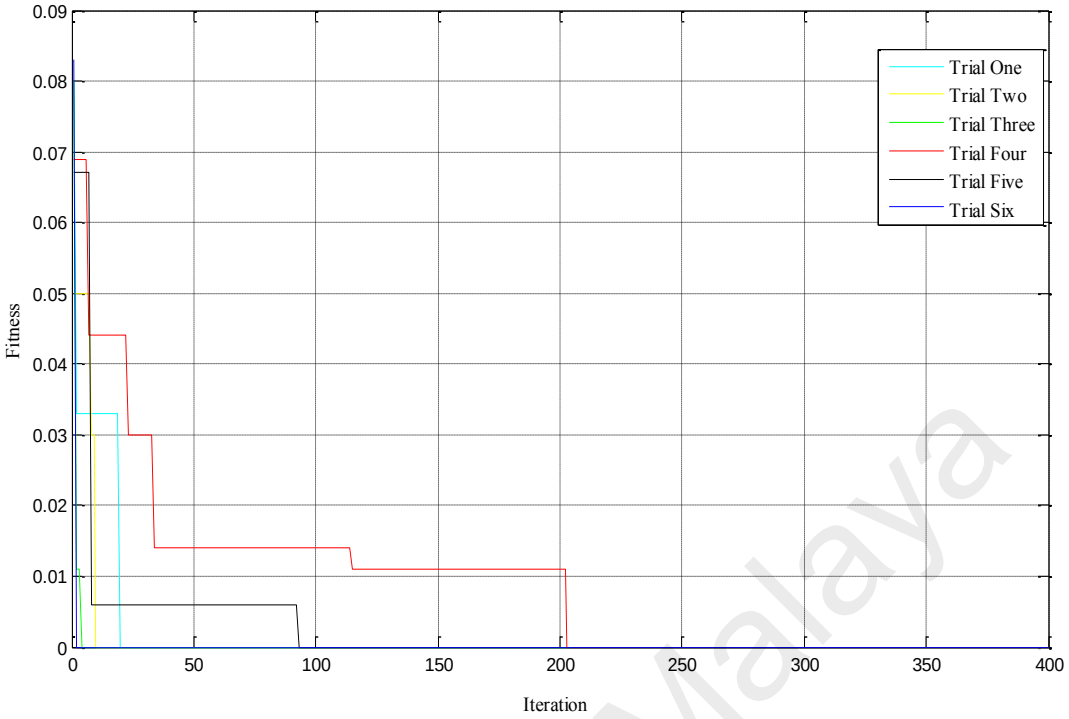

Figure 4.20: The convergence trend of BEP technique.

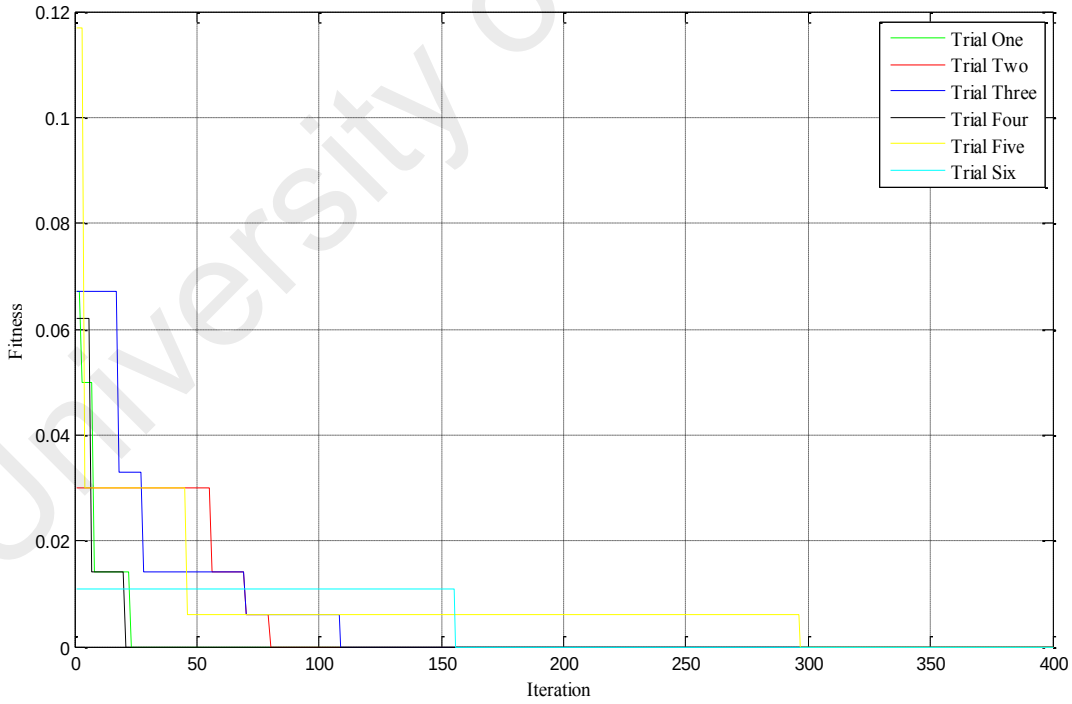

Figure 4.21: The convergence trend of BGA technique.

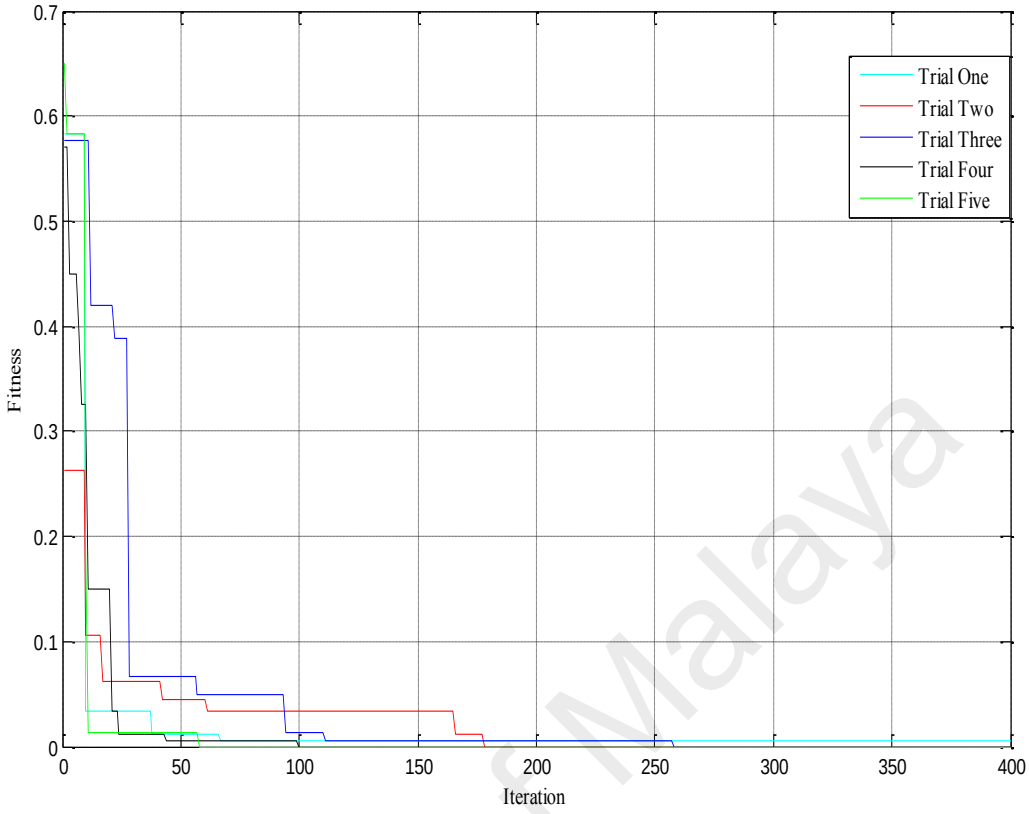

Figure 4.22: The convergence trend of BPSO technique.

4.3.3 Case Study 3: Comparison Between Different Load Shedding Techniques

This study compares the performance of the three metaheuristic methods; BEP, BGA, and BPSO for the UFLS technique. The performance of this technique is also compared with the FRPLS technique proposed in (Laghari et al., 2015).

(A) Load Increment of 1MW

Immediately after islanding, the system frequency begins to decline in the response to an excess load of (0.32 MW). Accordingly, the mini-hydro generators use their spinning reserve (0.48 MW) to recover the unbalance of power. The UFLS controller will only be activated when the total load power exceeds 5.8 MW. At 40s, the total power demand will be 6.68 MW. Table 4.11 shows that all load shedding techniques will shed the same amount of power (0.84 MW). However, the frequency deviation for each technique is

unequal due to the difference in execution time. The frequency responses of all UFLS controller are shown in Figure 4.23.

Table 4.11: The UFLS parameters for load increment of 1.0 MW after islanding

Parameter	BEP	BGA	BPSO	FRPLS technique proposed in (Laghari et al., 2015)
ΔP (MW)	1.0	1.0	1.0	1.0
Reserve (MW)	0.16	0.16	0.16	0.16
Total Load Shed Power (MW)	0.84	0.84	0.84	0.84
Shedding loads (MW)	Load 2 (0.069) Load 3 (0.15) Load 8 (0.645)	Load 2 (0.069) Load 3 (0.15) Load 8 (0.645)	Load 2 (0.069) Load 3 (0.15) Load 8 (0.645)	Load 2 (0.069) Load 3 (0.15) Load 8 (0.645)
Nadir Frequency (Hz)	49.3	49.25	48.8	48.55

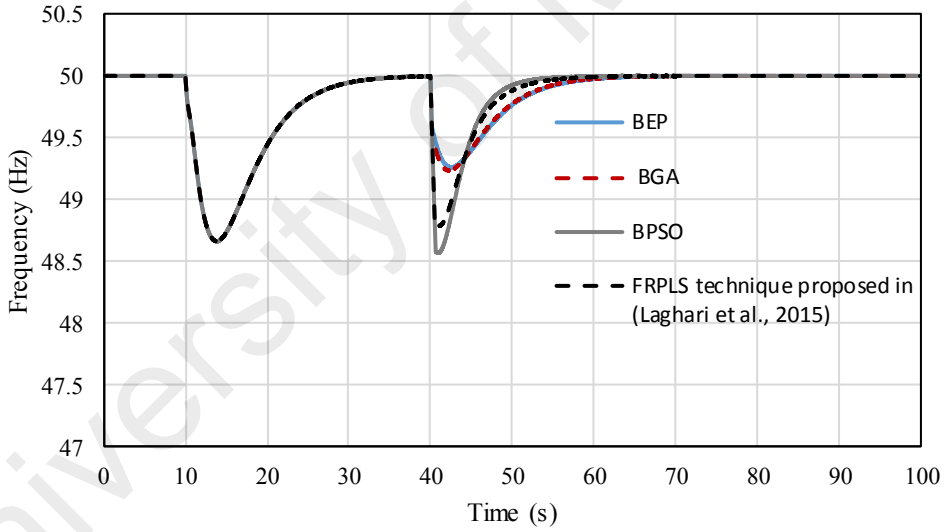

Figure 4.23: Frequency response for 1-MW load increment.

(B) Intentional Islanding at 1.56 MW Imbalance Power

In this scenario, the intentional islanding happened at t=10s when the solar radiation value is 500 W/m^2. Immediately after islanding, the system frequency begins to decline in response to an excess load (1.56 MW). Accordingly, the mini-hydro generators use their spinning reserve (0.48 MW), but this value is insufficient to cover the unbalance power. For this reason, load shedding techniques will be initiated to restore the system frequency.

Table 4.12 shows that all optimization techniques will shed the same amount of power (1.05 MW). However, Figure 4.24 shows that the BPSO technique fails to prevent the system frequency from dropping below 47.5 Hz, which leads to a total blackout. In fact, the large execution time of BPSO technique is the main reason of protection failure.

Table 4.12: UFLS parameter of intentional islanding at 1.56 MW imbalance power

Parameter	BEP	BGA	BPSO	FRPLS technique proposed in (Laghari et al., 2015)
ΔP (MW)	1.56	1.56	1.56	1.56
Reserve (MW)	0.48	0.48	0.48	0.48
Total Load Shed Power (MW)	1.08	1.08	1.08	1.08
Shedding loads (MW)	Load 7 (0.583) Load 5 (0.5)	Load 7 (0.583) Load 5 (0.5)	Load 7 (0.583) Load 5 (0.5)	Load 7 (0.583) Load 5 (0.5)
Nadir Frequency (Hz)	47.8	47.8	0	47.55

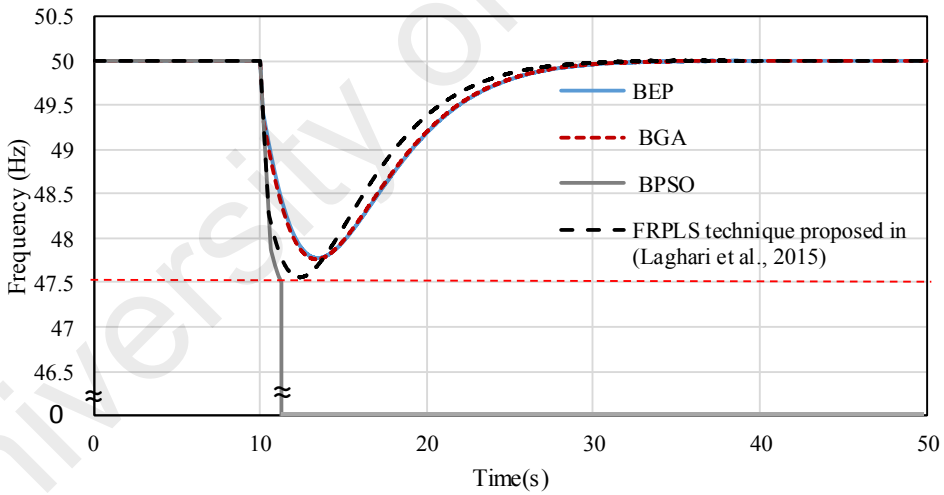

Figure 4.24: Frequency response of intentional islanding at 1.56 MW imbalance power

(C) Mini-hydro DG Tripping

Immediately after islanding at 10s, the system frequency begins to decline in the response to an excess load of (0.32 MW). Accordingly, the mini-hydro generators use their spinning reserve (0.48 MW) to recover the unbalance of power. The UFLS controller will only be activated when the total load power exceeds 5.8 MW. At 40s, a mini-hydro DG of (1.71 MW) is tripped from the islanded distribution network. Due to this, all load

shedding techniques are initiated to restore the system frequency. Table 4.13 shows that all load shedding techniques will shed the same amount of power (1.63 MW). However, Figure 4.25 shows that the BPSO technique and the FRPLS technique fail to stop the frequency deviation below 47.5 Hz. In fact, the large execution time of BPSO technique and FRPLS technique proposed in (Laghari et al., 2015) is the main reason of operation inability.

Table 4.13: The UFLS parameters for mini hydro DG tripping event

Parameter	BEP	BGA	BPSO	FRPLS technique proposed in (Laghari et al., 2015)
ΔP (MW)	1.71	1.71	1.71	1.71
Reserve(MW)	0.08	0.08	0.08	0.08
Total Load Shed Power (MW)	1.63	1.63	1.63	1.63
Shedding loads (MW)	Load 1(0.044) Load 4 (0.314) Load 6 (0.55) Load 9 (0.7)	Load 1(0.044) Load 4 (0.314) Load 6 (0.55) Load 9 (0.7)	Load 1(0.044) Load 4 (0.314) Load 6 (0.55) Load 9 (0.7)	Load 1(0.044) Load 4 (0.314) Load 6 (0.55) Load 9 (0.7)
Nadir Frequency (Hz)	49.2	49.1	0	0

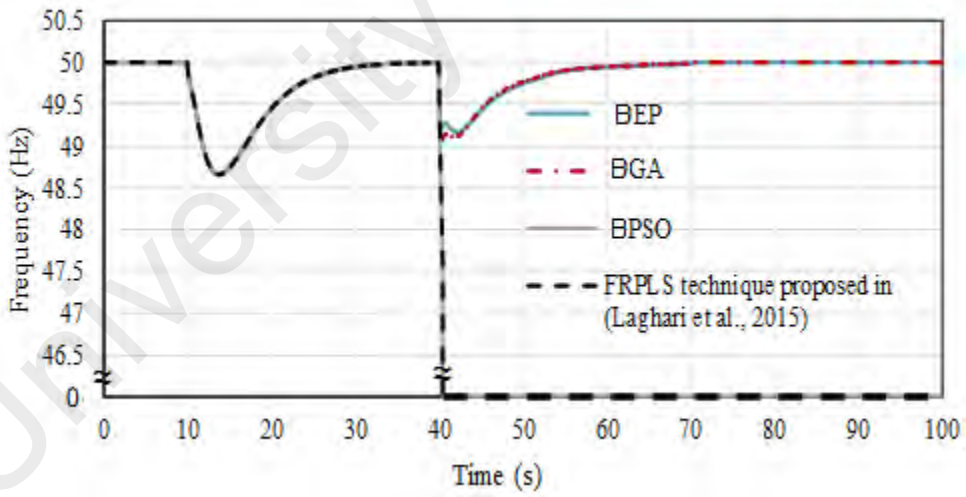

Figure 4.25: Frequency response for mini hydro DG tripping event.

4.4 Discussions

As discussed previously, it has become clear that the load shedding controller with fixed priority loads cannot shed the optimal combination of loads. Contrarily, the FRPLS technique is able to shed the optimal combination of loads. However, this technique still suffers from time delay, which affects the operation of the load shedding controller. For

this reason, three metaheuristic techniques; BEP, BGA, and BPSO can be applied to determine the optimal combination of load to be shed. Through comparative simulation study, the BEP technique requires less time to shed the optimal combination of loads compared to the BGA and BPSO method. Accordingly, the BEP method is selected for use with the UFLS technique to shed the optimal combination of loads from the islanding distribution network.

4.5 Summary

This chapter discusses modelling the distribution network used to validate the proposed UFLS technique. The effectiveness and robustness of this technique was investigated on 29-Bus test system for islanding events, DG tripping event, and load increment cases. Through the simulation results, it was proven that the proposed UFLS technique shed the optimal combination of loads compared to the conventional and adaptive techniques. This was achieved via metaheuristic methods and flexibility towards load shedding priority. Accordingly, the proposed UFLS technique is capable of restoring the network frequency without overshooting.

CHAPTER 5: VALIDATION OF PROPOSED FREQUENCY CONTROL SCHEME

5.1 Introduction

This chapter discusses the validation of proposed frequency control scheme by using the distribution network model. Various case studies, such as islanding, DG tripping event, load increments are performed to demonstrate the effectiveness of the proposed frequency control scheme for different PV penetration. In this chapter, the coordination between frequency control scheme and synchronization system is conducted to ensure a seamless reconnection process with the main grid.

5.2 Test System for Proposed Frequency Control Scheme

The test system considered in this research is a part of the Malaysian distribution network, which was modelled using PSCAD/EMTDC software, as shown in Appendix A, section A.2. To demonstrate the impact of high PV penetration level on frequency stability of islanded distribution network, four penetration scenarios were conducted. The first scenario considers the same network without any PV units, which represents a zero-penetration level. The second scenario considering the same network, while this time, the Bio-Mass generator is replaced by three PV units, each rated 0.5 MW, which represent 25% penetration level. The third scenario is similar to the second scenario however, four PV generation units are used to represent 33% penetration level, as shown in Figure 5.1. In the fourth scenario, Biomass and mini-hydro DGs are replaced by six PV units to represent 50% penetration level, which is expressed by the following equation

$$\text{Penetration level} = \frac{\text{Total PV Power}}{\text{Total load power}} \times 100\% \tag{5.1}$$

Due to the lack of reserve power available in the distribution network, two battery storage systems (BSS) are connected to the distribution network to provide frequency regulation services. The BSS is connected to the network via a step-up transformer (0.4 kV-11 kV) to provide 1MW AC output power at standard test conditions.

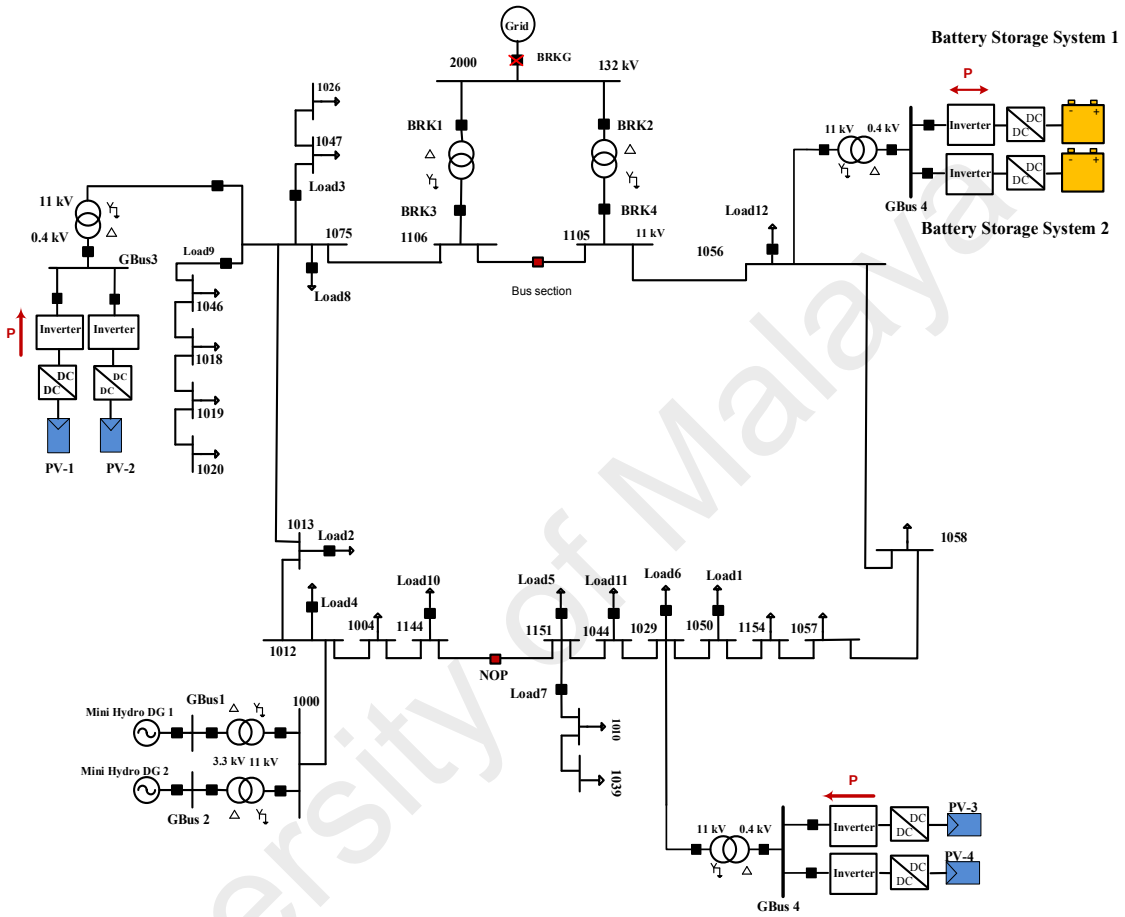

Figure 5.1: Distribution network used for validation of frequency control scheme

5.2.1 Mini-hydro DG Modelling

Two mini-hydro DGs are connected to the distribution network, each rated 2 MVA. The modelling of mini-hydro DG has been explained in section 4.2.1.

5.2.2 Modelling of Photovoltaic System

To validate the proposed frequency control scheme for high PV penetration, a different number of PV units are used based on the required penetration level. The modelling of PV unit has been explained in section 4.2.3.

5.2.3 Bio-Mass DG Modelling

This research utilizes a Bio-Mass DG rated 2 MVA capacity in the distribution network. The Bio-Mass DG is connected through a step-up transformer to increase the voltage level from 3.3 kV to 11 kV. The standard models for exciter, governor, and turbine from PSCAD/EMTDC library have been used to model the Bio-Mass DG. The Bio-Mass DG consists of a synchronous generator, governor, generic turbine and an excitation system. For the exciter model, an IEEE type AC1A excitation model is used. For governor, a mechanical hydraulic governor is used as per Figure 5.2, Table 5.1 shows the value for each parameter of the governor. Whereas the values of generic turbine model parameters are shown in Table 5.2.

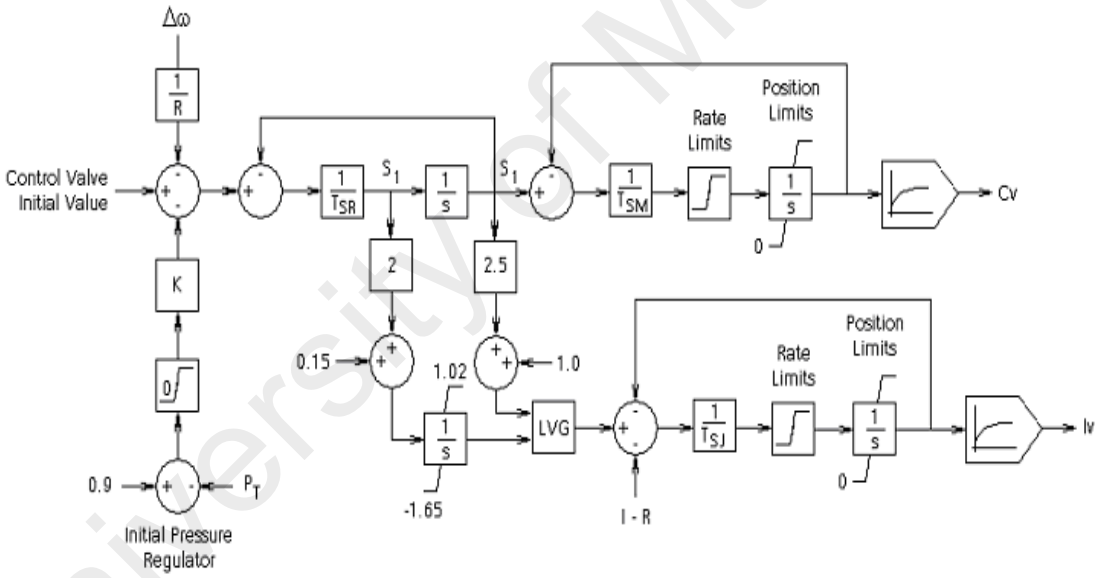

Figure 5.2: Mechanical-hydraulic control system governor model

Table 5.1: Mechanical-hydraulic governor parameters

Parameter	Value	Parameter	Value
Permanent Droop (R)	0.05 p.u	path Accelerator Bias	0.15 p.u
Speed Relay Time Constant	0.1 s	path Position Bias	1.0 p.u
Gate Servo Time Constant	0.2 s	Max Accelerator value	1.02 p.u
Max. CV Opening Rate	0.2 p.u/s	Min. Accelerator value	-1.65 p.u
Min. CV Opening Rate	-0.5 p.u/s	Servo Time Constant	0.2 s
Max. CV Servo Position	1.0 p.u	Min. Opening Rate	0.2 p.u/s
Min. CV Servo Position	0.0 p.u	Min. Closing Rate	-0.5 p.u/s
Path Accelerator Gain (K_1)	0.5 p.u	Max. servo Position	1.0 p.u
Path Position Gain (K_2)	2.5 p.u	Min. servo Position	0.0 p.u

For a steam turbine, this research uses Generic Turbine Mode, including Intercept Valve Effect. Figure 5.3 shows the block diagram of the steam turbine, while their parametric values are shown in Table 5.2.

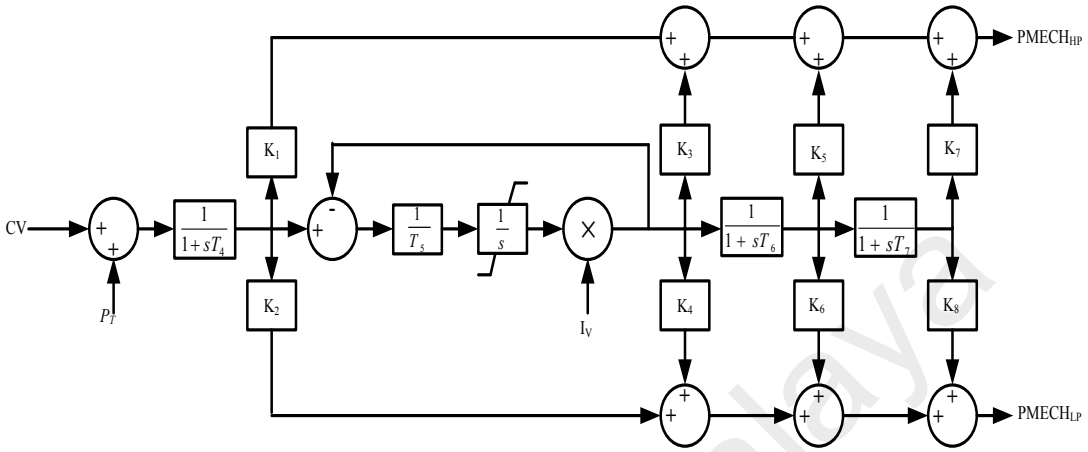

Figure 5.3: Block diagram of generic turbine mode including intercept valve effect

Table 5.2: Values of generic turbine model including intercept valve

Parameter	Value	Parameter	Value
K_1 fraction	0.299 p.u	K_8 fraction	0.695 p.u
K_2 fraction	0.001 p.u	Steam Chest Time Constant (T_A)	0.3 s
K_3fraction	0.001 p.u	Reheater Time Constant (T_5)	7.0 s
K_4 fraction	0.001 p.u	Reheater/Cross-over Time Constant (T_6)	0.0 s
K_5fraction	0.001 p.u	Cross-Over Time Constant (T_7)	0.5 s
K_6 fraction	0.001 p.u	Turbine Initial Output power	1.0 p.u
K_7 fraction	0.001 p.u	Max. Reheater Pressure Value (PR_{max})	1.0 p.u

5.2.4 Modelling of Battery Storage System

In this research, a reserve power of 2 MW capacity is required to compensate for the mini-hydro disconnection, which may occur in islanded distribution network. Therefore, two BSS are used; each provides of 1MW for 1 hour, with a terminal voltage of 600 V. The block diagram of BSS is shown in Figure 5.4. It consists of the battery bank, buck-boost converter, Bi-directional inverter filter, and step-up transformer (0.4/11kV).

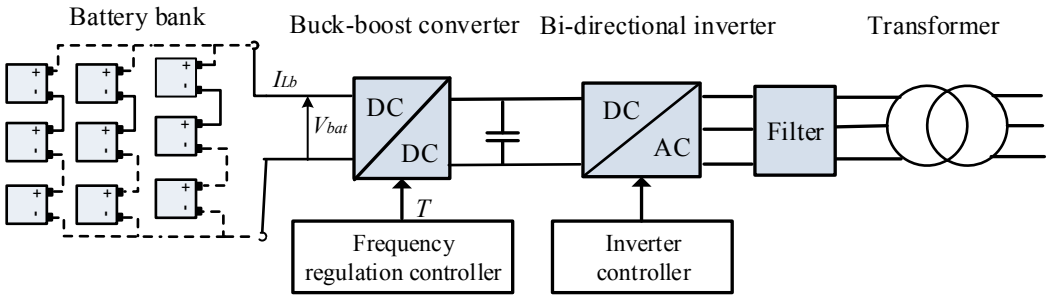

Figure 5.4: Block diagram of BSS.

5.2.4.1 The Battery Bank Model

The construction of battery bank is shown in Figure 5.5. It consists of eight strings connected in parallel; each string contains 375 lead acid battery (2V/200Ah) connected in series.

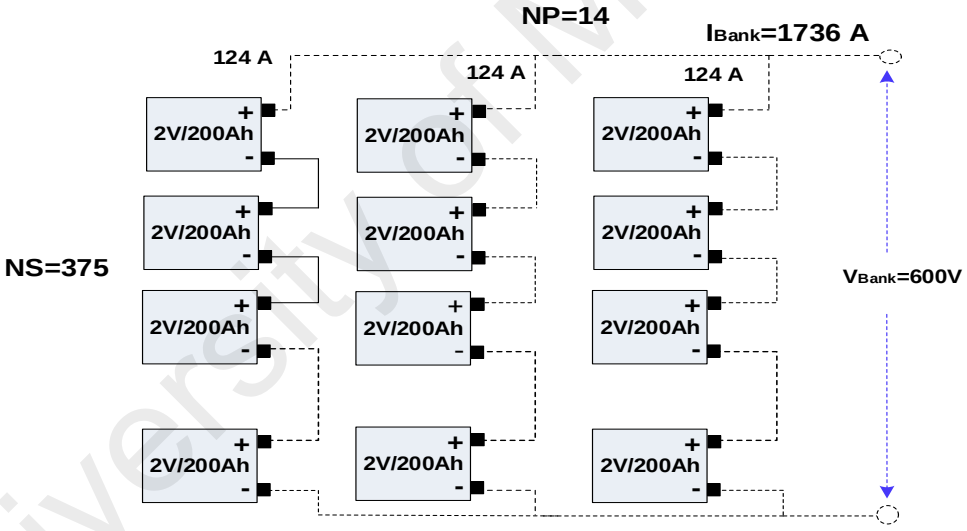

Figure 5.5: The construction of battery bank

The number of batteries connected in series and parallel can be calculated by:

$$N_P = \frac{I_{Bank}}{I_{Bat}} = \frac{1666\ A}{124\ A} = 13.45 \approx 14 \tag{5.2}$$

Where

$$I_{Bank} = \frac{P_{Bank}}{V_{Bank}} = \frac{1MW}{600V} = 1666\ A \tag{5.3}$$

$$N_S = \frac{V_{Bank}}{V_{Bat,min}} = \frac{600\ V}{1.6\ V} = 375 \tag{5.4}$$

Where I_{Bank} is the battery bank output current; P_{Bank} is the total output power of battery bank; V_{Bank} is the battery bank terminal voltage; I_{Bat}, $V_{B,min}$ are battery current at specific time and minimum battery voltage respectively, these two values are taken from Table 5.3.

Table 5.3: Technical specifications of lead acid battery cell (Vision CL200)

Nominal voltage	V	2V					
Nominal capcity	C_{10}	200Ah (20h)					
Internal resistance	R_0	< 0.1m Ohm					
Maximum Charge current	$I_{ch,Max}$	1000 A (5 s)					
Final Voltage		15 min	30 min	45 min	1h	5h	10h
1.6 V	Ampere	294	196	162	124	39.3	21.4
	Power	524	380	308	245	106	78
1.65	Ampere	280	187	155	120	38.4	21.2
	Power	499	364	299	235	104	76.6
1.7	Ampere	265	178	148	115	37.4	20.9
	Power	473	348	289	224	101	75
1.75	Ampere	250	169	141	110	36.3	20.5
	Power	446	331	280	213	98.0	73.5
1.8	Ampere	235	160	134	104	35.0	20.0
	Power	420	315	272	201	94.7	71.7

(A) The Battery Model

A generic dynamic battery model, which represent most popular types of rechargeable batteries, is considered in this research. The circuit models the transient behavior and internal resistance of the battery by a controlled voltage source in series with a constant resistance, as shown in Figure 5.6.

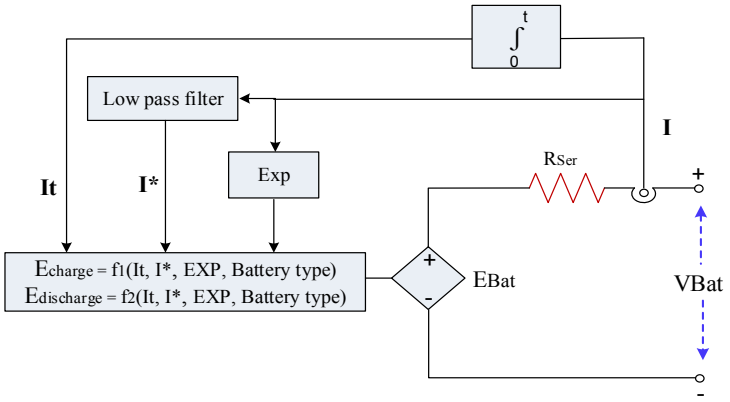

Figure 5.6: Generic dynamic battery model

In this research, the lead acid battery model is considered with the following equations for charging and discharging modes (Yong, Ramachandaramurthy, Tan, & Mithulananthan, 2015).

- Discharge model (I > 0)

$$V_{Bat} = E_0 - K \times \frac{Q}{Q - I_t} \times I_t - K \times \frac{Q}{Q - I_t} \times I^* - (R_{Bat} \times I_{Bat}) + C \quad (5.5)$$

Where

$$C = B \times |I_t| \times (-C + A) \quad (5.6)$$

- Charge model (I < 0)

$$V_{Bat} = E_0 - K \times \frac{Q}{Q - I_t} \times I_t - K \times \frac{Q}{I_t - 0.1 \times Q} \times I^* - (R_{Bat} \times I_{Bat}) + C \quad (5.7)$$

Where

$$C = B \times |I_t| \times (-C) \quad (5.8)$$

$$E_0 = V_{Full} + K + I_{Bat} \times R_{Bat} - A \quad (5.9)$$

Where V_{Bat} = Nonlinear voltage (V); E_0 = Constant voltage; K = Polarization constant (Ah^{-1}) or Polarization resistance (Ohms), I^* = Low frequency current dynamics (A); I_{Bat} = Battery current (A); I_t = Extracted capacity (Ah), Q = Maximum battery capacity (Ah), A = Exponential voltage (V), and B = Exponential capacity $(Ah)^{-1}$

All of the parameters mentioned above is available from the manufacturer's datasheet. However, polarization resistance K, exponential voltage A, and exponential capacity B need to be calculated from the discharge curve of the battery.

i Discharge Curve

A typical discharge curve is composed of three sections, as shown in Figure 5.7. The first section represents the exponential voltage drop when the battery is charged, the second section represents the charge that can be extracted from the battery until the voltage drops

below the battery nominal voltage, and the third section represents the total discharge of the battery when the voltage drops rapidly.

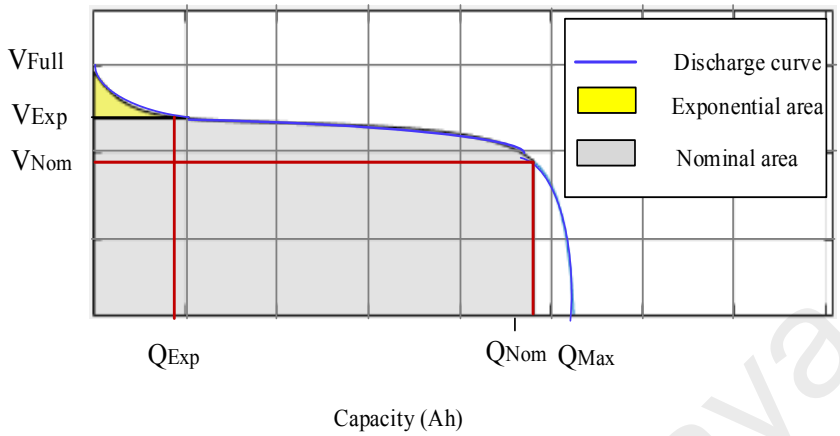

Figure 5.7: Typical Discharge Curve

ii Extract Battery Parameters from Discharge Curve

The typical discharge characteristic of a lead acid battery considered in this research is shown in Figure 5.8.

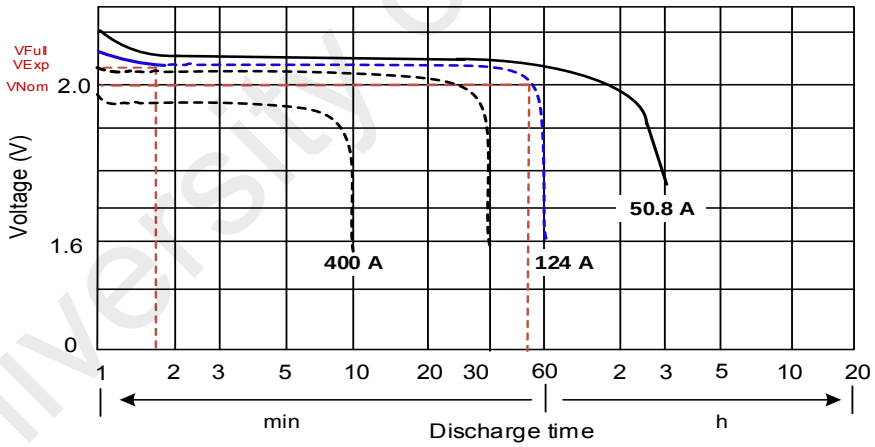

Figure 5.8: Discharge characteristics of (Vision CL200 2V 200Ah)

From the discharge curve shown in Figure 5.8 and the manufacturer datasheet presented in Table 5.3, the parameters of the discharge equation of battery can be calculated as follows (Tremblay, Dessaint, & Dekkiche, 2007):

$$A = V_{Full} - V_{Exp} = 2.05 - 2.02 = 0.03\ V \tag{5.10}$$

$$B = \frac{3}{Q_{Exp}} = \frac{3}{I_{Bat} \times discharge\ time} = \frac{3}{(124 \times 0.03)\ Ah} = 0.75\ Ah^{-1} \tag{5.11}$$

Where A is the voltage drop during the exponential zone (V). Then, the polarization voltage K can be deduced from the fully charged voltage (V_{Full}) and the third point (End of the nominal zone: Q_{Nom} and E_{Nom}):

$$K = \frac{\left(V_{Full} - V_{Nom} + A \times (e^{-B \times Q_{Nom}} - 1)\right) \times (Q_{Max} - Q_{Nom})}{Q_{Nom}} \tag{5.12}$$

$$K = \frac{\left(2.05 - 2.02 + 0.03 \times (e^{-0.75 \times 57} - 1)\right) \times (124 - 115)}{115} = 0.06\, V/Ah$$

$$E_0 = 2.05 + 0.06 + (124 \times 0.1 \times 10^{-3}) - 0.03 = 2.09\, V$$

5.2.4.2 Bi-directional Buck-Boost Converter Model

In this research, the Bi-directional buck-boost converter is used to control the active power flow between the battery and distribution network based on frequency deviation and battery State of Charge (SOC). This converter has two operation modes, as shown in Figure 5.9. For the over-frequency mode, the frequency management unit sends a command to DC/DC converter to work as a buck converter. In this situation, the IGBT-1 is initiated to charge the battery, and the current will flow from distribution network to the battery, while for the under-frequency mode, the frequency management unit sends a command to DC/DC converter to work as a boost converter. In this situation, the IGBT-2 is initiated to discharge the battery, and the current will flow from the battery to distribution network. In this converter, the switch (SW) is used to disconnect the battery, as per section 3.2.3.

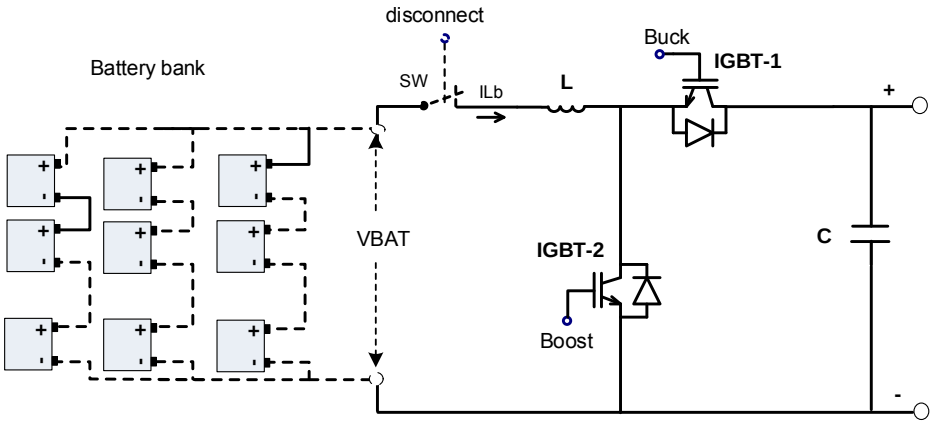

Figure 5.9: Bidirectional buck-boost converter.

The parameters of the bidirectional buck-boost converter used in the PSCAD simulation are shown in Table 5.4. The dc-link voltage is set to 800 V, where the VSC can work normally, and expressed by:

$$V_{dc} = \frac{2\sqrt{2}V_{LL}}{m\sqrt{3}} \tag{5.13}$$

Where V_{LL} is the RMS value of line-to-line inverter voltage at the grid side and m is the PWM duty cycle. Depending on the dc-link voltage, the battery voltage is determined to be 600 V suitable for charging and discharging the battery via the bidirectional converter. The quiescent duty ratio is expressed by:

$$D = \frac{V_{Batt}}{V_{dc}} = \frac{600}{800} = 0.75 \tag{5.14}$$

Because batteries have internal impedance, ripple current flowing into a battery can cause heating due to simple power dissipation heating. Therefore, the LC filter is necessary to decrease this ripple, and can be determined using:

$$L_f = \frac{D \times V_{Batt} \times (1-D)}{2f_{sw} \times \text{ICR} \times I_{O,Max}} = \frac{0.75 \times 600 \times (1-0.75)}{2 \times 10000 \times 0.2 \times 1736} = 16\ \mu H \tag{5.15}$$

$$C_f = \frac{D \times (1-D)}{16 \times fsw^2 \times L_f} \times \frac{V_{Batt}}{\text{CVRR} \times V_O} = \frac{0.75 \times (1-0.75)}{16 \times 10000^2 \times 30 \times 10^{-6}} \times \frac{600}{0.02 \times 800}$$

$$= 146\ \mu F \tag{5.16}$$

Where *D* is the PWM switching modulation index; ICR is the inductor current ripple ratio, usually ICR is 20%-40% of $I_{o,Max}$; CVRR is the capacitor voltage ripple ratio, usually CVRR is limited to less than 1~2% of the output voltage; f_{sw} is the switching frequency; $I_{o,Max}$ is the maximum output current from the converter; *Vo* is the output voltage of the converter.

Table 5.4: Parameters of bidirectional buck boost converter

Parameter Symbol Target	Parameter Symbol	Parameter value
Input Voltage	V_{IN}	700 V
Output Voltage	V_{OUT}	819 V
Switching Frequency	f_{SW}	10 KHz
Maximum Output Current	$I_{OUT, MAX}$	1428 A
The minimum inductance value	L_{min}	15 µH
The minimum capacitance value	C_{min}	133µF

5.2.4.3 Three Phase Bidirectional Inverter Model

The main aim of using a bidirectional inverter in this research is to exchange power between the distribution network and the BSS. The bidirectional DC-DC converter has two operational modes, the first is activated when the system's frequency exceeds the nominal value, where in this situation, the DC-DC converter operates as a rectifier to transfer the extra active power from the distribution network to battery. In the case of under-frequency events, the second mode is activated, where the converter operates as an inverter to transfer active power from the battery to the distribution network via the DC-DC converter. This active power is necessary to compensate for the power deficit in the distribution network.

5.3 Simulation Results of Frequency Control Scheme

The validation of the proposed frequency control scheme is divided into four case studies, where each represents a specific PV penetration level. Through each case study, various scenarios have been implemented to demonstrate the ability of frequency control scheme on stabilizing the frequency of the islanded distribution network. Furthermore, these scenarios show the voltage and phase synchronization process with the islanded distribution network with the main grid. The simulation case studies are summarized in Table 5.5.

Table 5.5: The simulation case studies

Case study	Mini-hydro-1	Mini-hydro-2	Bio-Mass	PV units	Penetration level of rotary DGs	Penetration level of PV	Scenario
1	√	√	√	0	80%	0%	**1** Islanding followed by load increament (0.5MW) without inertia
							2 Islanding followed by Bio-Mass DG trip
							3 Islanding followed by Bio-Mass DG without BSS
2	√	√	x	3	53%	25%	**1** Islanding followed by load increment (0.5MW) without inertia
							2 Islanding followed by mini-hydro DG trip
							3 Islanding followed by mini-hydro trip without BSS
							4 Islanding followed by mini-hydro trip **during night**
3	√	√	x	4	53%	33%	**1** Islanding followed by load increament (0.5MW) without inertia controller
4	√	x	x	6	27%	50%	**1** Islanding followed by load increament (0.5MW) without inertia controller
							2 Islanding followed by load increment (0.5MW) with inertia controller

5.3.1 First case study (80% rotary DGs and 0% PV penetration level)

First scenario: Islanding followed by load increment (0.5MW) without inertia controller

In this scenario, the intentional islanding occurred at t=10s. Immediately after islanding, the system frequency begins to decrease in the response to an excess load of (1.1 MW). Accordingly, both primary frequency control of BSS and the governor system of mini-hydro provide the required power to restore the frequency to an acceptable level. At 30s, a secondary frequency control from BSS is activated to bring back the distribution network to its nominal value of (50Hz), as shown in Figure 5.10. At 40s, the load increment will be 0.5 MW. Immediately after load increment, the system frequency begins to decline again in response to an excess load. In this situation, the UFLS controller will not be initiated because the least reserve power (mini-hydro & battery reserve) is sufficient to recover the network frequency. At 70 s, the phase controller is activated to synchronize the distribution network phase angle with the main grid. When the synchronization criteria of phase and voltage are achieved, the distribution network will be smoothly reconnected to the main grid, as shown in Figure 5.11 a) and b).

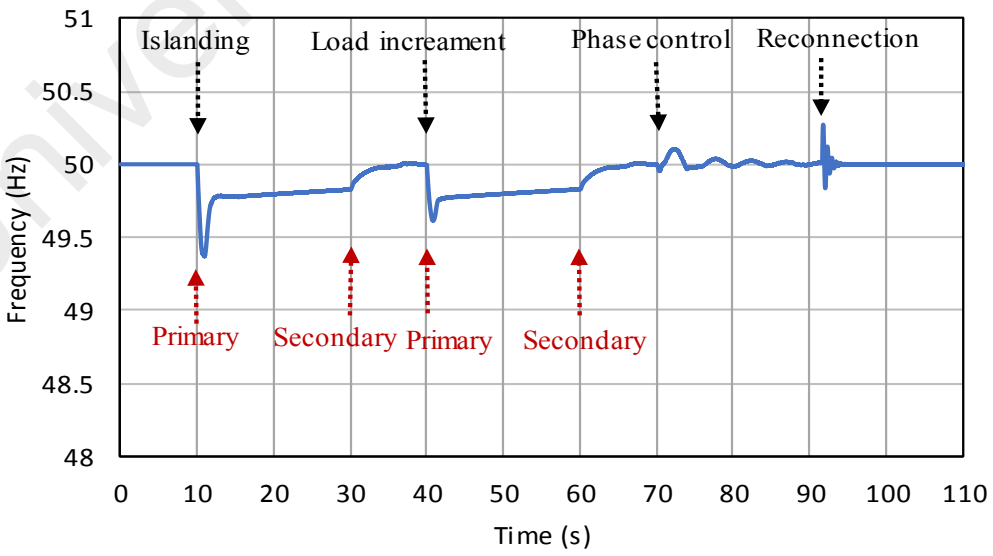

Figure 5.10: Frequency response of intentional islanding followed by load increment (first scenario/first case study)

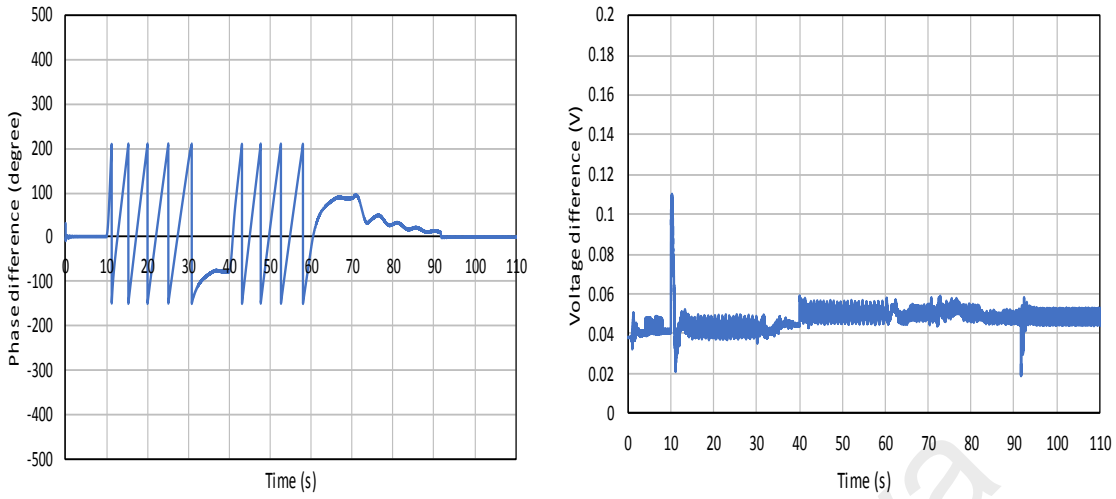

a) b)

Figure 5.11: a) Phase difference between distribution network and main grid for (first scenario/first case study) **b)** the voltage difference between distribution network and main grid for (first scenario/first case study)

Second scenario: Islanding followed by Bio-Mass DG trip

In this scenario, the distribution network will report the same response to the first scenario, however, at 40s, a biomass DG of (1.7 MW) is tripped from the network. Therefore, the system's frequency begins to decline in response to an excess load, as shown in Figure 5.12. In this situation, the UFLS controller will be initiated and shed load 4 (0.314 MW), because the least reserve power (1.4 MW) is insufficient to recover the network frequency. When the synchronization criteria of phase and voltage are achieved, as shown in Figure 5.13 a) and b), the distribution network will be smoothly reconnected to the main grid.

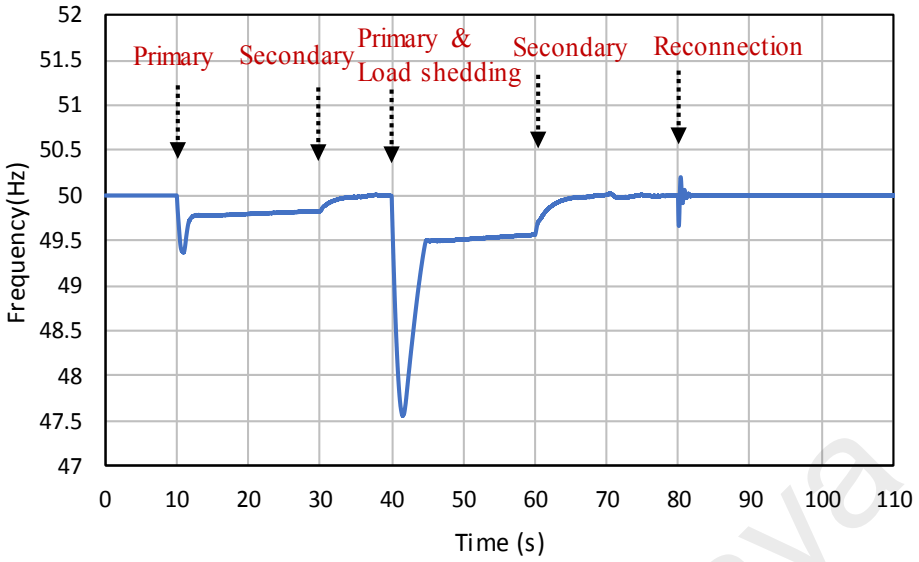

Figure 5.12: Frequency response for intentional islanding followed by Bio-Mass trip (first case study)

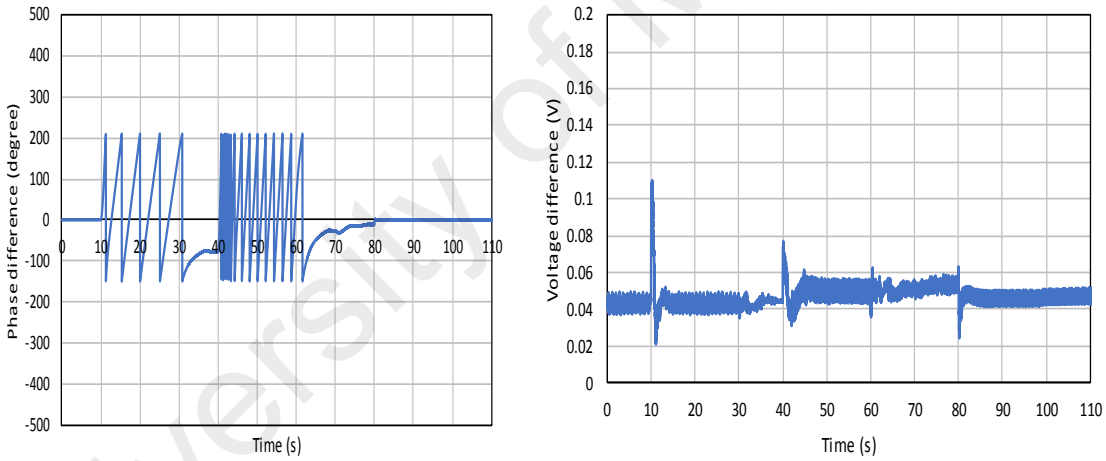

a) b)

Figure 5.13: a) The phase difference between distribution network and main grid for (second scenario/first case study) **b)** the voltage difference between distribution network and main grid for (second scenario/first case study)

Third scenario: Islanding followed by Bio-Mass DG trip without BSS

In this scenario, intentional islanding occurred at t=10s. Immediately after islanding, the system frequency begins to decline in response to an excess load of (1.1 MW). Accordingly, the UFLS is activated and shed load 7 (0.583 MW), since the reserve power

available from the three DGs is insufficient (0.52 MW). At 40s from islanding, a biomass DG (1.8 MW) is tripped from the network. Therefore, the system frequency begins to decline in response to the excess load, as shown in Figure 5.14. In this situation, the UFLS controller will be initiated and shed loads 3, 4, 8, 9 (1.8 MW).

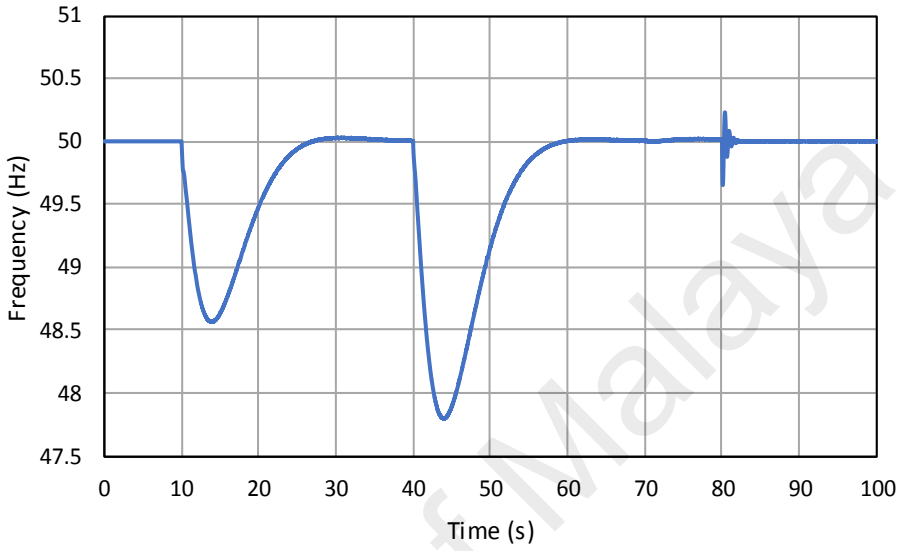

Figure 5.14: Frequency response for intentional islanding followed by Bio-Mass DG trip without BSS (first case study)

5.3.2 Second case study (53% rotary DGs and 25% PV penetration level)

First scenario: Islanding followed by load increment (0.5MW) without inertia controller

In this scenario, the distribution network has the same response to (**First scenario/First case study**), as shown in Figure 5.15. However, the rate of change of frequency is larger due to the reduced inertia response of the distribution network. When the synchronization criteria of the phase and voltage are achieved, as shown in Figure 5.16 a) and b), the distribution network will be smoothly reconnected to the main grid.

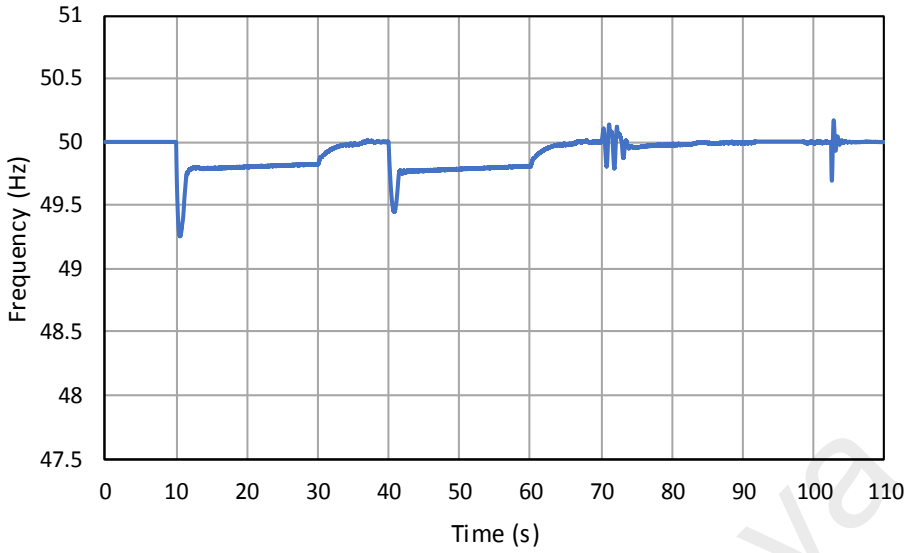

Figure 5.15: Frequency response of intentional islanding followed by load increament (0.5MW) without inertia controller

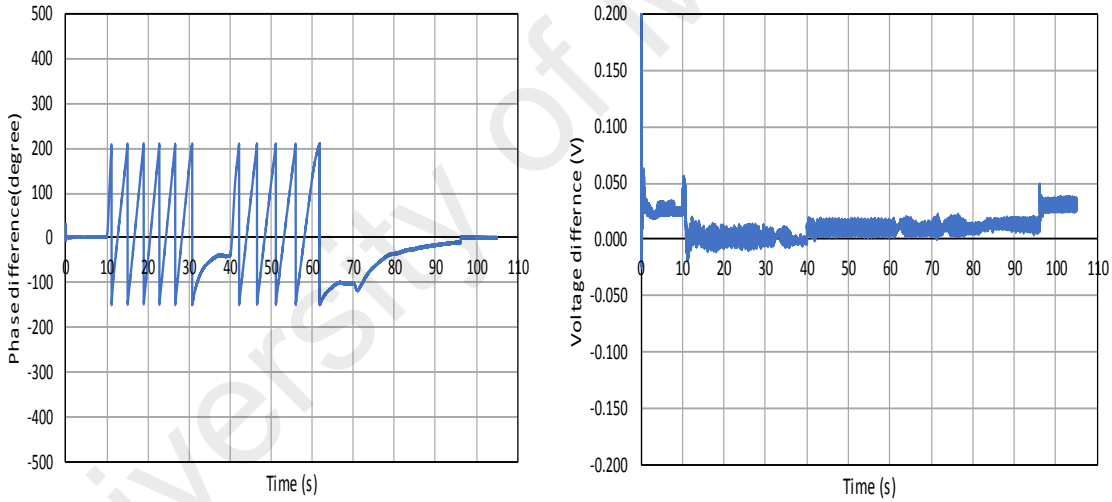

a) **b)**

Figure 5.16: a) The phase difference between distribution network and main grid (first scenario/second case study) **b)** The voltage difference between distribution network and main grid for (First scenario/Second case study)

Second scenario: Intentional islanding followed by mini-hydro trip with BSS

In this scenario, the distribution network has the same response to (**Second scenario/First case study**). However, at 10s, the rate of change of frequency is larger due to the reduced inertia response of distribution network, which will be detailed in the discussion section.

Furthermore, at 40s, a biomass DG (1.7 MW) is tripped from the network. Therefore, the system's frequency begins to decline in response to an excess load, as shown in Figure 5.17. In this situation, the UFLS controller will be activated and shed load 5 (0.5 MW), because the least reserve power (1.2 MW) is insufficient to recover the network frequency.

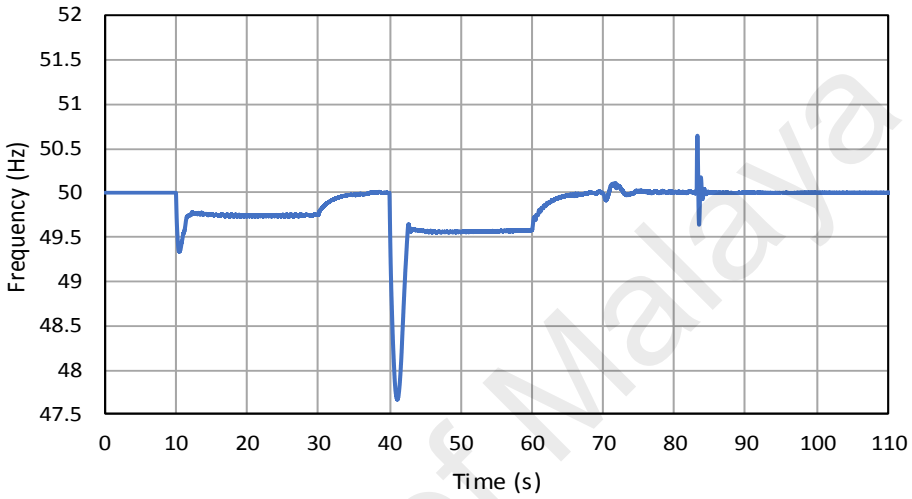

Figure 5.17: Frequency response for intentional islanding followed by mini-hydro trip (Second scenario/Second case study)

Third scenario: Islanding followed by mini-hydro trip without BSS

This scenario has been implemented to showcase the benefit of frequency regulation control by BSS. Intentional islanding occurred at t=10s. Immediately after islanding, the system frequency begins to decline in response to an excess load of (1.1 MW), as shown in Figure 5.18. Accordingly, UFLS is activated and shed loads 1, 2, 3, 4 (0.577 MW), since the reserve power available from the three DGs is insufficient (0.43 MW). At 40s from islanding, a biomass DG (1.8 MW) is tripped from the network. Accordingly, the system frequency begins to decline quickly, and the UFLS will not have the opportunity to shed the required loads in the appropriate timeframe. Therefore, the distribution network frequency will arrive at 47.5 Hz, which leads to a total black out.

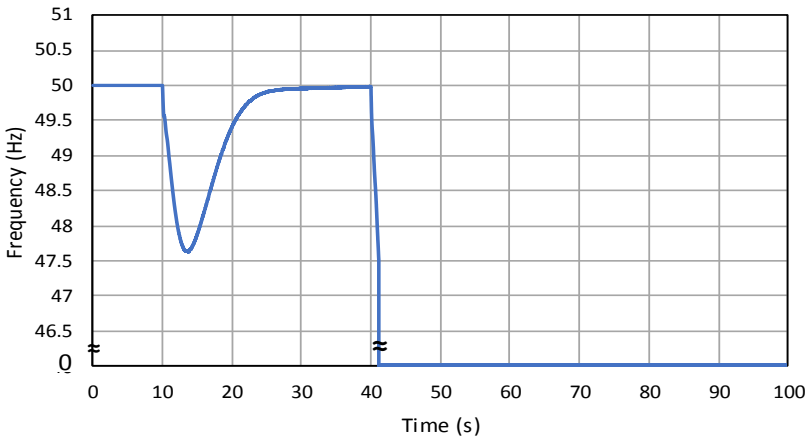

Figure 5.18: Frequency response of intentional islanding followed by mini-hydro trip without BSS

Fourth scenario: Islanding followed by mini-hydro trip during night

This scenario has been implemented to showcase the performance of the frequency control scheme when intentional islanding occurs in the night, where the PV units did not provide any power. Intentional islanding occurred at t=10s. Immediately after islanding, the system's frequency begins to decline in response to an excess load of (2.67 MW), as shown in Figure 5.19. Accordingly, the UFLS is activated and shed loads 1, 2, 3 (0.263 MW), since the reserve power available from the three DGs is insufficient (2.43 MW). At 40s from islanding, a mini-hydro DG (1.8 MW) is tripped from the network. Accordingly, the system frequency begins to decline quickly, and the UFLS is activated and shed loads 1, 5, 6, 8, 10 (1.85 MW).

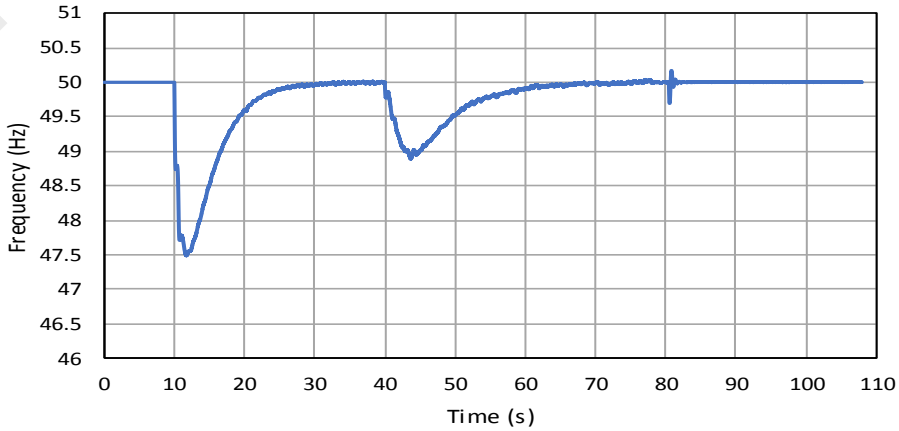

Figure 5.19: Frequency response of intentional islanding followed by mini-hydro trip during night

5.3.3 Third case study (53% rotary DGs and 33% PV penetration level)

This case study has been implemented to show the difference between frequency responses of the islanded distribution network at different PV penetration with fixed penetration level of rotating based DGs.

First scenario: Islanding followed by load increment (0.5MW) without inertia controller

This scenario has been implemented to showcase the effect of increasing the PV penetration level with fixed penetration level of rotating based DGs. As shown in Figure 5.20, the frequency response of distribution network in this scenario is similar to the frequency response of first scenario in the second case study.

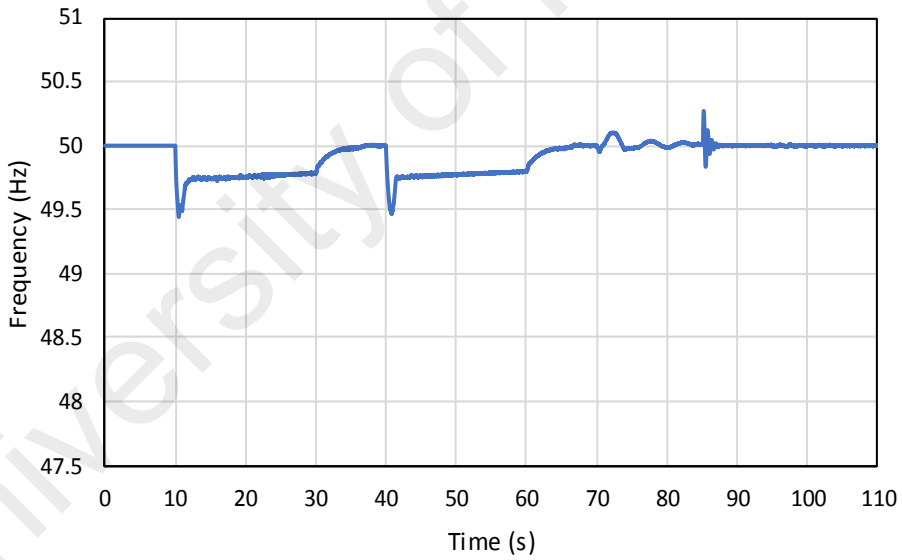

Figure 5.20: Frequency response of intentional islanding followed by load increment (0.5MW) for (first scenario/third case study)

5.3.4 Fourth case study (27% rotary DGs and 50% PV penetration level)

First scenario: Islanding followed by load increment (0.5MW) without inertia controller

This scenario has been implemented to show the importance of inertia controller at high PV penetration. From Figure 5.21, when the inertia controller is not activated, the

frequency will quickly drop. Therefore, the primary frequency control is unable to stop the frequency deviation. Furthermore, the UFLS controller will not have the opportunity to shed the required load in time.

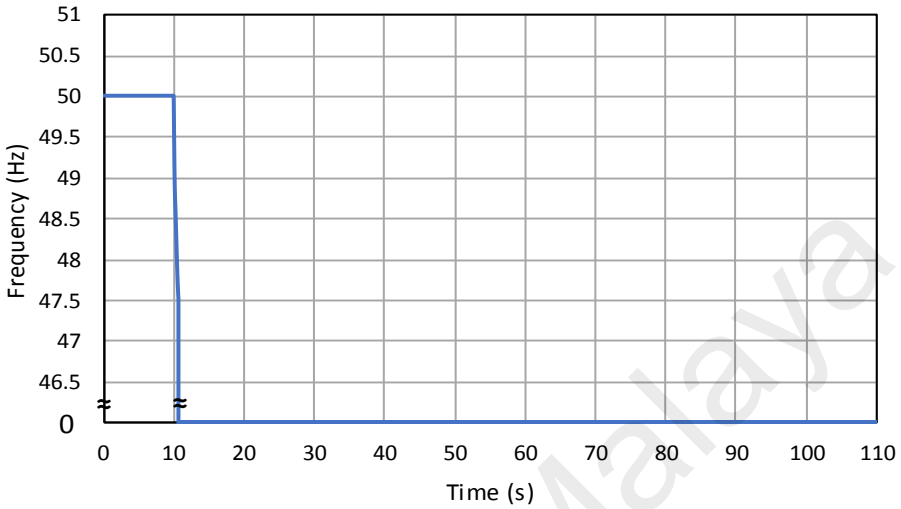

Figure 5.21: Frequency response of intentional islanding followed by load increment (0.5MW) for (first scenario/fourth case study)

Second scenario: Islanding followed by load increment (0.5MW) with inertia controller This scenario shows that the rate of change of frequency and the frequency deviation are larger than the first scenario in the first and second case studies, as shown in Figure 5.22. In fact, this difference is due to the reduced inertia response caused by the increase PV penetration.

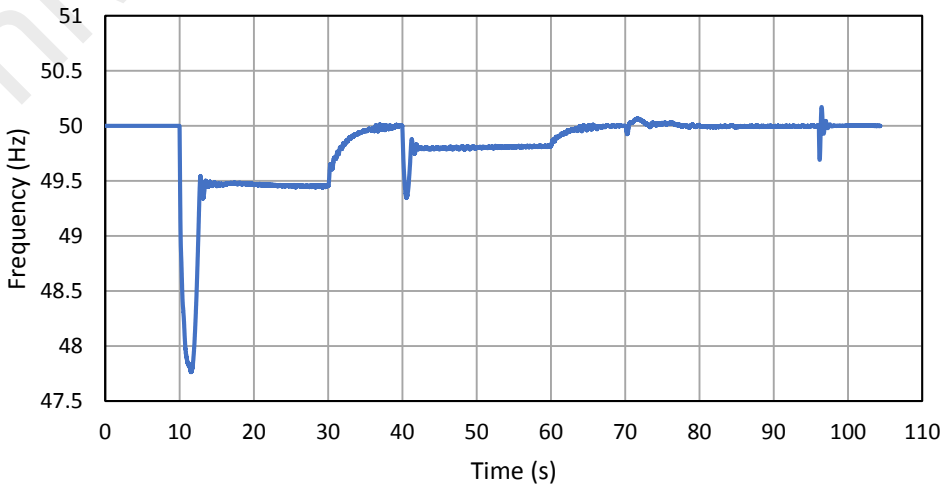

Figure 5.22: Frequency response of intentional islanding followed by load increment (0.5MW) for (second scenario/fourth case study)

5.4 Discussion

From the simulation results, when the PV penetration level increased from 0% →25% →50%, the rate of change of frequency of islanded distribution network will increase from 1.5 Hz/s →2.5 Hz/s→ 6.5 Hz/s at intentional islanding. Figure 5.23 shows the frequency response at different PV penetration levels (islanding, followed by 0.5 MW load increment). The selected areas shown in Figure 5.23 were enlarged to make it easier to see the difference between the different frequency responses.

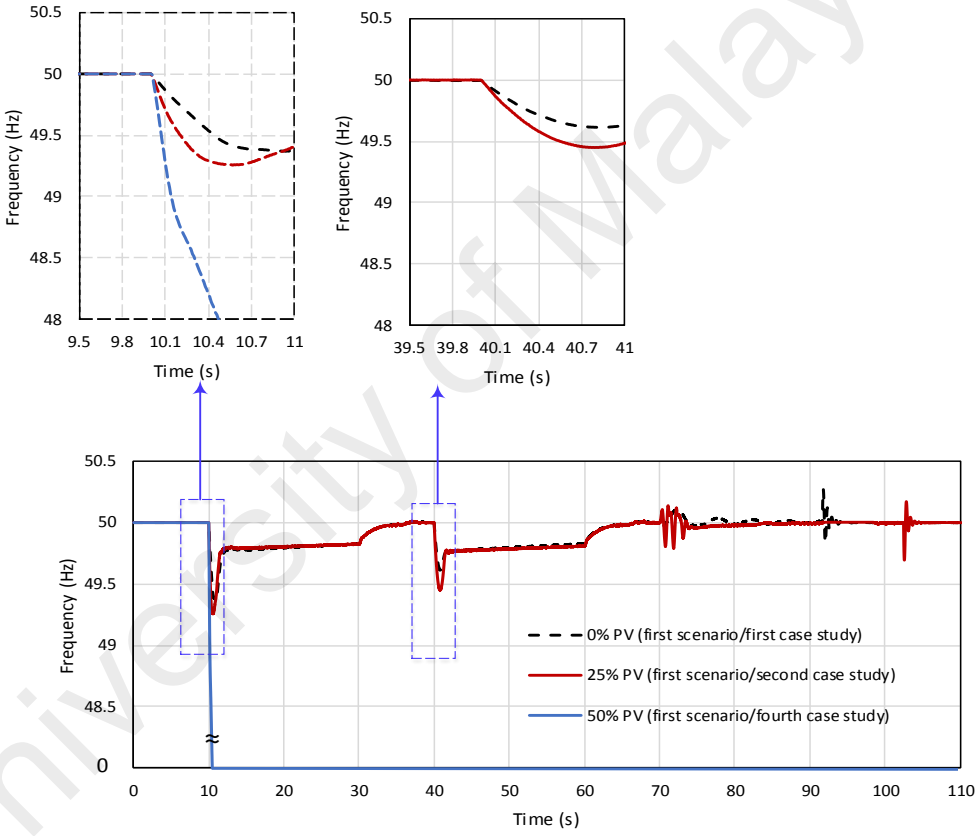

Figure 5.23: Frequency response comparison between different PV penetration levels

As shown in Figure 5.24, when the distribution network islanding takes place without inertia controller, the frequency drops below 47.5 Hz, which leads to a total blackout. However, when the inertia controller is used in (first scenario/fourth case study), it gives time for the primary frequency controller to be activated. In fact, the importance of inertia controller at low PV penetration level is lower, as shown in Figure 5.25, where the figure

shows that the rate of change of frequency slightly changes when the inertia controller is used.

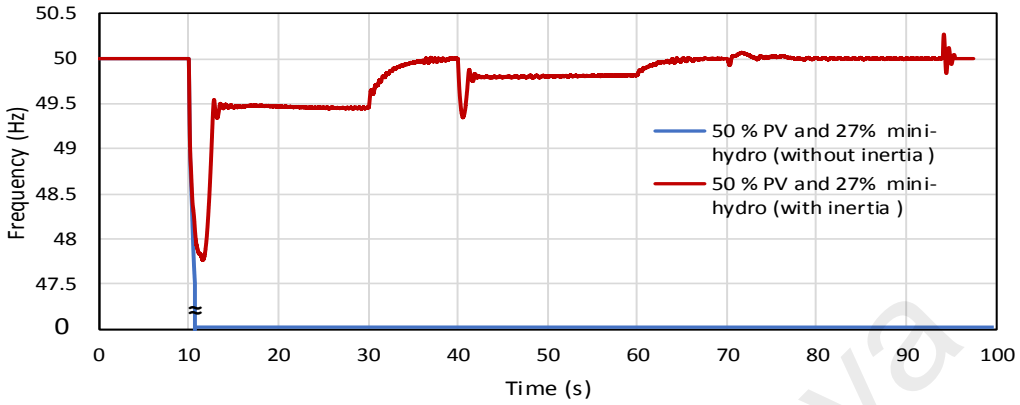

Figure 5.24: Frequency response for 50% PV penetration with and without inertia

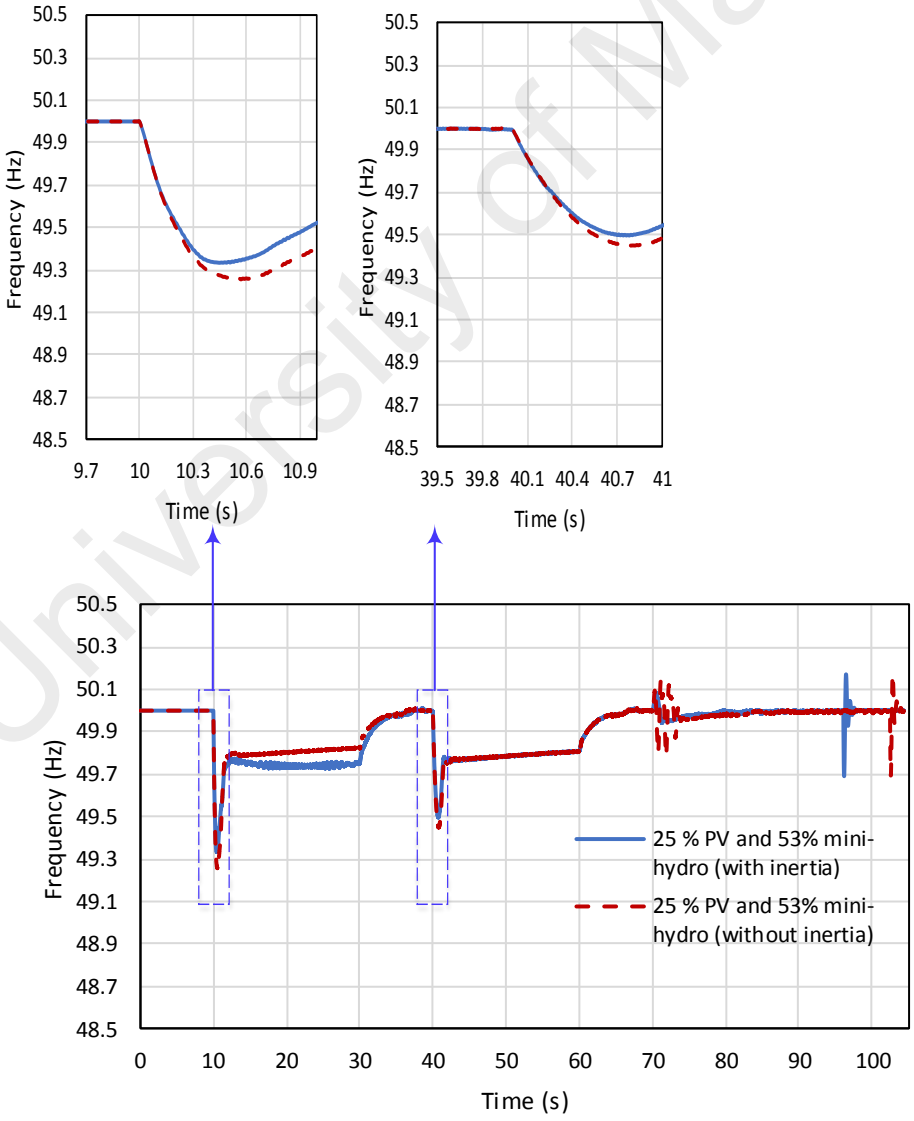

Figure 5.25: Frequency response for 25% PV penetration with and without inertia

From the simulation results, it is clear that increasing the PV penetration level with fixed penetration level of rotating based DGs did not increase the rate of change of frequency of the islanded distribution network. Figure 5.26 shows that when the PV penetration level is increased from 25% to 33% with fixed penetration level of mini-hydro, the rate of change of frequency will not change. The intentional islanding occurred at t=10s, the system frequency begins to decline in both scenarios. However, the frequency deviation is not similar due to different imbalance power. At 40s, the load increment will be 0.5 MW. Immediately after load increment, the system frequency begins to decline at the same rate of change of frequency.

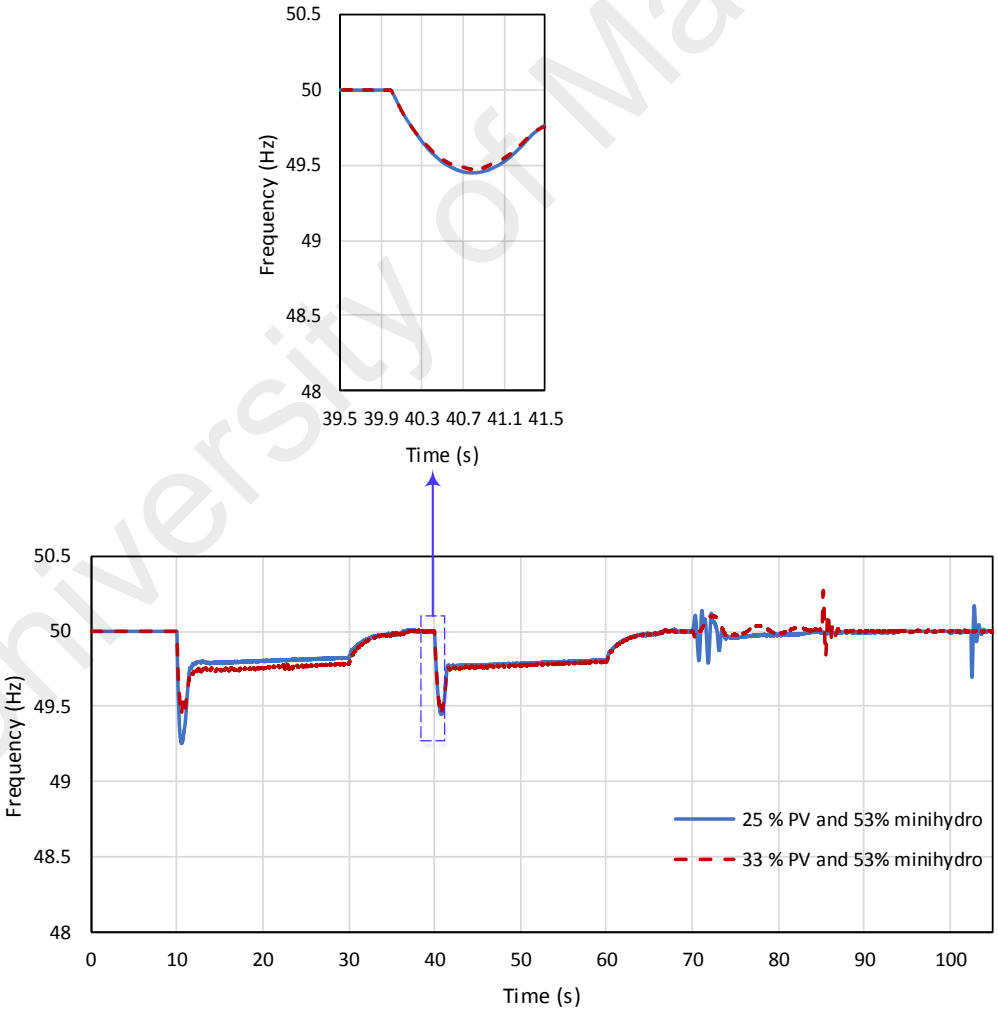

Figure 5.26: Frequency responses for two penetration level of PV with fixed penetration level of mini-hydro generation

The main contributions of inertia and frequency regulation controllers proposed in this research compared with controllers proposed in literature are summarized in Tables 5.6 and 5.7, respectively. As shown in Table 5.6, this research proposes an inertia controller to allow the PV to provide inertial response based on the ROCOF value, which is not accounted for in literature. In terms of frequency regulation controller, for the first time, this research used BSS to provide both primary and secondary frequency services. Also, in this research, a CCS is designed to coordinate the operation of the frequency regulation controller, and manage the charging and discharging states of BSS.

With regards to the proposed UFLS technique, Table 5.7 shows that the new technique uses the metaheuristic method to select the optimal combination loads to be shed from random and fixed priority loads. This advantage prevents the over-shedding or under-shedding problems, and increase the stability of the distribution network. As shown in Table 5.7, the execution time of FRPLS technique to select the optimal combination of loads is 0.5 second, while for the proposed UFLS technique, only 0.154 second is required to make that decision. As discussed in chapter 3, The delay time that includes the measurements, communication, and circuit breaker operation time is assumed to be 0.1 second, based on practical considerations (Laghari et al., 2015). Accordingly, the total execution time of FRPLS controller to shed the loads is 0.6 second, while for proposed UFLS controller, only 0.254 second is required.

Table 5.6: Comparison between inertia and frequency regulation controllers proposed in this research and controllers proposed in the literature

	Technique	Controller	Advantages	Disadvantages
Controllers proposed in literature	Deloading of PV	Voltage controller	(A) Fast response due to electronic converter (B) Improve frequency regulation services (C) Simple controller based on classical PI	(A) Some power lost due to the deloading technique (B) The controller does not adapt; a classical PI is used without tuning
		Voltage controller based on Intelligent Algorithm tuning PI	(A) Fast response due to electronic converter (B) The controller adapts according to different changes	(A) Some power lost (B) Low reliability
	Deloading (PV) + ESS	Voltage controller (PV) + Primary frequency controller (ESS)	(A) High reliability (ESS is used) (B) No power loss (C) Improve frequency regulation services	(A) High cost due to ESS (B) Provide only primary frequency control
	Inertia response controller	Hidden inertia Emulation	(A) No power loss (B) Allow the wind turbine to increase the network inertial response by releasing the stored power from the rotated blade	(A) Low reliability (B) The controller does not adapt; a classical PI is used without tuning
		Fast power reserve		
	Deloading of wind turbine	Speed control	Fast response due to electronic converter	(A) The controller does not adapt; a classical PI is used without tuning (B) Limited by rated speed
		Pitch angle control	It can be used to control the wind turbine after rated speed	(A) Slow response due to mechanical movements (B) The controller does not adapt; a classical PI is used without tuning
		Speed control based on Intelligent Algorithm	The controller adapts according to different changes	(A) Low reliability (B) Provide only primary frequency control
	Deloading of wind turbine + ESS	Speed control + Primary frequency controller (ESS)	(A) High reliability (ESS is used) (B) Improve frequency regulation services	High cost due to ESS
Controllers proposed in this research	Deloading	Inertia controller by PV	The PV generation provide inertial response to the distribution network	The deloading amount is constant
	Frequency regulation by BSS	Primary and secondary frequency controller	(A) Provide primary and secondary frequency services that improve network stability (B) High reliability (BSS is used)	(A) The controller does not adapt; a classical PI is used without tuning (B) High cost due to BSS

Table 5.7: Comparison between UFLS technique proposed in this research and technique proposed in the literature

UFLS technique	**References**	**Method used in UFLS technique**	**Priority of shedding loads**	**The ability to shed the optimal combination of loads**	**Time consumed in selecting the optimal combination of loads**	**Effect of network configuration on the UFLS technique**
Conventional UFLS technique	(Tang et al., 2013; Zin et al., 2004)	Predetermined frequency steps	Fixed priority load	Suffers from over-shedding or under-shedding	No time consumed (fixed priority load)	The predetermined steps need to be selected according to the network's configuration
Adaptive UFLS technique	(Marzband et al., 2016; Rudez & Mihalic, 2011)	Swing equation				This technique does not depend on the network's configuration
Computational Intelligence Based Load Shedding Techniques	(Mokhlis et al., 2012; Sallam & Khafaga, 2002)	Fuzzy logic method		Suffers from over-shedding or under-shedding	No time consumed (fixed priority load)	These techniques need to be trained using network data, therefore, it depends on network configuration
	(Sanaye-Pasand & Davarpanah, 2005)	Genetic algorithm method				
	(Amraee et al., 2006)	PSO method				
	(Hooshmand & Moazzami, 2012; Javadian et al., 2013)	ANN method				
Fixed and random priority load shedding technique	(Laghari et al., 2015)	Swing equation	Fixed and random priority load (consider all combinations of loads)	Shedding the optimal combination of loads	0.5 second (ten random priority loads and two fixed priority loads)	This technique does not depend on the network's configuration
Proposed UFLS technique	In this research	Swing equation	Fixed and random priority load with metaheuristic methods	Shedding the optimal combination of loads	0.154 second (ten random priority loads and two fixed priority loads)	This technique does not depend on the network's configuration

5.5 Summary

This chapter detailed the modelling of the distribution network used to validate the proposed frequency control scheme. The effectiveness and robustness of the proposed frequency control scheme were investigated on a part of the Malaysian distribution network for islanding events, DG tripping event, and load increment cases. Through simulation results, the proposed scheme can stabilize the frequency of the islanded distribution network. Furthermore, when the proposed frequency control scheme was coordinated with the synchronization system, the islanded distribution network can smoothly reconnect to the main grid. Therefore, the frequency control scheme proposed in this thesis is applicable to real distribution networks.

CHAPTER 6: CONCLUSION AND FUTURE WORK

6.1 Introduction

Research on the islanding operation of distribution networks is progressing to the level that allows the DG-RES such as PV to continue working after being islanded from the main grid. However, the islanding of distribution network with high PV penetration is normally accompanied by several frequency stability issues. First, after islanding, the power reserve is insufficient for the load demand, which subsequently decreases the frequency of the network. Second, the islanding distribution network suffers from low inertial constant, which increases the rate of change of frequency. Therefore, this research proposed a frequency control scheme for the distribution network to address the frequency stability issues occurring after islanding.

6.2 Overall Conclusion

The four main objectives of this research, as outlined in Chapter 1, have been fulfilled. The following describes the outcome for each objective:

An inertia controller is proposed for PV units using the deloading technique. Through this technique, the PV units can be set to operate below the maximum power point to reserve some amount of power. This reserve power is released immediately whenever needed, such as when there is a disturbance in the distribution network. This operation mimics the synchronous generator's inertial response. From the simulation results presented in Chapter 5, it was found that the proposed inertia controller reduced the rate of change of frequency, and therefore provides an opportunity for frequency regulation controller to be activated. In the case where the frequency is decreasing under the allowable limit, the frequency regulation controllers will react.

These frequency regulation controllers consist of primary and secondary frequency controllers. These controllers will regulate the discharge power from the Battery Storage System (BSS) into the distribution network. Through the simulation results presented in Chapter 4, it was found that the primary frequency controller is able to stabilize the network frequency within the acceptable limit (49.5 Hz to 50 Hz). Furthermore, the secondary frequency controller was able to return the network frequency to its nominal value (50Hz). In the case where the frequency controllers fail to restore the frequency, the proposed UFLS controller will be activated.

The proposed UFLS controller used metaheuristic techniques (BEP, BGA, BPSO) technique to determine the optimal combination of loads to be shed from ten random priority loads. A comparison in terms of computation time between these metaheuristic techniques revealed that UFLS based on BEP was 30% and 82% less than BPSO and BGA, respectively. Based on this result, the performance of UFLS based on BEP was then compared with Adaptive and FRPLS techniques. It was found that the proposed UFLS shed the most optimal combination of loads, which is indicated by the none overshot of frequency.

To manage the operation of frequency control scheme and perform grid reconnection, a Centralized Control System (CCS) was modeled in this research. This CCS consist of a frequency management unit, UFLS controller, and reconnection controller. Through the simulation results presented in Chapter 5, the CCS succeeded in coordinating between frequency control scheme and other synchronization controllers. Therefore, the islanded distribution network was smoothly reconnected to the main grid.

6.3 Future Work

This research proposes a frequency control scheme for islanded distribution network with high PV penetration. To improve the proposed research, the following are recommendations for future works:

(1) In this research, only the technical aspect of proposed frequency control scheme has been considered. It is recommended to investigate the economic feasibility of this scheme as follows:

A) Investigate the economic analysis of inertia controller, considering the power loss caused by PV deloading and the market power price for inertia response.

B) Calculate the revenue from using battery storage system to provide frequency regulation, considering the price of battery storage system, life time of battery, and the market power price for frequency regulation.

C) Implement an economical comparison study between different energy storage systems to select the most revenue system.

(2) This research assumes that the BSS provides frequency regulation services. It is recommended that the impact of using other storage systems, such as hydro pumping, super-capacitor, and flywheel be studied as well.

(3) It is recommended that the grid disconnection process and islanding detection techniques, such as passive, active and remote techniques, be investigated to realize a comprehensive control system.

(4) In this work, the frequency control scheme was applied for a 29-bus part of Malaysian distribution network. In future works, the researcher can use models with larger scale network. Thus, the efficiency and competency of the proposed scheme can be observed and compared.

REFERENCES

Adhikari, S., & Li, F. (2014). Coordinated vf and pq control of solar photovoltaic generators with mppt and battery storage in microgrids. IEEE Transactions on Smart Grid, 5(3), 1270-1281.

Ali, S.Q., & Hasanien, H.M. (2012). Frequency control of isolated network with wind and diesel generators by using adaptive artificial neural network controller. International Review of Automatic Control, Praise Worthy Prize, 5(2).

Aman, M., Jasmon, G., Naidu, K., Bakar, A., & Mokhlis, H. (2013). Discrete evolutionary programming to solve network reconfiguration problem. Paper presented at the IEEE TENCON Spring Conference.

Amraee, T., Mozafari, B., & Ranjbar, A. (2006). An improved model for optimal under voltage load shedding: Particle swarm approach. Paper presented at the IEEE Power India Conference.

Anderson, P., & Mirheydar, M. (1992). An adaptive method for setting underfrequency load shedding relays. IEEE Transactions on Power Systems, 7(2), 647-655.

Arani, M.F.M., & El-Saadany, E.F. (2013). Implementing virtual inertia in dfig-based wind power generation. IEEE Transactions on Power Systems, 28(2), 1373-1384.

Basso, T. (2004). Ieee standard for interrconnecting distributed resources with the electric power system. Paper presented at the IEEE Pes Meeting.

Best, R.J., Morrow, D.J., McGowan, D.J., & Crossley, P.A. (2007). Synchronous islanded operation of a diesel generator. IEEE Transactions on Power Systems, 22(4), 2170-2176.

Bevrani, H., Habibi, F., Babahajyani, P., Watanabe, M., & Mitani, Y. (2012). Intelligent frequency control in an ac microgrid: Online pso-based fuzzy tuning approach. IEEE Transactions on Smart Grid, 3(4), 1935-1944.

Bhatt, R., & Chowdhury, B. (2011). Grid frequency and voltage support using pv systems with energy storage. Paper presented at the North American Power Symposium (NAPS).

Bianchi, F.D., De Battista, H., & Mantz, R.J. (2007). Wind turbine control systems.

Caldon, R., Stocco, A., & Turri, R. (2008). Feasibility of adaptive intentional islanding operation of electric utility systems with distributed generation. Electric Power Systems Research, 78(12), 2017-2023.

Castro, L.M., Fuerte-Esquivel, C.R., & Tovar-Hernández, J.H. (2012). Solution of power flow with automatic load-frequency control devices including wind farms. IEEE Transactions on Power Systems, 27(4), 2186-2195.

Chamana, M., & Chowdhury, B.H. (2013). Droop-based control in a photovoltaic-centric microgrid with battery energy storage. Paper presented at the North American Power Symposium (NAPS).

Chen, C.-R., Tsai, W.-T., Chen, H.-Y., Lee, C.-Y., Chen, C.-J., & Lan, H.-W. (2011). Optimal load shedding planning with genetic algorithm. Paper presented at the IEEE Industry Applications Society Annual Meeting (IAS).

Datta, M., Senjyu, T., Yona, A., Funabashi, T., & Kim, C.-H. (2011). A frequency-control approach by photovoltaic generator in a pv–diesel hybrid power system. IEEE Transactions on Energy Conversion, 26(2), 559-571.

De Almeida, R.G., & Lopes, J.P. (2007). Participation of doubly fed induction wind generators in system frequency regulation. IEEE transactions on power systems, 22(3), 944-950.

De Brito, M.A.G., Galotto, L., Sampaio, L.P., e Melo, G.d.A., & Canesin, C.A. (2013). Evaluation of the main mppt techniques for photovoltaic applications. IEEE transactions on industrial electronics, 60(3), 1156-1167.

Dehghanpour, K., & Afsharnia, S. (2015). Electrical demand side contribution to frequency control in power systems: A review on technical aspects. Renewable and Sustainable Energy Reviews, 41, 1267-1276.

Delille, G., François, B., & Malarange, G. (2010). Dynamic frequency control support: A virtual inertia provided by distributed energy storage to isolated power systems. Paper presented at the IEEE PES Innovative Smart Grid Technologies Conference Europe (ISGT Europe).

Díaz-González, F., Hau, M., Sumper, A., & Gomis-Bellmunt, O. (2014). Participation of wind power plants in system frequency control: Review of grid code requirements and control methods. Renewable and Sustainable Energy Reviews, 34, 551-564.

Díaz-González, F., Hau, M., Sumper, A., & Gomis-Bellmunt, O. (2015). Coordinated operation of wind turbines and flywheel storage for primary frequency control support. International Journal of Electrical Power & Energy Systems, 68, 313-326.

Dong, J., Xue, G., Dong, M., & Xu, X. (2015). Energy-saving power generation dispatching in china: Regulations, pilot projects and policy recommendations—a review. Renewable and Sustainable Energy Reviews, 43, 1285-1300.

Dreidy, M., Mokhlis, H., & Mekhilef, S. (2017). Application of meta-heuristic techniques for optimal load shedding in islanded distribution network with high penetration of solar pv generation. Energies, 10(2), 150.

Eberhart, R.C., & Shi, Y. (2000). Comparing inertia weights and constriction factors in particle swarm optimization. Paper presented at the Evolutionary Computation Conference.

Eid, B.M., Rahim, N.A., Selvaraj, J., & El Khateb, A.H. (2014). Control methods and objectives for electronically coupled distributed energy resources in microgrids: A review. IEEE Systems Journal, 1-13.

El-Sadek, M. (1998). Preventive measures for voltage collapses and voltage failures in the egyptian power system. Electric power systems research, 44(3), 203-211.

El Itani, S., Annakkage, U.D., & Joos, G. (2011). Short-term frequency support utilizing inertial response of dfig wind turbines. Paper presented at the IEEE Power and Energy Society General Meeting.

Energypedia.(2016).Hydropower basics. Retrieved from https://Energypedia.info/wiki/Hydro_Power_Basics.

Faranda, R., & Leva, S. (2008). Energy comparison of mppt techniques for pv systems. WSEAS transactions on power systems, 3(6), 446-455.

Gonzalez-Longatt, F., Chikuni, E., & Rashayi, E. (2013). Effects of the synthetic inertia from wind power on the total system inertia after a frequency disturbance. Paper presented at the International IEEE Conference of Industrial Technology (ICIT).

Hansen, A.D., Altin, M., Margaris, I.D., Iov, F., & Tarnowski, G.C. (2014). Analysis of the short-term overproduction capability of variable speed wind turbines. Renewable Energy, 68, 326-336.

Hoke, A., & Maksimović, D. (2013). Active power control of photovoltaic power systems. Paper presented at the IEEE Technologies for Sustainability (SusTech) Conference.

Hooshmand, R., & Moazzami, M. (2012). Optimal design of adaptive under frequency load shedding using artificial neural networks in isolated power system. International Journal of Electrical Power & Energy Systems, 42(1), 220-228.

Hsu, C.-T., Chuang, H.-J., & Chen, C.-S. (2011). Adaptive load shedding for an industrial petroleum cogeneration system. Expert Systems with Applications, 38(11), 13967-13974.

Hsu, C.-T., Kang, M.-S., & Chen, C.-S. (2005). Design of adaptive load shedding by artificial neural networks. IEE Proceedings-Generation, Transmission and Distribution, 152(3), 415-421.

Hua, C., & Shen, C. (1998). Study of maximum power tracking techniques and control of dc/dc converters for photovoltaic power system. Paper presented at the 29th Annual IEEE Power Electronics Specialists Conference.

Javadian, S., Haghifam, M.-R., Bathaee, S., & Firoozabad, M.F. (2013). Adaptive centralized protection scheme for distribution systems with DG using risk analysis for protective devices placement. International Journal of Electrical Power & Energy Systems, 44(1), 337-345.

Jayawardena, A., Meegahapola, L., Perera, S., & Robinson, D. (2012). Dynamic characteristics of a hybrid microgrid with inverter and non-inverter interfaced renewable energy sources: A case study. Paper presented at the IEEE International Power System Technology Conference (POWERCON).

Josephine, R., & Suja, S. (2014). Estimating pmsg wind turbines by inertia and droop control schemes with intelligent fuzzy controller in indian development. Journal of Electrical Engineering and Technology, 9(4), 1196-1201.

Kakimoto, N., Takayama, S., Satoh, H., & Nakamura, K. (2009). Power modulation of photovoltaic generator for frequency control of power system. IEEE Transactions on Energy Conversion, 24(4), 943-949.

Ketabi, A., & Fini, M.H. (2017). Adaptive underfrequency load shedding using particle swarm optimization algorithm. Journal of Applied Research and Technology, 15(1), 54-60.

Keung, P.-K., Li, P., Banakar, H., & Ooi, B.T. (2009). Kinetic energy of wind-turbine generators for system frequency support. IEEE Transactions on Power Systems, 1(24), 279-287.

Knudsen, H., & Nielsen, J.N. (2005). Introduction to the modeling of wind turbines. Wind power in power systems, 525-585.

Kuala Lumpur-Post (Producer). (2016). Earthquake: No signs of structural damage to kenyir dam. Retrieved from http://www.kualalumpurpost.net/earthquake-no-signs-of-structural-damage-to-kenyir-dam/kenyir-dam/.

Kundur, P., Balu, N.J., & Lauby, M.G. (1994). Power system stability and control (Vol. 7): McGraw-hill New York.

Laghari, J., Mokhlis, H., Bakar, A.H.A., Karimi, M., & Shahriari, A. (2012). An intelligent under frequency load shedding scheme for islanded distribution network. Paper presented at the International IEEE Power Engineering and Optimization Conference (PEDCO) Melaka, Malaysia.

Laghari, J., Mokhlis, H., Karimi, M., Bakar, A.H.A., & Mohamad, H. (2015). A new under-frequency load shedding technique based on combination of fixed and random priority of loads for smart grid applications. IEEE Transactions on Power Systems, 30(5), 2507-2515.

Lamchich, M.T., & Lachguer, N. (2012). Matlab simulink as simulation tool for wind generation systems based on doubly fed induction machines: INTECH Open Access Publisher.

Lashof, D., Yeh, S., Carter, S., Doniger, D., Murrow, D., & Johnson, L. (2014). Cleaner and cheaper: Using the clean air act to sharply reduce carbon pollution from existing power plants, delivering health, environmental, and economic benefits. Natural Resources Defence Council (NRDC). Retrieved from http://assets.fiercemarkets.net/public/sites/energy/reports/nrdcreport1.pdf

Marzband, M., Moghaddam, M.M., Akorede, M.F., & Khomeyrani, G. (2016). Adaptive load shedding scheme for frequency stability enhancement in microgrids. Electric Power Systems Research, 140, 78-86.

Mauricio, J.M., Marano, A., Gómez-Expósito, A., & Ramos, J.L.M. (2009). Frequency regulation contribution through variable-speed wind energy conversion systems. IEEE Transactions on Power Systems, 24(1), 173-180.

Mekhilef, S., Safari, A., Mustaffa, W., Saidur, R., Omar, R., & Younis, M. (2012). Solar energy in malaysia: Current state and prospects. Renewable and Sustainable Energy Reviews, 16(1), 386-396.

Miao, L., Wen, J., Xie, H., Yue, C., & Lee, W.-J. (2015). Coordinated control strategy of wind turbine generator and energy storage equipment for frequency support. IEEE Transactions on Industry Applications, 51(4), 2732-2742.

Mishra, S., & Sekhar, P. (2013). A novel controller for frequency regulation in a hybrid system with high pv penetration. Paper presented at the IEEE Power & Energy Society General Meeting.

Mokhlis, H., Laghari, J., Bakar, A., & Karimi, M. (2012). A fuzzy based under-frequency load shedding scheme for islanded distribution network connected with DG. International Review of Electrical Engineering, 7, 4992-5000.

Morren, J., De Haan, S.W., Kling, W.L., & Ferreira, J. (2006). Wind turbines emulating inertia and supporting primary frequency control. IEEE Transactions on Power Systems, 21(1), 433-434.

Morren, J., Pierik, J., & De Haan, S.W. (2006). Inertial response of variable speed wind turbines. Electric power systems research, 76(11), 980-987.

Okou, A., Akhri, O., Beguenane, R., & Tarbouchi, M. (2012). Nonlinear control strategy insuring contribution of pv generator to voltage and frequency regulation. Paper presented at the 6th International Power Electronics, Machines and Drives (PEMD) Conference.

Oluwadare, S.A., Iwasokun, G.B., Olabode, O., Olusi, O., & Akinwonmi, A.E. (2016). Genetic algorithm-based cost optimization model for power economic dispatch problem. British Journal of Applied Science & Technology, 15(6).

Paish, O. (2002). Small hydro power: Technology and current status. Renewable and sustainable energy reviews, 6(6), 537-556.

Pappu, V.A.K., Chowdhury, B., & Bhatt, R. (2010). Implementing frequency regulation capability in a solar photovoltaic power plant. Paper presented at the North American Power Symposium (NAPS), 2010.

Pasand, M.S., & Seyedi, H. (2007). New centralized adaptive under frequency load shedding algorithms. Paper presented at the Large Engineering Systems Conference on Power Engineering.

Pradhan, C., & Bhende, C. (2015). Adaptive deloading of stand-alone wind farm for primary frequency control. Energy Systems, 6(1), 109-127.

Rahmann, C., & Castillo, A. (2014). Fast frequency response capability of photovoltaic power plants: The necessity of new grid requirements and definitions. Energies, 7(10), 6306-6322.

REN, R. (2012). Global status report. Renewable energy policy network. Retrieved from http://www.ren21.net/Portals/0/documents/Resources/GSR2012_low%20res_FINAL.pdf

REN, R. (2016). Renewables global status report. Renewable energy policy network. Retrieved from http://www.ren21.net/wp-content /uploads/ 2016/05/ GSR_2016_Full_Report_lowres.pdf

Revel, G., Leon, A.E., Alonso, D.M., & Moiola, J.L. (2014). Dynamics and stability analysis of a power system with a pmsg-based wind farm performing ancillary services. IEEE Transactions on Circuits and Systems I: Regular Papers, 61(7), 2182-2193.

Rudez, U., & Mihalic, R. (2011). Monitoring the first frequency derivative to improve adaptive underfrequency load-shedding schemes. IEEE Transactions on Power Systems, 26(2), 839-846.

Sa-ngawong, N., & Ngamroo, I. (2013). Optimal fuzzy logic-based adaptive controller equipped with dfig wind turbine for frequency control in stand alone power system. Paper presented at the IEEE Innovative Smart Grid Technologies-Asia (ISGT Asia).

Sadati, N., Amraee, T., & Ranjbar, A. (2009). A global particle swarm-based-simulated annealing optimization technique for under-voltage load shedding problem. Applied Soft Computing, 9(2), 652-657.

Saffarian, A., & Sanaye-Pasand, M. (2011). Enhancement of power system stability using adaptive combinational load shedding methods. IEEE Transactions on Power Systems, 26(3), 1010-1020.

Sallam, A., & Khafaga, A. (2002). Fuzzy expert system using load shedding for voltage instability control. Paper presented at the Large Engineering Systems Conference.

Sanaye-Pasand, M., & Davarpanah, M. (2005). A new adaptive multidimensioanal load shedding scheme using genetic algorithm. Paper presented at the Canadian Conference on Electrical and Computer Engineering, 2005.

Sasikala, J., & Ramaswamy, M. (2011). Fuzzy based load shedding strategies for avoiding voltage collapse. Applied Soft Computing, 11(3), 3179-3185.

SEDA. (2015). Annual report. Retrieved from http://seda.gov.my

Serban, I., Teodorescu, R., & Marinescu, C. (2013). Energy storage systems impact on the short-term frequency stability of distributed autonomous microgrids, an analysis using aggregate models. IET Renewable Power Generation, 7(5), 531-539.

Sharma, H., & Singh, J. (2013). Run off river plant: Status and prospects. International Journal of Innovative Technology and Exploring Engineering (IJITEE), 3, 210-213.

Shekarchian, M., Moghavvemi, M., Mahlia, T., & Mazandarani, A. (2011). A review on the pattern of electricity generation and emission in malaysia from 1976 to 2008. Renewable and Sustainable Energy Reviews, 15(6), 2629-2642.

Stockwell, A. (2009). 'The crucible of the malayan nation': The university and the making of a new malaya, 1938–62. Modern Asian Studies, 43(05), 1149-1187.

Sun, Y.-z., Zhang, Z.-s., Li, G.-j., & Lin, J. (2010). Review on frequency control of power systems with wind power penetration. Paper presented at the International Conference of Power System Technology (POWERCON).

Tang, J., Liu, J., Ponci, F., & Monti, A. (2013). Adaptive load shedding based on combined frequency and voltage stability assessment using synchrophasor measurements. IEEE Transactions on power systems, 28(2), 2035-2047.

Terzija, V.V. (2006). Adaptive underfrequency load shedding based on the magnitude of the disturbance estimation. IEEE Transactions on Power Systems, 21(3), 1260-1266.

Thakur, P., & Singh, A.J. (2014). Study of various crossover operators in geneticalgorithms. International Journal of Advanced Research in Computer Science and Software Engineering, 4(3).

Thresher, R., Robinson, M., & Veers, P. (2007). To capture the wind. IEEE Power and Energy Magazine, 5(6), 34-46.

Tielens, P., De Rijcke, S., Srivastava, K., Reza, M., Marinopoulos, A., & Driesen, J. (2012). Frequency support by wind power plants in isolated grids with varying generation mix. Paper presented at the IEEE Power and Energy Society General Meeting.

TNB. (2013). TNB technical guidebook on grid-interconnection of photovoltaic power generation system to LV and MV networks. Retrieved from http://www.seda.gov.my

Tremblay, O., Dessaint, L.-A., & Dekkiche, A.-I. (2007). *A generic battery model for the dynamic simulation of hybrid electric vehicles*. Paper presented at the IEEE Vehicle Power and Propulsion Conference.

Ulbig, A., Borsche, T.S., & Andersson, G. (2014). Impact of low rotational inertia on power system stability and operation. IFAC Proceedings Volumes, 47(3), 7290-7297.

Ullah, N.R., Thiringer, T., & Karlsson, D. (2008). Temporary primary frequency control support by variable speed wind turbines—potential and applications. IEEE Transactions on Power Systems, 23(2), 601-612.

Vahedi, H., & Karrari, M. (2013). Adaptive fuzzy sandia frequency-shift method for islanding protection of inverter-based distributed generation. IEEE Transactions on Power Delivery, 28(1), 84-92.

Van, T.V., Visscher, K., Diaz, J., Karapanos, V., Woyte, A., Albu, M., . . . Federenciuc, D. (2010). Virtual synchronous generator: An element of future grids. Paper presented at the IEEE PES Innovative Smart Grid Technologies Conference Europe (ISGT Europe).

VATTENFALL. (2016). Geesthacht pumped-storage power plant. Retrieved from http://powerplants.vattenfall.com/geesthacht

Vidyanandan, K., & Senroy, N. (2013). Primary frequency regulation by deloaded wind turbines using variable droop. IEEE Transactions on Power Systems, 28(2), 837-846.

Wachtel, S., & Beekmann, A. (2009). Contribution of wind energy converters with inertia emulation to frequency control and frequency stability in power systems. Paper

presented at the 8th international workshop on large-scale integration of wind power into power systems as well as on transmission networks for offshore wind farms, Bremen, Germany.

Watson, L.D., & Kimball, J.W. (2011). Frequency regulation of a microgrid using solar power. Paper presented at the Twenty-Sixth Annual IEEE Applied Power Electronics Conference and Exposition (APEC).

Wharburton, D., Fisher, B., & Zema, M. (2014). Renewable energy target scheme. report of the expert panel. Retrieved from http://apo.org.au/system/files/41058/apo-nid41058-82456.pdf

Wong, E., Yusof, M., Mansor, M., Anbazhagan, D., Ong, S., & Sekaran, S. (2009). Disruption of adeb gene has a greater effect on resistance to meropenems than adea gene in acinetobacter spp. Isolated from university malaya medical centre. Singapore medical journal, 50(8), 822-826.

Wu, D., Tang, F., Dragicevic, T., Vasquez, J.C., & Guerrero, J.M. (2014). Autonomous active power control for islanded ac microgrids with photovoltaic generation and energy storage system. IEEE Transactions on Energy Conversion, 29(4), 882-892.

Wu, L., & Infield, D.G. (2013). Towards an assessment of power system frequency support from wind plant—modeling aggregate inertial response. IEEE Transactions on Power Systems, 28(3), 2283-2291.

Wu, Z., Gao, W., Wang, J., & Gu, S. (2012). A coordinated primary frequency regulation from permanent magnet synchronous wind turbine generation. Paper presented at the IEEE Power Electronics and Machines in Wind Applications.

Xu, D., & Girgis, A.A. (2001). Optimal load shedding strategy in power systems with distributed generation. Paper presented at the IEEE Power Engineering Society Winter Meeting.

Yao, W., & Lee, K.Y. (2011). A control configuration of wind farm for load-following and frequency support by considering the inertia issue. Paper presented at the IEEE Power and Energy Society General Meeting.

Yong, J.Y., Ramachandaramurthy, V.K., Tan, K.M., & Mithulananthan, N. (2015). Bi-directional electric vehicle fast charging station with novel reactive power compensation for voltage regulation. International Journal of Electrical Power & Energy Systems, 64, 300-310.

Yu, M., Dyśko, A., Booth, C.D., Roscoe, A.J., & Zhu, J. (2014). A review of control methods for providing frequency response in VSC-HVDC transmission systems. Paper presented at the 49th International Universities Power Engineering Conference (UPEC).

Yusof, N.A., Mohd Rosli, H., Mokhlis, H., Karimi, M., Selvaraj, J., & Sapari, N.M. (2017). A new under-voltage load shedding scheme for islanded distribution system based on voltage stability indices. IEEJ Transactions on Electrical and Electronic Engineering.

Zarina, P., Mishra, S., & Sekhar, P. (2012a). Deriving inertial response from a non-inertial pv system for frequency regulation. Paper presented at the IEEE International Conference on Power Electronics, Drives and Energy Systems (PEDES).

Zarina, P., Mishra, S., & Sekhar, P. (2012b). Photovoltaic system based transient mitigation and frequency regulation. Paper presented at the Annual IEEE India Conference (INDICON).

Zarina, P., Mishra, S., & Sekhar, P. (2014). Exploring frequency control capability of a pv system in a hybrid pv-rotating machine-without storage system. International Journal of Electrical Power & Energy Systems, 60, 258-267.

Zhang, Z.-S., Sun, Y.-Z., Lin, J., & Li, G.-J. (2012). Coordinated frequency regulation by doubly fed induction generator-based wind power plants. IET Renewable Power Generation, 6(1), 38-47.

Zhang, Z., Wang, Y., Li, H., & Su, X. (2013). Comparison of inertia control methods for dfig-based wind turbines. Paper presented at the IEEE ECCE Asia Downunder (ECCE Asia).

Zhangjie, C., Xiaoru, W., & Jin, T. (2012). Control strategy of large-scale dfig-based wind farm for power grid frequency regulation. Paper presented at the 31st Chinese Control Conference (CCC).

Zhou, S., Kang, L., Sun, J., Guo, G., Cheng, B., Cao, B., & Tang, Y. (2010). A novel maximum power point tracking algorithms for stand-alone photovoltaic system. International journal of control, automation and systems, 8(6), 1364-1371.

Zin, A.M., Hafiz, H.M., & Aziz, M. (2004). A review of under-frequency load shedding scheme on tnb system. Paper presented at the Proceedings of Power and Energy Conference PECon.